Project: PNII-ID-PCE-2012-4-0299

Project title: "Nuclear astrophysics studies at IFIN-HH"

Intermediate report December 2015

1. Introduction

This is an intermediate report for the project identified above, done at the beginning of Dec. 2015, after 25+ months since the start of its financing. The project was submitted in April 2012 and its financing started only on Sept 2, 2013 for a duration that became 37 months, after three contract amendments. It has the IFIN-HH internal number PNII 27/2013 and some documents may identify it with this number. Due to a late start and financial truncation, some of the objectives may not be as stated in the original proposal, in spite of the efforts of the project director. First, after only 3 months of regular financing in 2013, the funds for the project were cut to about 55% of those scheduled for 2014 and a 11 months extension into 2016 was given. For 2015 the funds were first cut to a similar percent, then supplemented in November with 120,000 lei. These lead the Project Director (PD) (or Principal Investigator - PI), to some changes in program's objectives, mostly to their order - not their substance, and in particular of the use of funds. Funds in this project had to be, at several points, complemented with funds from other projects, in particular for the acquisition of equipment. These are clearly shown where the case, and in the financial documents. Some of the changes were inherent to such a project, which included in its original form, written almost 4 years ago, proposals that depended on the approval of experiments at foreign laboratories, and after approval, on the scheduling of those experiments at installations where the competition is tough and arduous. They also involve collaborations with groups from outside IFIN-HH, and the timing of joint activities had to be correlated with them.

2. General report

In last year's report I started from part *C. Project description* from the proposal of April 2012 [1], used a convention to identify the main objectives, and discussed in detail where we stood exactly a year ago [2]. I will not go on exactly the same format this year, but will refer only briefly to those objectives and go directly into the report of physics results of the last period.

C2.1 *Start a research group in the Department of Nuclear Physics (DFN) of IFIN-HH.*

This was one of the stated objectives. A Nuclear Astrophysics Group (NAG) was formally and factually put together. The situation is the following at this time:

- The post-doc employed for a two-years period, dr. Daniela Chesneanu, ended her participation in the project when she left the institute at the very end of 2014.

- Soon after that, I could hire on the project two debutant physicists, Alexandra Chilug and Dana Tudor, who both have master degrees from the Faculty of Physics of the University of Bucharest. So far their integration in the group is very good and they were both instrumental in realizing the scientific program of 2015, in particular of the measurements done at IFIN-HH installations.
- The collaboration with dr. Florin Carstoiu and his assistant, V. Balanica, both of Department of Theoretical Physics (DFT) of IFIN-HH, has continued this year too, along the lines of the program established earlier.
- The collaboration with dr. George Pascovici has also continued, but informally, because dr. Pascovici is retired and does not want to re-enter into a contractual work agreement. His advice on equipment and its electronics, to our group and other groups in IFIN-HH, was obtained when necessary. This has helped, given the financial cuts mentioned above.

The activities of 2015 were concentrated on the lines stated in the amended contract:

a) Construction and tests off-line and in-beam of the ASTROBOX 2 detector at Texas A&M University
b) Experiments in IFIN-HH to determine reaction cross sections for the $^{13}C + {}^{12}C$ system through direct measurements at very low energies (II)
c) Trojan Horse Method measurements (THM) $^{12}C+{}^{12}C$ at LNS Catania and Bucharest.

In addition work was done:

d) on the proposed RIKEN project and
e) on the theory to obtain and describe nucleus-nucleus potentials (optical model potentials) needed for the interpretation of the various indirect methods we propose for nuclear astrophysics.

The results of these activities will be presented in the next section of this report. Some of the results were reported previously in 8 articles published or submitted for publication. Six of those were presented at international conferences and four had to pass peer review before being included in the respective volumes. Some were presentations of members of our group from Bucharest, some were presented by our external collaborators. Two articles were submitted for publication in November.

At the beginning of 2015, the volume [3]:

"Exotic Nuclei and Nuclear/Particle Astrophysics (V). From Nuclei to Stars", ***Proceedings CSSP14***, L. Trache, D. Chesneanu and C.A. Ur (eds.), AIP Conf. Proc. Series, **vol. 1645**,

a 437 pages book, was published by one of the most prestigious publishing houses: the American Institute of Physics, New York, USA. The conference *Carpathian Summer School of Physics 2014*, Sinaia, Romania and the volume of its proceedings were realized and partially supported from this project.

The next edition *Carpathian Summer School of Physics 2016* was approved by the Scientific Council of IFIN-HH to take place also in Sinaia, June 26 – July 9, 2016. It will be organized by a committee based partially on NAG and supported in part by this project.
The front matter of the volume and the pdf files of the articles are appended at the end of this report.

3. Specific objectives

3.1 Construction and tests off-line and in-beam of the detector AstroBox2 (AB2) at Texas A&M University

Last year we discussed in [2] the design of a new version of a detector to measure β-delayed proton emission, of its micromegas component – the main active part of the detector, and have shown its use for measuring very low energy protons, as well as the connection between these measurements and the determination of astrophysical reaction rates for proton induced reaction rates dominated by resonances. We will not repeat those here, but only describe briefly the detector built and the test measurements done at the Cyclotron Institute, Texas A&M University, in College Station, TX.

The active part of the detector, the micromegas was built for us by a group at CERN, the inventors of such devices. The body of the detector was designed by my former student and current post-doc in Texas, dr. A. Saastamoinen. Its design and realization was actively pursued by us and by our collaborator from CEA/IRFU Sacaly, France, dr. E. Pollacco. Schematically it was shown in Figure 5 of last year's report. The detector was put together in the spring of 2015 and on April 20-28, 2015, we had beams for tests of the detector. The main difference from AstroBox 1 [4] is that it does not have anymore a cylindrical symmetry (on an axis perpendicular to the beam), but is more appropriate to the geometry of the beam and its stopping in the gas of the detector. Another difference is that it has 29 separated pads and correspondingly 29 signals, compared with 3 only for AstroBox 1 (AB1).

The tests that were done, were:

- Off-beam tests using ^{55}Fe and ^{241}Am sources
- In-beam commissioning of the detector using a ^{25}Si radioactive beam separated by the MARS spectrometer. The radioactive specie we used, ^{25}Si, is very appropriate for a test of a new proton detector, as it is a good, well known, β-delayed proton emitter with a large βp-branching. It was produced at a reasonable rate from a primary beam of ^{28}Si at 40 MeV/nucleon on a ^{27}Al solid target. The result was actually a cocktail of secondary beams, a benefit for the identification of the beam in AB2.
- In-beam measurements for the ^{23}Al secondary beam, which is the main focus of the physics for these measurements.

The same scheme of measurements was used in 2012 on a test of AB1. The first two parts of the tests went very well, and the commissioning of the AB2 detector was a success. So appeared to be the last measurement, for which we reserved the last 4 days of the experiment. The primary beam of ^{24}Mg at 45 MeV/nucleon was delivered successfully to us on Friday April 24, and the next day the secondary beam of ^{23}Al was selected and was stopped in the middle of the AB2. All seemed to work well for us and it was only a matter of 2 more days of active beamtime to obtain the desired results. Unfortunately, Sunday April 26 a thunderstorm hit the city and produced a blackout that has stopped the cyclotron. The measurement could not be restarted and was incomplete. The data need still be fully analyzed to see if the reconstruction of all signals from adding the adjacent pads improved the statistics to the point we need. After this full analysis the collaboration will decide if the measurement has to be re-done. We will describe these results at a later time.

3.2 Experiments in IFIN_HH to determine reaction cross sections for the ^{13}C+^{12}C system through direct measurements at very low energies (II)

The second of the objectives of this project was to perform experiments for determination of fusion reaction cross section of ^{13}C+^{12}C at deep sub-barrier energies through direct measurements. We shall report on this part more thoroughly. A first experiment was carried out in Sept-Oct 2014 and preliminary reports on those results were presented and published [5,6]. After we analyzed, in collaboration with our colleagues from IMP China, the data from the last year experiment, we obtained a factor of 1.5 between our results and the previous experiments. So we decided to continue the experiment this year to see where this factor comes from and to go even at lower energies that we reached last year (5.2 MeV in laboratory frame). During last year's experiment a total of 23 targets were irradiated at different beam energies in steps of 0.2 MeV between 5.2-6.8 MeV (in laboratory frame). Last year's results are shown in Fig. 1:

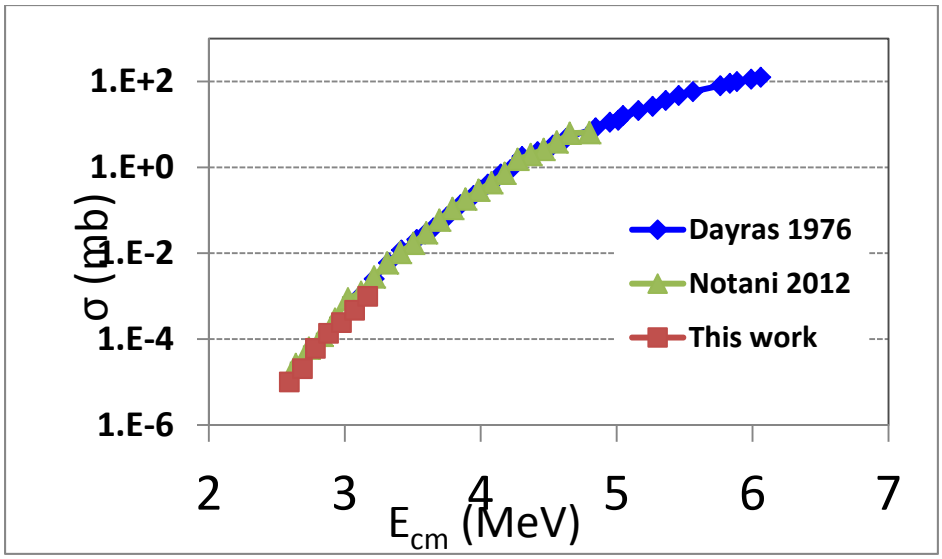

Figure 1. Cross section of the ^{12}C (^{13}C,p)^{24}Na reaction obtained from the past year experiment. The results from the previous experiments are also shown.

The modified S factor S* is defined as: $S^*(E) = \sigma(E)Ee^{\frac{87.21}{\sqrt{E}}+0.46E}$. A normalization factor of 1.5 has been applied to the data obtained from the last year experiment to be comparable with the past ones.

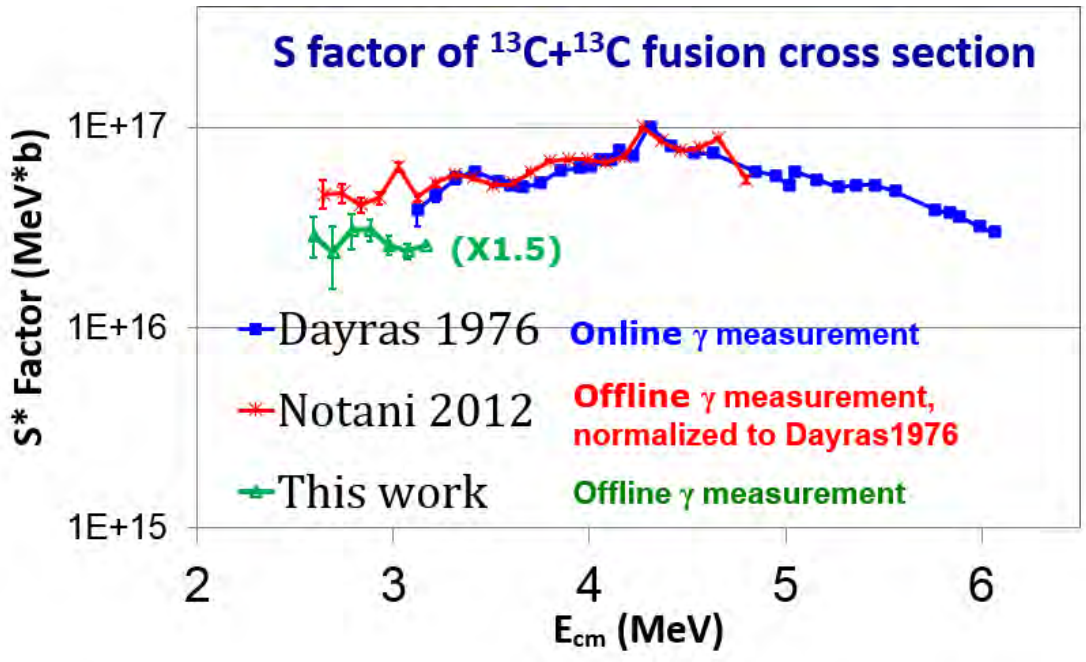

Figure 2. Modified astrophysical S* factor.

For this year we proposed at the “Spring Campaign of experiments 2015” PAC at IFIN-HH the experiment “Measurement of ^{13}C+^{12}C fusion cross section at deep sub-barrier energies in

IFIN-HH", which was approved with highest priority was and performed in collaboration with our colleagues from IMP China in October 2015. Our objectives for the proposed experiment were to:

A. Certify the absolute values of the cross sections measured by further testing calibrations.
B. Determine the relative contribution of the channels: activation vs. total cross section at a few energies by measuring prompt gamma rays and activation gamma rays.
C. Extend the measurements to lower energies using the microBq lab.
D. Use of beta-gamma coincidences to further clean the background in the spectra with the aim of going to even lower energies than those foreseen with the current method.

For this objectives we had requested 26 days for beam time at 3MV Tandem Accelerator:

- 1 day for in-beam γ-ray measurements
- 14 days for decay measurements
- 11 days for trying the β-γ coincidence measurements.

However we only had allocated 15 days for beam time, therefore we could do all planned experiments A-C, but could not perform all the β-γ coincidence measurements (D), could only test the procedure and determine the efficiency we can attain for it in our laboratory and with the detectors, electronics and data acquisition systems available.

$^{13}C+^{12}C$ experimental arrangement and procedure at 3 MV Tandem Accelerator. Measurements, data and preliminary results

We have established a program at IFIN-HH Bucharest-Magurele to test the possibility to make direct measurements for nuclear astrophysics using the new 3 MV Tandetron and an ultra-low background laboratory situated in a salt mine at about 2.5 hours drive north of Bucharest. After initial tests of accelerator performances, like beam intensities, stability of beam energies and intensities for long periods of time, and of the logistics involved by irradiations and de-activation measurements at separate locations, we concluded that we could be competitive for reactions induced by alphas and light ions [7]. We report here on extensive tests using the above case proposed with our colleagues from IMP Lanzhou and CAS Beijing.

One of the important questions in nuclear astrophysics is the carbon burning scenario. This process represents the third stage of stellar evolution of massive stars. Until now fusion reaction have only been measured at energies well above the region of astrophysical interest because of the extremely low cross section and signal/background ratio. In stellar environments the reaction rates are estimated by extrapolating measurements done at higher energies, extrapolations that imply a certain degree of uncertainty. For the $^{13}C+^{12}C$ fusion reaction the situation is more complicated because of the resonances occurring below the Coulomb barrier. In contrast with these resonances in the $^{13}C+^{12}C$ fusion reaction, the $^{13}C+^{12}C$ fusion cross reaction behaves more regularly. Therefore direct measurements at the Gamow window energies are essential, but very difficult to carry due to the background from the cosmic rays, terrestrial environment etc. We can make improvements using irradiation de-activation sequences: we irradiate probes at the new 3

MV Tandetron accelerator and move the probes for de-activation measurements in the ultra-low background laboratory in the salt mine. The preliminary results are presented here.

During the experiment, the ^{13}C beam in the laboratory energy range of E_{Lab}= 11 – 4.6 MeV (E_{cm} =5.28-2.21 MeV), with steps of 0.2 MeV, impinged on 1.5 mm thick natural carbon targets. Intensities in the range of 0.02-15pμA were used in different runs.

We have made a number of activation and measurements. In total 35 target were irradiated at different energies and we went down to the lowest energy ever reached of 4.6 MeV in laboratory frame where the cross section was 0.24 nb (in absolute value).

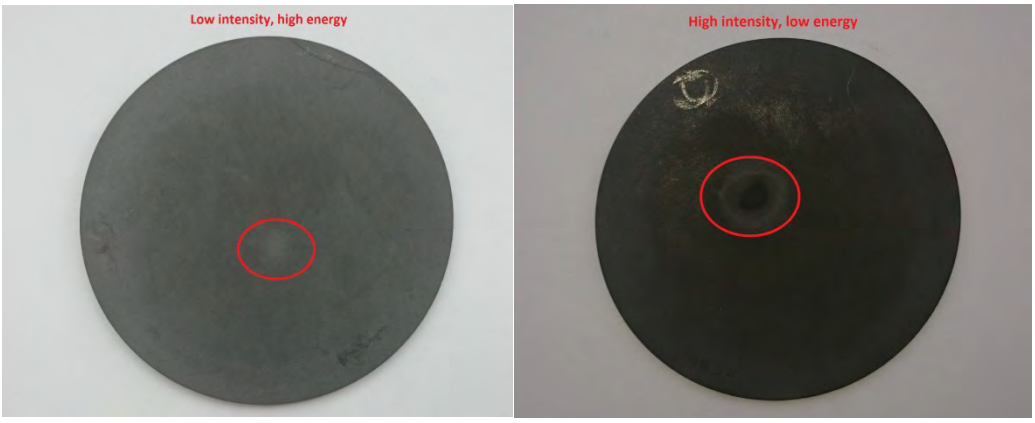

Figure 3. Examples of beam marks on targets irradiated at different energies and different beam currents.

The experiment contained two parts: one of on-line and one of offline measurements. During the prompt gamma-rays measurements we were able to see the opened channels for this reaction.

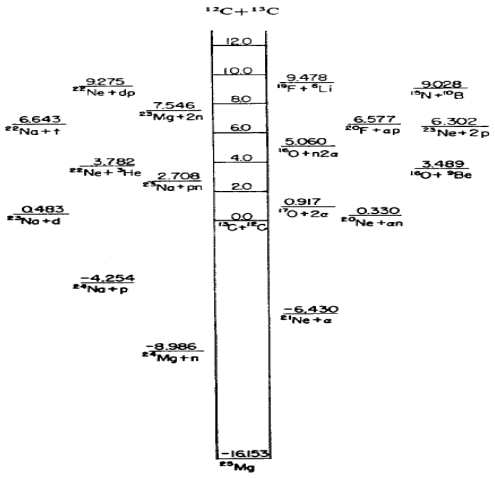

Figure 4. Thresholds for decay of ^{25}Mg relative to the separation energy for $^{13}C+^{12}C$. The locations of bombarding energies (c.m) of 2, 4, 6 MeV, etc. are indicated [8].

For the proton evaporation channel we performed measurements of the two gamma rays of ^{24}Mg.

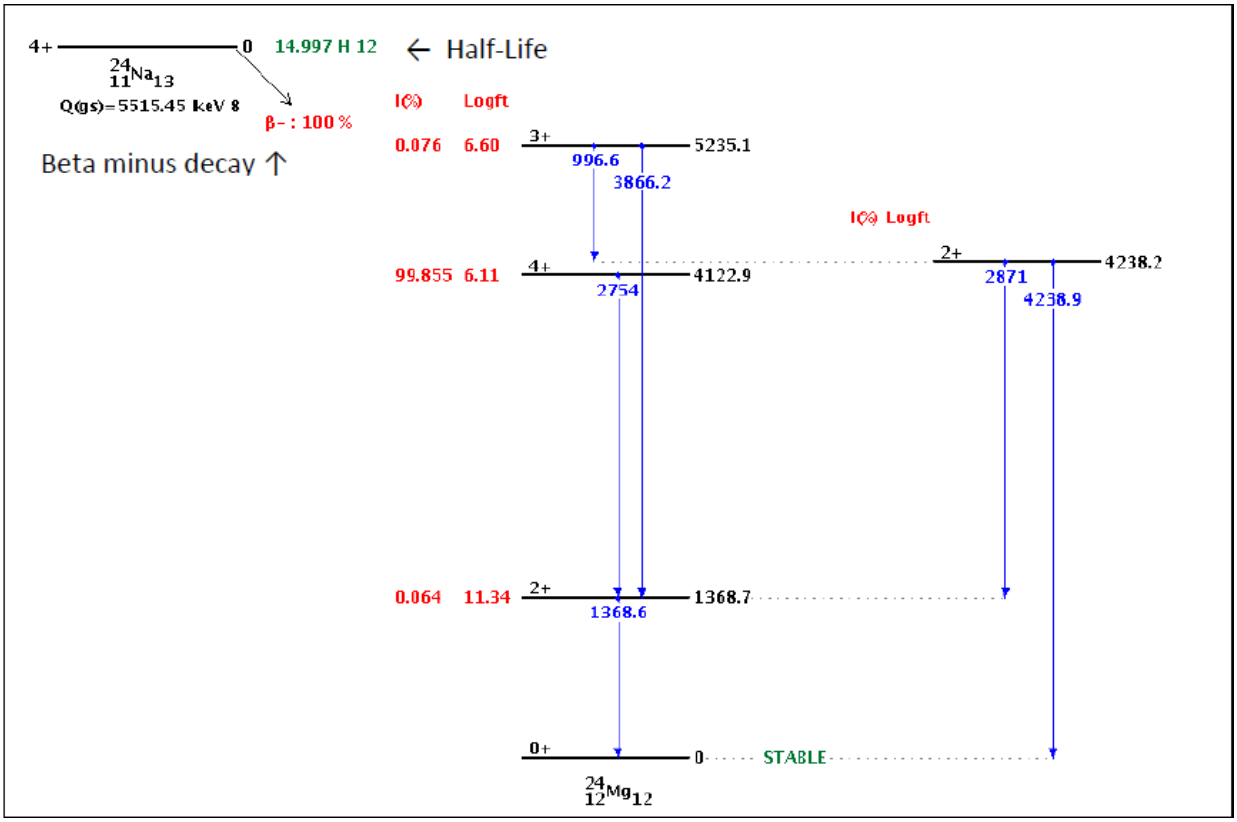

Figure 5. The decay scheme of ^{24}Na. Note the around 99.9% beta decay branch with half-life of 15 hours to the 4^+ state of ^{24}Mg, and then to the ground state via the emission of two gamma rays of energies 2754 keV and 1368.63 keV [9].

Preparation of experimental set-up

The resonances from the ^{13}C+^{12}C fusion reaction make it very difficult to measure in the Gamow window, so to be able to test the predictive power of various models and establish a reliable upper limit for the cross section, we studied the ^{13}C+^{12}C fusion cross section at deep sub-barrier energies. The machine has a maximum voltage of 3.2 MV, and it can run as low as 200 kV. During tests we have proven that the accelerator has high and stable beam current in the range of tens of μA for the prolific negative ions (^{12}C, ^{13}C, ^{28}Si, ^{197}Au) and we consider it suitable for α and light ion beams (0.2-1 MeV per nucleon).

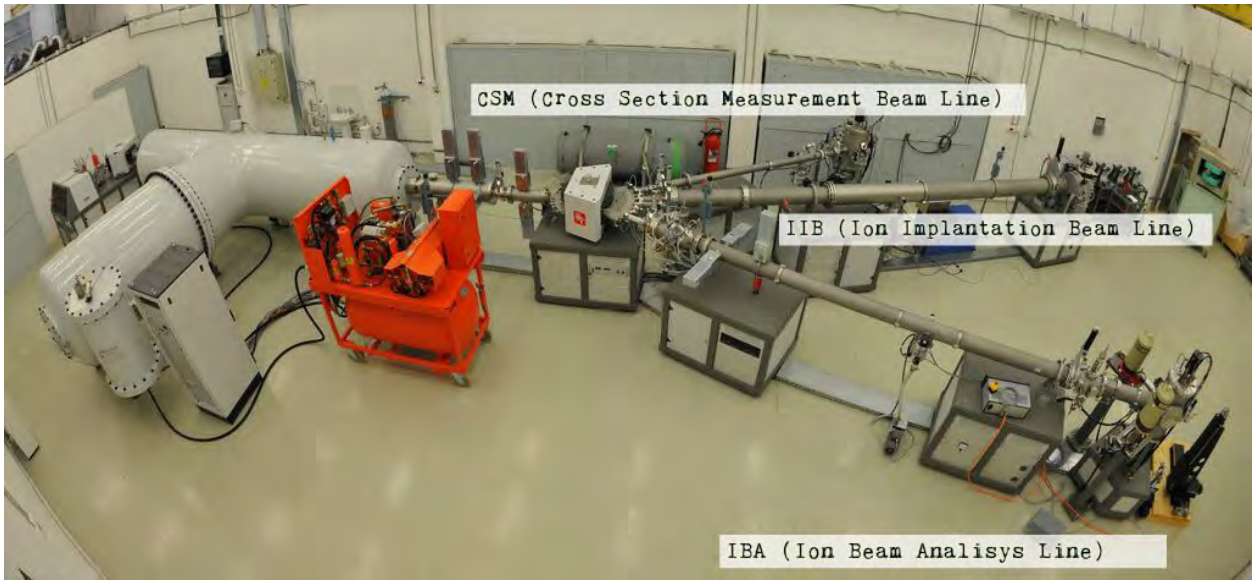

Figure 6. The 3 MV Tandetron Accelerator at IFIN-HH [10].

The reaction we chose $^{13}C+^{12}C$ has the advantage that leads to an activation product with a half-life allowing for the transportation and efficient de-activation measurement. Therefore, one of our interests was focused on the proton evaporation channel ^{12}C (^{13}C, p)^{24}Na and the other one on the prompt gamma-rays measurements, because we were able to use one HPGe detector with relative efficiency of 100% placed at 55^0in extension of the reaction chamber of accelerator Cross Section Measurements line. The irradiation chamber was electrically isolated, acting as a Faraday cup for current integration.

Prompt gamma rays measurements

We measured the prompt gamma-rays during the irradiation with a ^{13}C beam of 1.5 mm thickness natural carbon targets. The prompt emission spectra were measured using a spectroscopy system consisting of a coaxial high-purity germanium (HPGe) detector, signal amplifier and a multichannel analyzer. The experimental set-up is shown in Figure 7. The HPGe detector used is a 100% efficiency (relative to a standard 3”x 3” NaI crystal) detector. The detector was placed at 55^0 in extension of the reaction chamber of accelerator Cross Section Measurements line. The HPGe detector was shielded along its length and on the front face with 5 cm thick lead bricks.

Figure 7. HPGe detector 100% relative efficiency placed at 55^0 at the reaction chamber.

For prompt gamma ray measurements we were able to analyze only the spectra of irradiated targets at beam energies higher than 6.4 MeV (laboratory frame) because the background inside the accelerator hall is too high. The difference between two different beam energies can be seen in Figure 8.

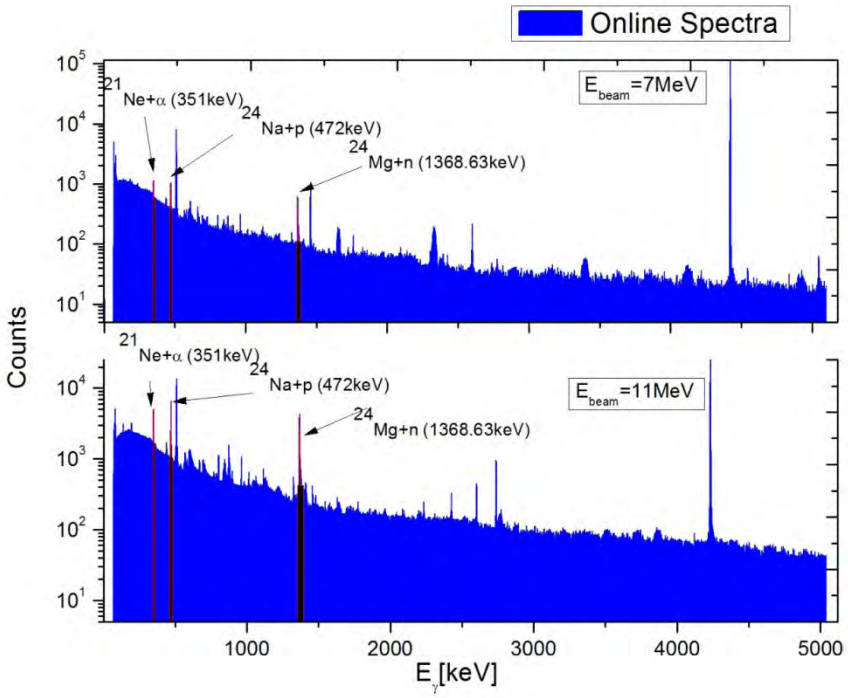

Figure 8. A typical γ-ray spectrum obtained with a ^{13}C beam on a natural carbon target. The origins of the prominent transitions are indicated by the associated light particle evaporated from the compound nucleus.

We have succeeded to measure and analyze the α-particle, proton and neutron exit channels independently and to compare the relative agreement for these three cases and this fact is an important feature of the present method for deducing absolute total cross sections.

In the preliminary analysis we calculated the corresponding yields for each opened channel which helped us to see the contribution of each channel at the total reaction cross section. For computing the yields we took into account the beam current, density of targets, irradiation time, the photo-peak efficiency for selected gamma rays and charge state. A representation of these yields is shown in Figure 9.

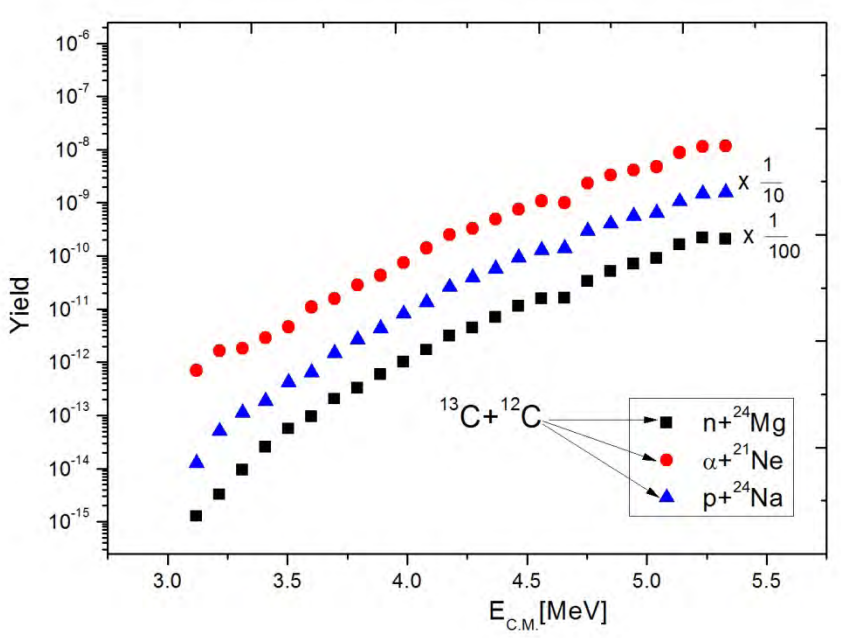

Figure 9. Calculated yields for opened channels.

Using these yields we calculate the reaction cross section using the formula:

$$\bar{\sigma}(E) = \frac{1}{N_v}\frac{dY(E)}{dE}\frac{dE}{dx}$$

where N_v is the number density of target nuclei present in the target, dE/dx is the stopping power and Y is the yield.

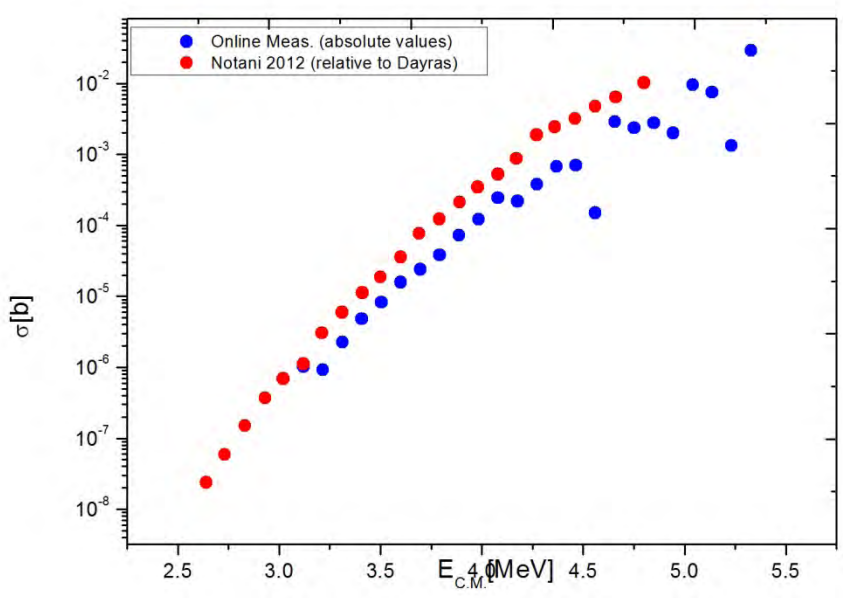

Figure 10. The absolute value of total fusion cross section.

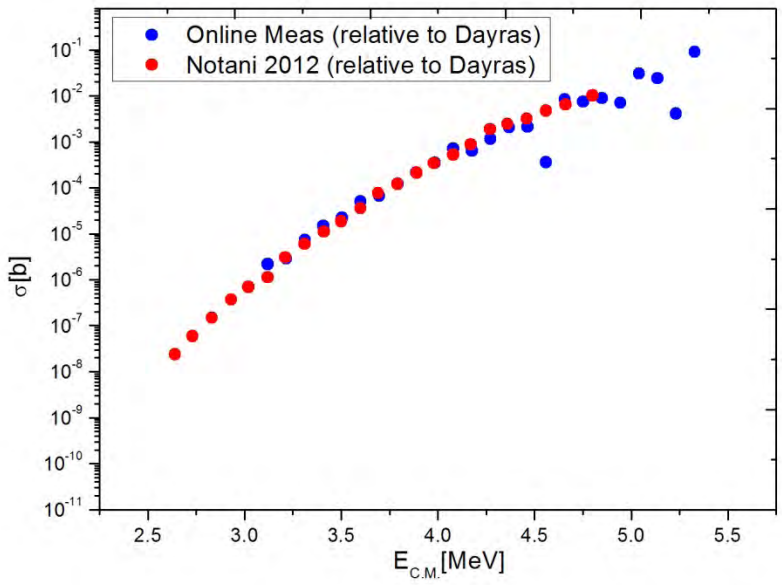

Figure 11. The relative values of total fusion cross section.

Decay measurements at the low background laboratory (GammaSpec) and at the ultra-low background laboratory (μBq) in the salt mine

Thick target yield for the $^{12}C(^{13}C,p)^{24}Na$ fusion reaction was determined through the measurement of the gamma-ray yield following the beta-decay of ^{24}Na ($T_{1/2}$=15 h) at low background laboratory GammaSpec at the ground level (in IFIN-HH) and the ultra-low background laboratory μBq (in Unirea salt mine at Slanic). At the μBq we could see a significant reduction of radiation background compared with GammaSpec as is shown in Figure 13 (a) and Figure 13 (b).

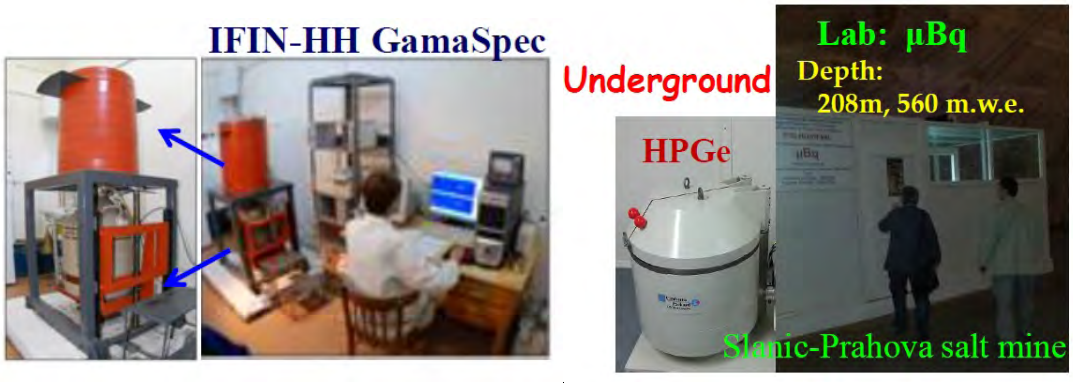

Fig. 12 GammaSpec and μBq Laboratories.

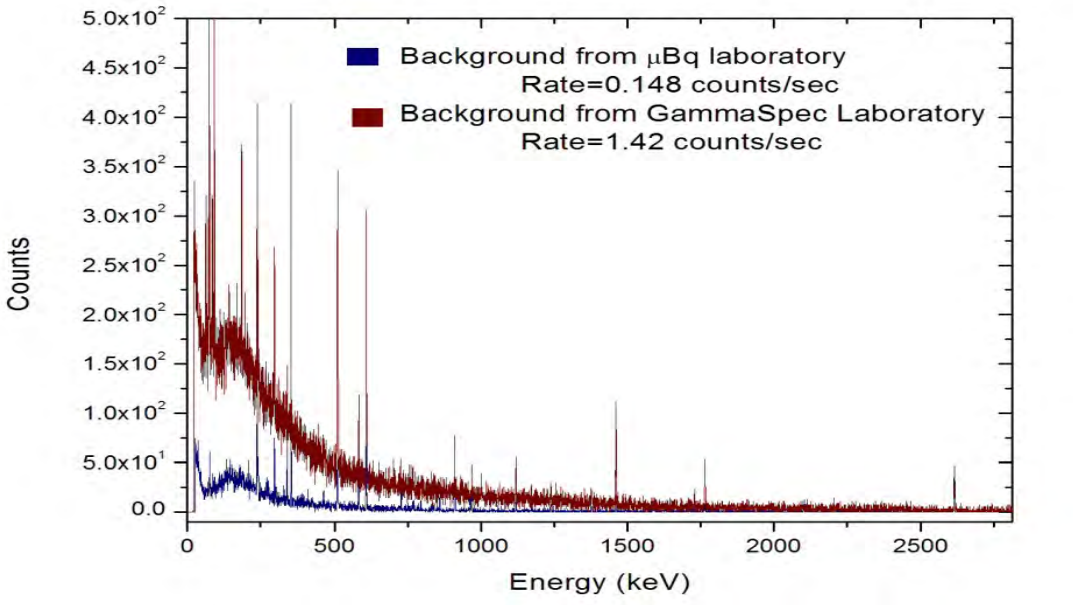

Figure 13 (a). Comparison between background from laboratories (GammaSpec and μBq).

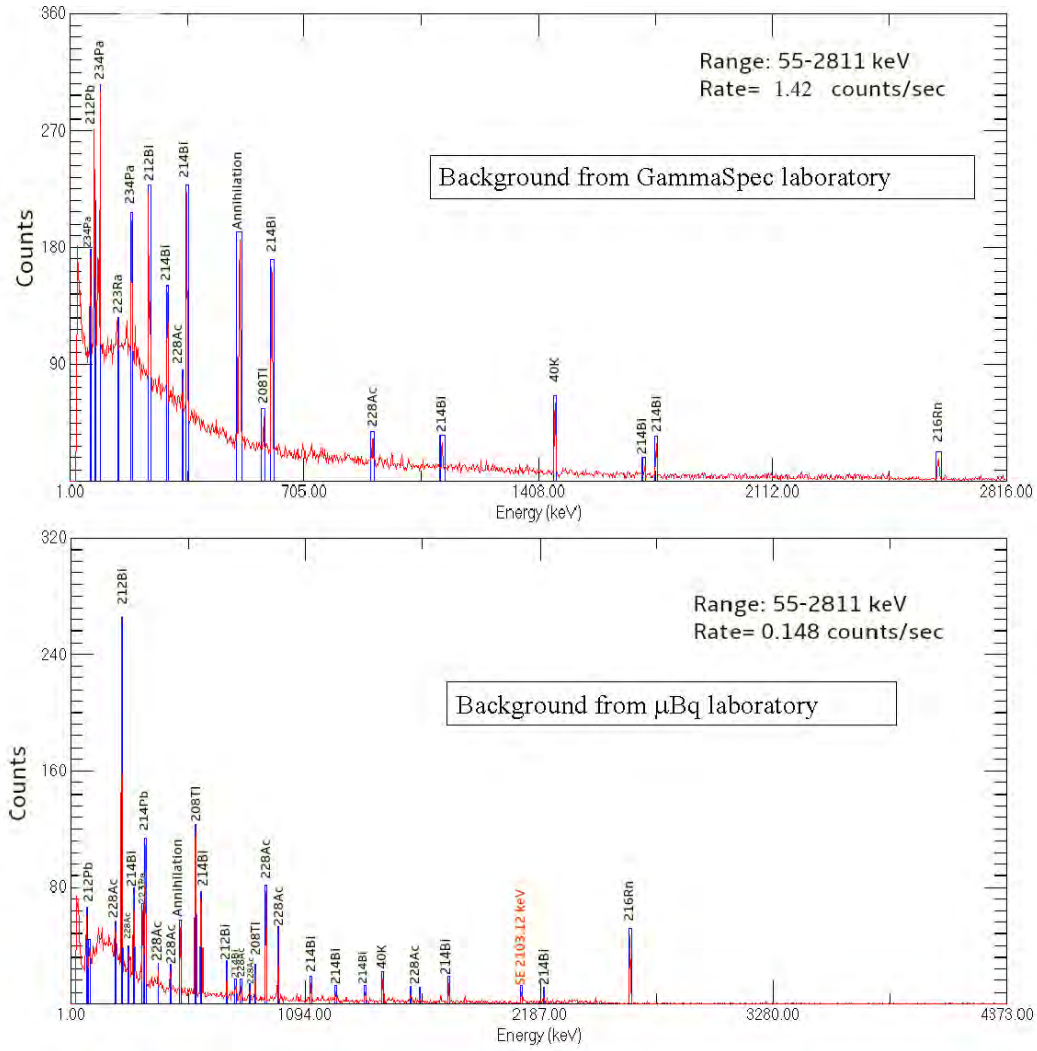

Figure 13 (b). Identification of the isotopes from the background in each laboratory.

In these laboratories the cascading gamma rays (1369 and 2754 keV) were detected with shielded HPGe detectors with 30% relative efficiency (at GammaSpec) and 120% (at μBq in the salt mine). In the next figure (Fig.14) are presented two spectra of two targets irradiated with the same beam energy, measured in both laboratories.

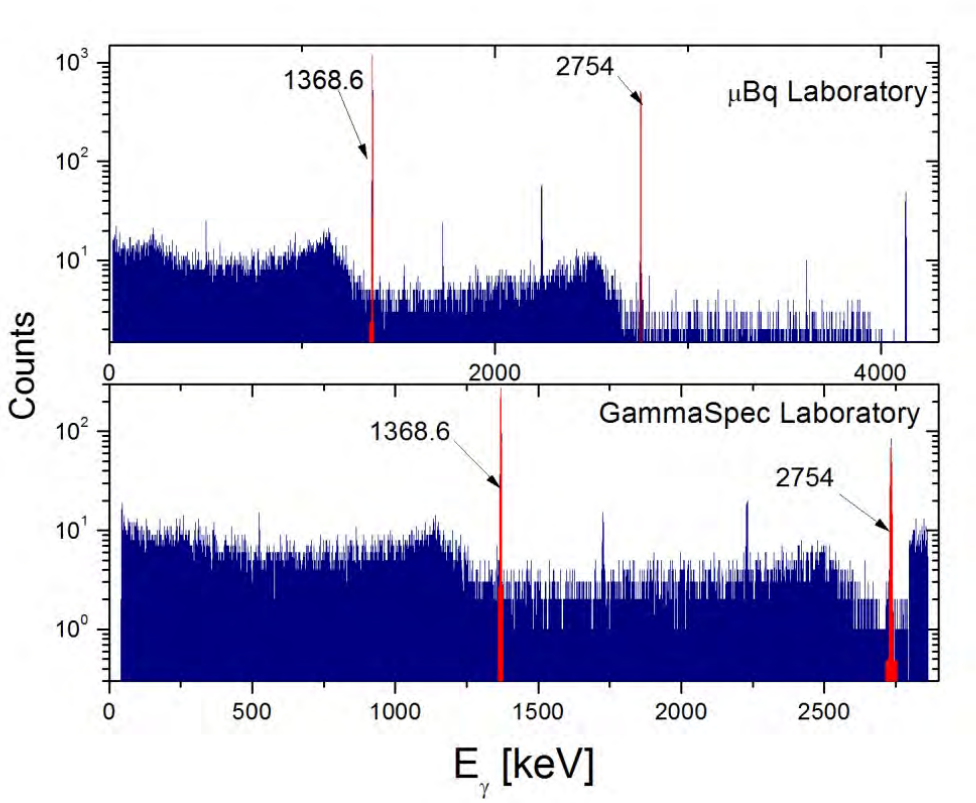

Figure 14. Measured spectra of a target irradiated at 8.6 MeV.

There were measured at GammaSpec Laboratory the targets which were irradiated at energies $E_{beam} \geq 5.8$ MeV (in lab. frame) because of the too high background for such measurements. For energies between 5.8-4.6 MeV (in lab. frame) the samples were measured in μBq Laboratory. After that, the $^{12}C(^{13}C,p)^{24}Na$ cross sections was calculated starting from the following equation:

$$\Delta R = I\Delta t\bar{\sigma}(E)N_v$$

where ΔR is the production rate and IΔt means the integrated beam current.

To obtain the total fusion cross section we used the correction factors obtained from interpretation of online measurements, for proton evaporation channel (f=0.319292 for absolute values and f=0.17921 for relative values). The results are shown in next figures.

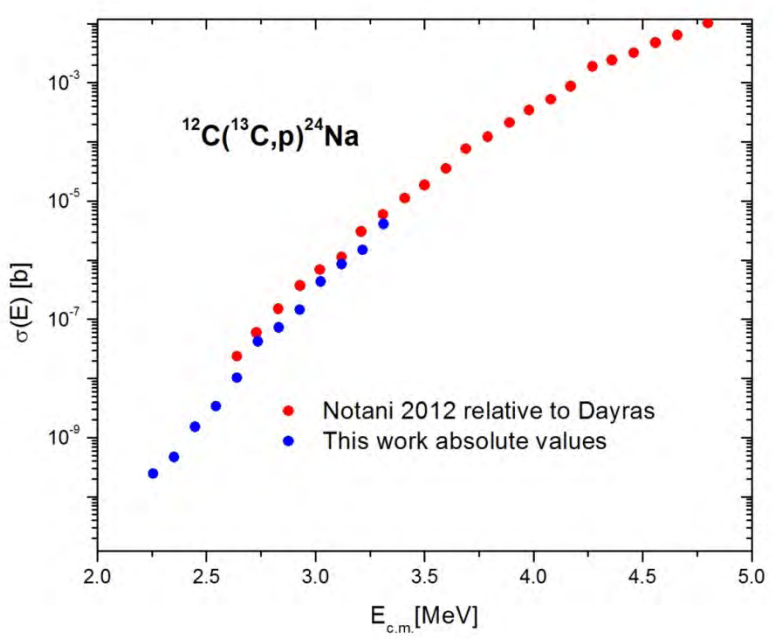

Figure 15. The absolute values of total cross section.

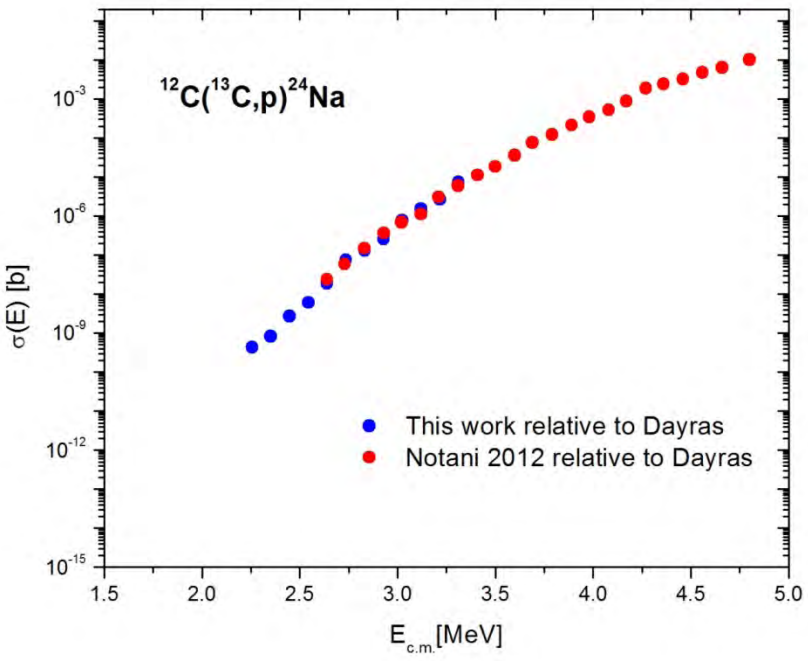

Figure 16. The relative values of total cross section.

In conclusion of these preliminary results, during this year experiment we have made a number of progresses:

- Measurements of proton, neutron and alpha channels at high energies with gamma spectroscopy.
- Pushing the lowest energy to 4.6 MeV, a new world record and we achieved a reasonable statistics.

The preliminary interpretation of data shows that our relative values match with those from the previous experiments (see Figure 17 and Figure 18).

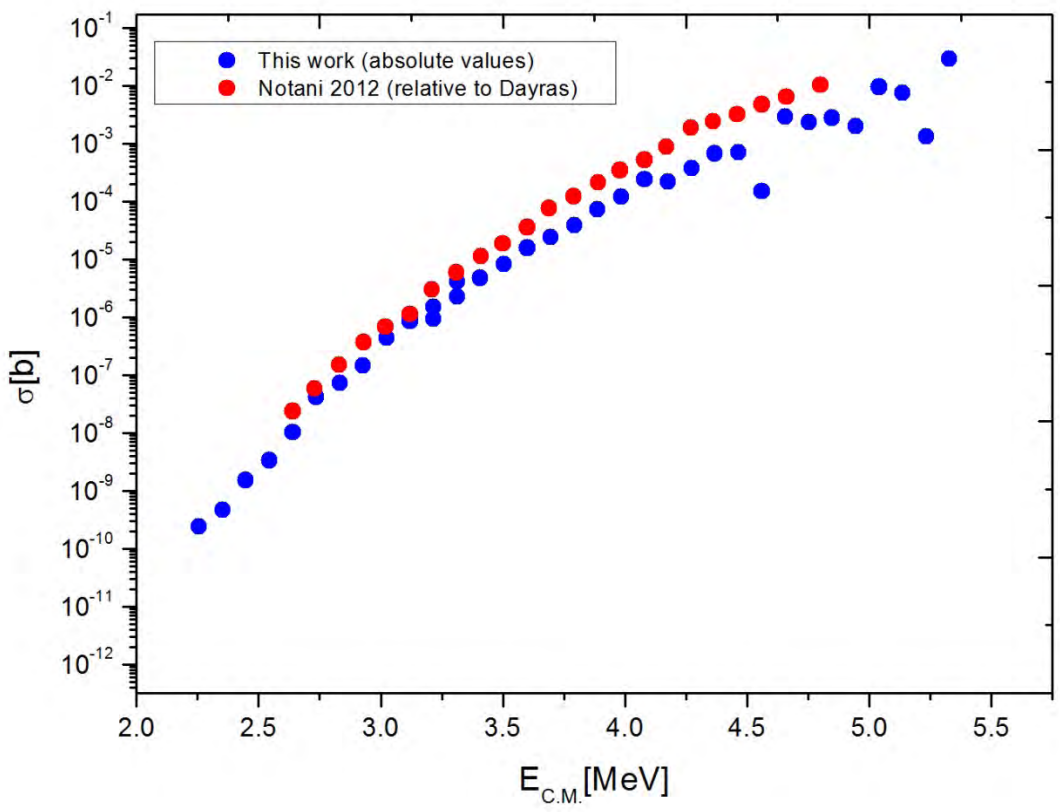

Figure 17. Absolute values of total fusion cross section for E_{cm} between 2.26-5.33 MeV.

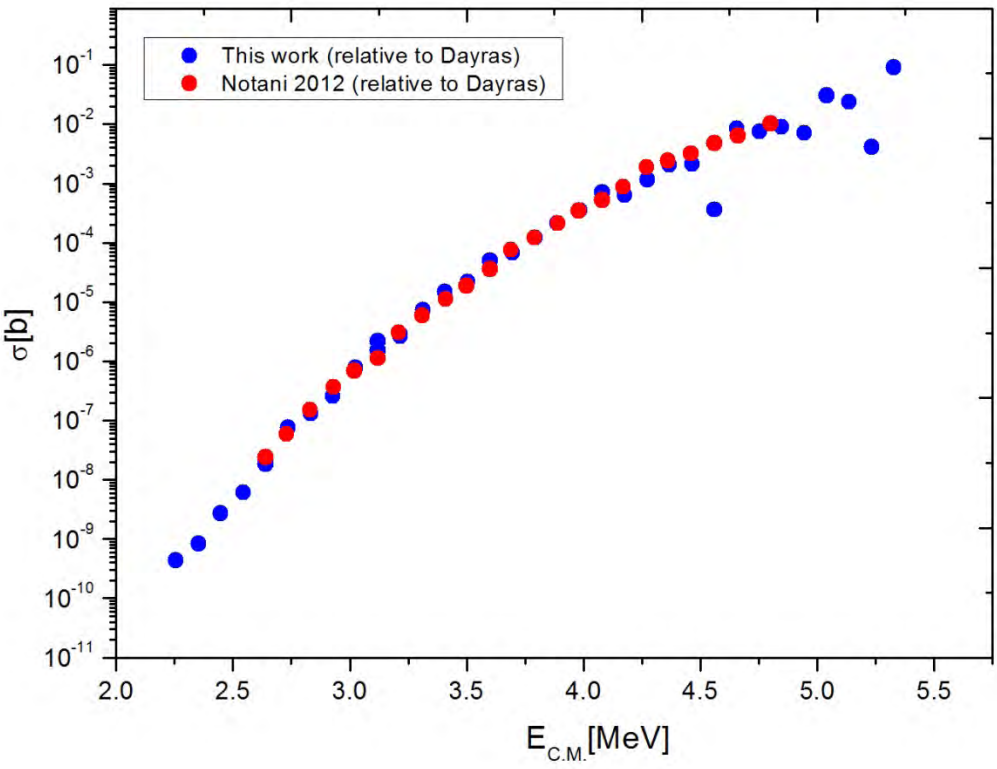

Figure 18. Relative values of total fusion cross section for E_{cm} = 2.26-5.33 MeV.

3.3 Trojan Horse Method measurements for the $^{12}C+^{12}C$ system

Test measurements were done in Bucharest, at the 9 MV FN tandem accelerator together with the group of prof. Claudio Spitaleri from the University of Catania and INFN LNS to check if this reaction can be studied using the Trojan Horse Method. This is an indirect type of measurement and the motivation is the same reaction as for our $^{13}C+^{12}C$ direct measurements. The test was done using a ^{16}O beam on ^{12}C targets. The beam was delivered on the beamline no. 4 (at 0 degree) in the large target chamber existent there. The setup was used before in Bucharest, but this time the reaction chamber was much improved. The test aimed at deciding if the method could work in this combination beam-target. Unfortunately the answer was NO = the projectile ^{16}O does not have a clear cluster structure in its ground state (a $^{12}C+\alpha$ clusterization) to allow for the quasi-free reaction mechanism. The experiment is not possible. However, we have a student that has written a diploma on the THM and is continuing toward a master thesis on similar subjects.

3.4 Preparations and tests of the detection system to be used in the RIKEN experiment: breakup of ^{9}C

In February 2015 a test experiment was carried out at the HIMAC accelerator in Chiba, Japan, for the detector assembly prepared to be used for the 9C breakup experiment proposed and approved by the PAC of the RIBF (Radioactive Ion Beam facility) of RIKEN, Japan. The test was done together with the collaborating groups from RIKEN, Louisiana State University, Washington University in St. Louis and Texas A&M University. The main subject of the tests was the newly designed and built dual gain integrated preamplifiers. The test was successful. While it is part of the program of this project, the proposal and the participation at these tests was financed from another grant, therefore I will skip the details of the experiments and the results.

3.5 Optical Model Potentials for nucleus-nucleus collisions

We have a long-term program to understand and describe nucleus-nucleus collisions in terms of one interaction potential, the optical model potential (OMP). A good understanding of all phenomena occurring in the elastic nucleus-nucleus scattering, which are used typically to extract OMP, and the interpretation of the origin of different aspects, including the well know potential ambiguities, are of crucial importance for finding and justifying the procedures used for predicting nucleus-nucleus OMP in the era of radioactive nuclear beams (RNB) (see ours based on double folding in Ref. 11). The reliability of these potentials is crucial in the correct description of a number of reactions, from elastic to transfer, to breakup, at energies ranging from a few to a few hundred MeV/nucleon. Of particular interest for us is to support the absolute values of the calculated cross sections for reactions used in indirect methods for nuclear astrophysics, see references [12-14] for the most recent results.

In this framework, the theoreticians involved in this project treated in two related papers submitted for publication to Romanian Journal of Physics [15,16] the case of heavy ion orbiting, one of the phenomena found over the years to occur is special cases of elastic scattering, well understood semi-classically, but not well documented by specific examples. We do not extent the discussion here, but attach the pdf files of the submitted articles.

4. Related activities and achievements

A number of activities were proposed and pursued constantly in the past two years. The justification behind it were detailed last year [2], I do not repeat it here. Below is a list of international conferences with participation from our group. In all cases the project director was invited to give lectures on nuclear astrophysics subjects, including news from the IFIN-HH facilities. The juniors of the group were participating to international schools on nuclear

astrophysics or nuclear physics subjects. Some of the participations were not financed from this grant.

Project director participated in several meetings:

- 12^{th} Russbach Winter school on nuclear astrophysics, in Russbach, Austria. March 11-14, 2015. Invited lecture "Nuclear astrophysics with Radioactive Ion Beams".
- International Conference ISTROS 2015, Casta-Papiernica, Slovakia. Invited lecture on Nuclear Astrophysics.
- International Workshop "Weakly Bound Exotic Nuclei", Natal, Brasil, May 23-30, 2015. Invited talk "Nuclear Astrophysics with Radioactive Ion Beams".
- Gordon Research Conference "Confluence of Structure and Reactions", in New London, NH, SUA, May 31-June 6, 29015. Invited talk.
- Shanghai, China – invited talk at SINAP: "Nuclear Astrophysics and IFIN-HH"
- Nucleus-Nucleus Conference 2015, Catania, Italy, member of International Advisory Committee.
- EuNPC Groningen, The Netherlands, Aug. 31 – Sep 3, 2015. Co-author several presentations.
- International Conference "Processes in Isotopes and Molecules", Cluj-Napoca, Romania, Sept. 23-25. Invited talk "Isotopes and molecules in current nuclear physics"

Physicists Alexandra Chilug and Dana Tudor participated at the JINR school in Borovets, Bulgaria.

Physicist Chilug Alexandra has participated and presented the proposal of the experiment "Measurement of $^{13}C+^{12}C$ fusion cross section at deep sub-barrier energies in IFIN-HH" at the "Spring Campaign of experiments 2015" PAC at IFIN-HH.

Physicists Chilug Alexandra and Tudor Dana attended schools on our research subjects: the JINR Dubna school in Borovets, Bulgaria and at the 8^{th} European Summer School on Experimental Nuclear Astrophysics, St. Tecla, Italy. Sep. 13-20, 2015.

Physicist Tudor Dana has presented the last year experimental results on "Measurement of $^{13}C+^{12}C$ fusion cross section at deep sub-barrier energies in IFIN-HH" at the8^{th} European Summer School on Experimental Nuclear Astrophysics, St. Tecla, Italy. Sep. 13-20, 2015 (Young session).

5. Conclusions

From the above report and documents attached, we conclude, as we did a year ago, that the objectives for the latest year of this project were fulfilled in both spirit and letter. Some of the activities proposed over 3.5 years ago could not be done in their letter, due to the fact that they

are affected not only by local financial problems, but by external ones, like availability of beam time at large RNB facilities (RIBF at RIKEN, Japan and MARS at TAMU, USA), and possibly, by shifts in the short term tactics, while keeping the focus of the strategy of research: nuclear astrophysics in IFIN-HH. Many of the efforts are already bearing fruit and this shows in experimental setups available, in results and even in publications. Furthermore, the young members of the NAG group are building experience, are collaborating well with colleagues in DFN and IFIN-HH in general, and even attracting other students toward the group and its subjects.

References

[1] L. Trache – Project proposal, April 2012. File C Descrierea proiectului.pdf.

[2] Project PBN-II-ID-PCE-2012-4-0299, Raport de faza, Dec. 2014 (in English)

[3] L. Trache, D. Chesneanu and C.A. Ur (eds.), "Exotic Nuclei and Nuclear/Particle Astrophysics (V). From Nuclei to Stars", *Proceedings CSSP14*, , AIP Conf. Proc. Series, **vol. 1645**, New York, 2015.

[4] E. Pollacco, L. Trache et al., Nucl. Instr. Meth. Phys. Res. **A 723**, 102 (2013).

[5] D. Tudor, A. Chilug et al, Proc. of St. Tecla school, Eur. J. Phys, Conf. Series, 2016, in press

[6] N.T. Zhang, X.D. Tang, H. Chen, D. Chesneanu, M. Straticiuc, L. Trache, K.A. Li, Y.J. Li, D.G. Ghita, I. Burducea, R. Margineanu, A. Pantelica and C. Gomoiu - *Proc. of OMEG15*, in press.

[7] D. Chesneanu et al. in "Exotic Nuclei and Nuclear/Particle Astrophysics (V). From Nuclei to Stars", *Proceedings CSSP14*, L. Trache, D. Chesneanu and C.A. Ur (eds.), AIP Conf. Proc. Series, **1645**, 311 (2015).

[8] R. A .Dayras, R.G. Stokstad, Z. E. Switkowski and R. M .Wieland, Nucl. Phys. A 625, 152-188, 1976.

[9] P. M. Davies, A dissertation submitted to the Department of Physics at the University of Surrey, 2009.

[10] I. Burducea, M. Straticiuc, D.G. Ghita, D.V. Mosu, C.I. Calinescu, N.C. Podaru, D.J.W. Mous, I. Ursu, N.V. Zamfir, Nuclear Instruments and Methods in Physics Research B 359, 1219, 2015.

[11] L. Trache, A. Azhari, H. L. Clark, C. A. Gagliardi, Y.-W. Lui, A. M. Mukhamedzhanov, R. E. Tribble, F. Carstoiu Phys. Rev. C 61, 024612(2000).

[12] T. Al-Abdullah, F. Carstoiu, X. Chen, H. L. Clark, C. A. Gagliardi, Y.-W. Lui, A. Mukhamedzhanov, G. Tabacaru, Y. Tokimoto, L. Trache, R. E. Tribble, and Y. Zhai, Phys. Rev. C 89, 025809 (2014). “Astrophysical reaction rate for F17(*p*,*γ*)Ne18 from the transfer reaction C13(O17,O18)C12”.

[13] M. McCleskey, A. M. Mukhamedzhanov, L. Trache, R. E. Tribble, A. Banu, V. Eremenko, V. Z. Goldberg, Y.-W. Lui, E. McCleskey, B. T. Roeder, A. Spiridon, F. Carstoiu, V. Burjan, Z. Hons, and I. J. Thompson, Phys. Rev. C 89, 044605 (2014).

[14] T. Al-Abdullah, F. Carstoiu, C. A. Gagliardi, G. Tabacaru, L. Trache, and R. E. Tribble, Phys. Rev. C 89, 064602 (2014)

[15] F. Carstoiu, M. Lassaut, L. Trache and V. Balanica, “Heavy Ion Orbiting and Regge Poles (I)”, Romanian Journal of Physics, 2015, submitted.

[16] F. Carstoiu, M. Lassaut, L. Trache and V. Balanica, Heavy Ion Orbiting and Regge Poles (II)”, Romanian Journal of Physics, 2015, submitted.

Consideram ca obiectivele acestei faze au fost integral indeplinite.

Responsabil Proiect
Dr. Livius Trache

Responsabili Etapa
Dr. Livius Trache
Phys. Alexandra Chilug
Phys. Dana Tudor

Front Matter for Volume 1645

Citation: AIP Conference Proceedings **1645**, frontmatter (2015); doi: 10.1063/v1645.frontmatter
View online: http://dx.doi.org/10.1063/v1645.frontmatter
View Table of Contents: http://scitation.aip.org/content/aip/proceeding/aipcp/1645?ver=pdfcov
Published by the AIP Publishing

Volume 1645

Workshops and summer schools

Exotic Nuclei and Nuclear/ Particle Astrophysics (V). From Nuclei to Stars

Carpathian Summer School of Physics 2014

Sinaia, Romania
13–26 July 2014

Editors
Livius Trache, Daniela Chesneanu and Calin Alexandru Ur

AIP | Proceedings

proceedings.aip.org

ISBN 978-0-7354-1284-2
ISSN 0094-243X

AIP

EXOTIC NUCLEI AND NUCLEAR/PARTICLE ASTROPHYSICS (V). FROM NUCLEI TO STARS

Vol. 1645

Workshops and summer schools

Exotic Nuclei and Nuclear/Particle Astrophysics (V). From Nuclei to Stars

Carpathian Summer School of Physics 2014

Sinaia, Romania

13–26 July 2014

Editors

Livius Trache

Daniela Chesneanu

"Horia Hulubei" Institute for Physics and Nuclear Engineering, Bucharest-Magurele, Romania

Calin Alexandru Ur

"Horia Hulubei" Institute for Physics and Nuclear Engineering, Bucharest-Magurele, Romania

Extreme Light Infrastructure – Nuclear Physics, Bucharest-Magurele, Romania

All papers have been peer reviewed.

Sponsoring Organizations

Ministry of National Education

ATHENA network of ENSAR

Nuclear Astrophysics Virtual Institute

Endorsed by the European Physical Society

iGroup

CAEN

Canberra

AIP Publishing

Melville, New York, 2015

AIP Proceedings

Volume 1645

To learn more about AIP Proceedings visit **http://proceedings.aip.org**

Editors

Livius Trache
Daniela Chesneanu
"Horia Hulubei" Institute for Physics
and Nuclear Engineering
Str. Reactorului no. 30
P.O. Box MG-6
Bucharest-Magurele, Romania

E-mail: livius.trache@nipne.ro
chesneanu@nipne.ro

Calin Alexandru Ur
"Horia Hulubei" Institute for Physics
and Nuclear Engineering
Str. Reactorului no. 30
P.O. Box MG-6
Bucharest-Magurele, Romania

Extreme Light Infrastructure – Nuclear Physics
P.O. Box MG-6
Bucharest-Magurele, Romania

E-mail: calin.ur@eli-np.ro

ISBN 978-0-7354-1284-2
ISSN 0094-243X
Printed in the United States of America

AIP Conference Proceedings, Volume 1645
Exotic Nuclei and Nuclear/Particle Astrophysics (V). From Nuclei to Stars
Carpathian Summer School of Physics 2014

Table of Contents

Organized by

"Horia Hulubei" National Institute for Physics and Nuclear Engineering (IFIN-HH), Bucharest-Magurele, Romania and
Texas A&M University (TAMU), College Station, Texas, USA

Sponsored also by

Ministry of National Education, Bucharest, Romania
ATHENA network of ENSAR
Nuclear Astrophysics Virtual Institute, Germany (NAVI)
Endorsed by the European Physical Society
iGroup
CAEN
Canberra

International Advisory Committee:

M. Ahmed (Duke)
T. Aumann (Darmstadt)
F. Azaiez (Orsay)
C. Bertulani (Commerce, TX)
S. Bishop (Munich)
M. El Eid (Beirut)
F. Ferroni (Rome)
Z. Fulop (Debrecen)
F. Gulminelli (Caen)
M. Hass (Rehovot)
J. Jose (Barcelona)
T. Kajino (Tokyo)
K.-L. Kratz (Mainz)
K. Langanke (Darmstadt)
T. Motobayashi (Tokyo)
N. Pietralla (Darmstadt)
Zs. Podolyak (Surrey)
H. Rebel (Karlsruhe)
W. Sandner (Berlin)
H. Schatz (East Lansing)
A. Smirnov (Trieste)
B. Sherrill (East Lansing)
O. Sorlin (Caen)
C. Spitaleri (Catania)
T. Tajima (Irvine)
M. Wiescher (Notre Dame)
N. V. Zamfir (Bucharest)

Organizing Committee:

Livius Trache *and* Robert Tribble*: chairs*
Daniela Chesneanu *and* Calin Alexandru Ur*: scientific secretaries*
Dan Cozma, Nicu Marginean *and* Denis Stanca (IFIN-HH), Gabriel Tabacaru, Antti Saastamoinen *and* Alexandra Spiridon (TAMU): *members*

Technical Secretariat:

Alexandra Olteanu – financial director
Denisa Cranganu

LIST OF SUMMER SCHOOLS OF PHYSICS HELD IN THE CARPATHIANS*

Along the times, different names were used for the summer schools of physics organized in the Carpathians: Predeal International SSP, Brasov SSP and Carpathian SSP. Here, to the best of our current knowledge, the history of these schools, including the names of the organizers and the published Proceedings:

1964 - According to oral tradition: a session organized by IFA where V.G. Soloviev (JINR Dubna, USSR) attended as sole foreign lecturer.

There is a large gap here in our memory …

1974 - *Proceedings of the International School on Nulcear Physics - Predeal, Romania, September 1974*, editor: A. Ciocanel et al. Editura Academiei RSR, Bucharest, Romania, 1976. 446 pp.

1976 - *"Heavy Ion Physics" Predeal International Summer School - Predeal, Romania, Sep. 1976*, editors: Valentin Ceausescu, I. A. Dorobantu. Central Institute of Physics Publ., Bucharest, Romania, 1977. 589 pp.

1978 - *"Heavy Ion Physics" Proceedings - Predeal International School 1978,* editors: A. Berinde, V. Ceausescu, I.A. Dorobantu. Central Institute of Physics Publ., Bucharest, Romania, 1978. 1219 pp.

1979. *"Recent Advances in Statistical Mechanics" Proceedings - Brasov International School, Aug. – Sep. 1979*, editor: A. Corciovei, Central Institute of Physics Publ., Bucharest, Romania, 1980.

1980 – *"Critical Phenomena In Heavy Ion Physics", Brasov International School, 1980*. Organizing Committee: directors: M. Petrascu, A.A. Raduta, scientific secretaries: G. Stratan, V. Zoran. *Proceedings* - Central Institute Of Physics Publ., Bucharest, Romania, 1982. 1124 pp.

1981 - *"Gauge Theories: Fundamental Interactions and Rigorous Results" Proceedings - International Summer School of Theoretical Physics Poiana Brasov, Romania "*. Organizers: V Ceausescu, G. Costache and V. Georgescu. Editors: P. Dita, V. Georgescu and R. Purice, published in "Progress in Physics", vol 5, "Critical Phenomena", Basel, Stuttgart: Boston Birkhauser, 1982. ISBN 3-7643-3095-3.

1982 – *"Nuclear Collective Dynamics" - Lectures of the 1982 International Summer School Of Nuclear Physics Poiana Brasov, Romania, 26 August - 7 September 1982,* editors: D. Bucurescu, V. Ceausescu, N.V. Zamfir, World Scientific Publishing, Singapore, 1983.

1983 - *"Critical Phenomena" – Proceedings of the Brasov School Conference.* Organizers: V Ceausescu, G. Costache and V. Georgescu. Editors: V. Ceausescu, G. Costache and V. Georgescu published in "Progress in Physics", vol 11, "Critical Phenomena", Basel, Stuttgart: Birkhauser Boston, 438 pp, 1985. ISBN 3-7643-3289-1.

1984 - *"Atomic and Nuclear Heavy Ion Interactions" - proceedings of the 15th Course of the Brasov International School in Physics, Poiana Brasov, Romania, August 28 - September 8, 1984.*

First Part: *"Atomic Physics"*, editors: Al Berinde, I.A. Dorobantu, V. Zoran , Central Institute of Physics Publ., Bucharest, Romania, 1986. 482 pp.

Second Part: *"Nuclear Physics"*, editors: G. Semenescu, I.A. Dorobantu, N.V. Zamfir. Central Institute of Physics Publ., Bucharest, Romania, 1986. 761 pp.

1986 - Poiana Brasov International Summer School of Physics.
"Symmetries and Semiclassical Features of Nuclear Dynamics". Invited Lectures of the 1986 International Summer School Held at Poiana Brasov, Romania, September 1-13, 1986. Series: Lecture Notes in Physics, Vol. 279, Raduta, A.A. (Ed.), Springer Verlag, Berlin, 1987. ISBN 978-3-540-17926-9.

1988 - *"Recent Advances In Nuclear Physics" - Lectures of the 1988 International Summer School Of Nuclear Physics, August 30th - September 9th, 1988, Poiana Brasov, Romania*, editors: M. Petrovici, N.V. Zamfir, World Scientific, Singapore, 1989. 537 pp.

1990 –*"Nuclear Structure Recent Advances In Nuclear Structure" – Proceedings - Predeal, Romania, August 28th - September 8th 1990*, editors: D. Bucurescu, G. Cata-Danil, N.V. Zamfir, World Scientific, Singapore, 1991. 514 pp.

1991 - "New Trends in Theoretical and Experimental Nuclear Physics" – Proceedings - Predeal International Summer School of Physics, Predeal, Romania, Aug 26th – Sep 7th 1991, editors: A.A. Raduta, D.S. Delion, I.I. Ursu, World Scientific, Singapore, New Jersey, London, Hong Kong, 1992. ISBN 981-02-0906-1C

1992 - Predeal International summer school of physics, NATO Advanced Study Institute, Org: V. Zoran, A Calboreanu., L. Trache, V. Florescu.
"Topics in Atomic and Nuclear Collisions" Proceedings of a NATO ASI held in Predeal, Romania, August 31-September 11, 1992. Series: Nato Science Series B, Vol. 321 Remaud, B.; Calboreanu, A.; Zoran, V. (Eds.), Springer Verl., Berlin, 1994, 478pp. ISBN 978-0-306-44662-7

1995 – *"Collective Motion And Nuclear Dynamics" – Proceedings - Predeal International Summer School, August 28th - September 9th , 1995, Predeal, Romania*,

editors: A.A.Raduta, D. Bucurescu, D.S.Delion, I.I. Ursu. World Scientific, Singapore, 1996. 571 pp. ISBN 98102252882.

1998 Predeal International Summer School.
"Structure and Stability of Nucleon and Nuclear Systems". Proceedings of Predeal International Summer School, Predeal, Romania. AA Raduta, II Ursu and S Stoica (eds.), World Scientific, Singapore, 1999. ISNB-10: 981023774X.

2000 - *Predeal International Summer School of Physics: "Nuclei far from stability and Astrophysics"*. Organizers: DN Poenaru and H. Rebel, directors. 28.08- 08.09 2000. Proc of NATO Advanced Study Institute on "Nuclei Far from Stability and Astrophysics", eds. DN Poenaru, H. Rebel and J. Wentz. NATO Science series, II Mathematics, Physics and Chemistry, vol. 17. Kluwer Academic Publishers, Dordrecht, Boston, London, 2001.

2005 – *"Exotic Nuclei and Nuclear/Particle Astrophysics" – Proceedings - Carpathian Summer School of Physics 2005, Mamaia-Constanta, Romania, June 13th – June 24th , 2005*, editors: S. Stoica, L. Trache and R. Tribble, New Jersey: World Scientific Publishing Co. Pte. Ltd., 484 pp, 2006. ISBN 981-270-007-2

2006 – *"Collective Motion And Phase Transitions In Nuclear Systems" - Proceedings - The Predeal International Summer School In Nuclear Physics, Predeal, Romania August 28th - September 9th , 2006*, Editors: A.A. Raduta; V. Baran; A.C. Gheorghe; I. Ursu , World Scientific Publ., Singapore, 2007. 672 pp. ISBN 9789812700834

2007 – *"Exotic Nuclei and Nuclear/Particle Astrophysics (II)" – Proceedings: The Carpathian Summer School of Physics 2007, Sinaia, Romania, August 20th – 31st , 2007*, editors: L. Trache and S. Stoica. American Institute of Physics (AIP), Conference Proceedings, vol. 972, Melville, New York, 2008. 617pp. ISBN 978-0-7354-0490-8, ISSN 0094-243X.

2010 – *"Exotic Nuclei and Nuclear/Particle Astrophysics (III) – From Nuclei to Stars" Proceedings - Carpathian Summer School of Physics 2010, Sinaia, Romania, June 20th – July 3rd, 2010.* Editors: L. Trache, S. Stoica and A. Smirnov; American Institute of Physics (AIP), Conference Proceedings, vol. 1304, Melville, New York, 2010. ISBN 978-0-7354-0859-3, ISSN 0094-243X.

2012 – *"Exotic Nuclei and Nuclear/Particle Astrophysics (IV) – From Nuclei to Stars" Proceedings - Carpathian Summer School of Physics 2012, Sinaia, Romania, June 20th – July 3rd, 2012.* Editors: Livius Trache and Paula Gina Isar; American Institute of Physics (AIP), Conference Proceedings, vol. 1498, Melville, New York, 2012. ISBN 978-0-7354-1112-8, ISSN 0094-243X.

2014 – *"Exotic Nuclei and Nuclear/Particle Astrophysics (V) – From Nuclei to Stars" Proceedings - Carpathian Summer School of Physics 2014, Sinaia, Romania, July 13th – 26th, 2014.* Editors: Livius Trache, Daniela Chesneanu and Calin Alexandru Ur; American Institute of Physics (AIP), Conference Proceedings, Melville, New York, to be published.

This list was compiled by Livius Trache with assistance from Ion I. Ursu, Denise Cranganu and Adriana Mihai. If you have any suggestions, or further information, please write at dir.sci@nipne.ro. Thanks!

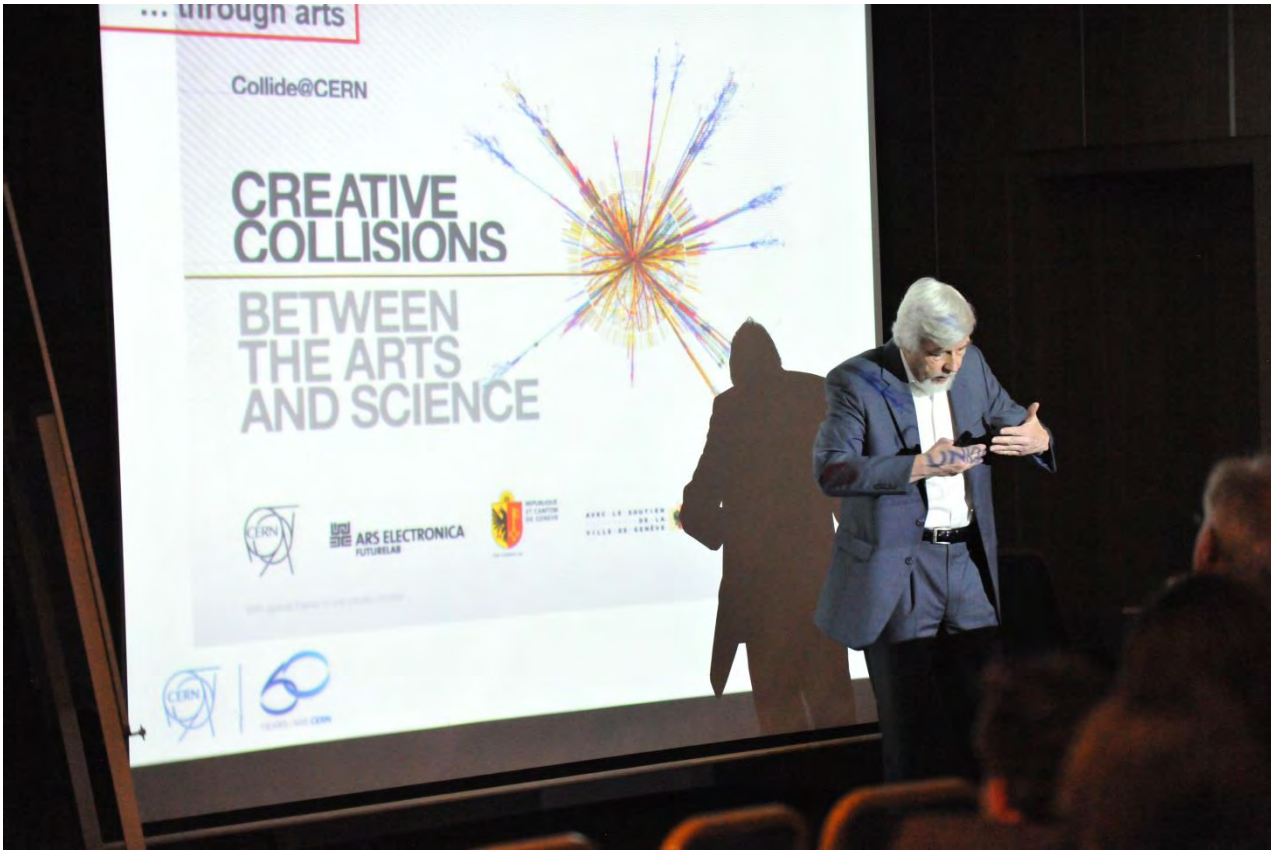

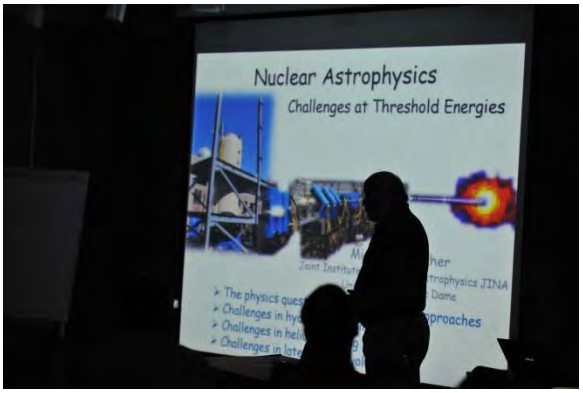

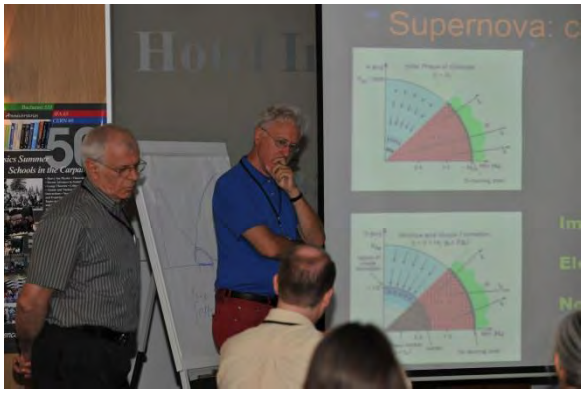

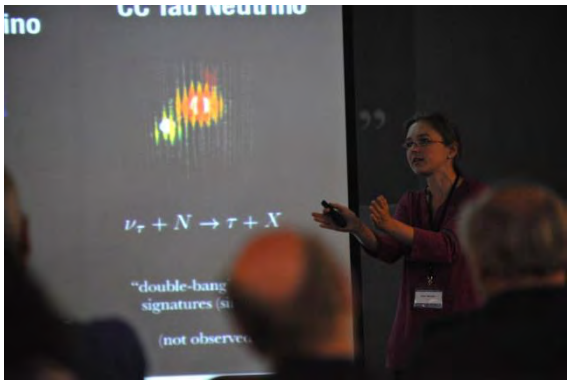

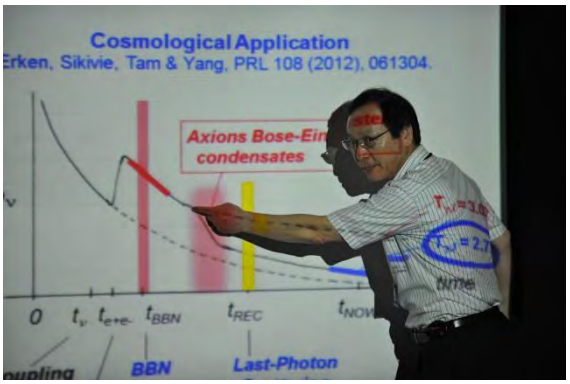







Carpathian Summer School of Physics 2014

Conference Program

Sunday, July 13th , 2014	16.00-Registration of participants 20.00- Welcome Party

Monday, July 14th, 2014	
Introduction (I) **Chair: Livius Trache**	
9:00 - 9:15	Opening
9:15 - 9:55	*C. Bertulani (I)*: Quasi–Free Scattering and Knockout Reactions with Rare Isotopes
9:55 - 10:50	*M.C. Wiescher (I)*: Nuclear Astrophysics – Challenges at Threshold Energies
10:50 - 11:10	Coffee break
11:10 - 12:00	*K. Langanke (I)*: Core collapse supernovae - from the view of a nuclear theorist
12:00 - 12:50	*B.S. Meyer (I)*: Synthesis of Radioactive Nuclei and Secondary Supernova Machine
13:00 - 15:00	Lunch
Afternoon Session **Chair: Karlheinz Langanke**	
15:00 - 15:50	*R. Diehl*: Gamma Ray Astronomy: Lessons from cosmic radioactive nuclei
15:50 - 16:10	Coffee break
16:10 - 17:05	*J. Lattimer (I)*: Introduction to Neutron stars I
17:05 - 18:00	*I. Mocioiu*: News about nus
18:00 - 18:15	*M. Karus*: Calibration of Photo Sensors for the Space–Based Cosmic Ray Telescope JEM–EUS
18:15 - 18:30	*M. Holl*: Quasi–Free Scattering from Relativistic Neutron–Deficient Carbon
18:30 - 18:45	*A. Slemer*: Advanced Stellar Evolution and Related Nuleosynthesis

Tuesday, July 15th, 2014	
Introduction (II) **Chair: Carlos Bertulani**	
9:00 - 9:55	*K-L Kratz (I)*: Astrophysical, observational and nuclear-structure aspects of r-process nucleosynthesis
9:55 - 10:50	*M.C. Wiescher (II)*: Nuclear Astrophysics – challenges at threshold energies
10:50 - 11:10	Coffee break
11:10 - 12:00	*T. Kajino*: Big-Bang and Supernova Neutrinos and Nucleosynthesis
12:00 - 12:50	*B.S. Meyer (II)*: Synthesis of Radioactive Nuclei and Secondary Supernova Machine
13:00 - 15:00	Lunch
Afternoon Session **Chair: Dan Cozma**	
15:00 - 15:50	*K. Langanke (II)*: Core collapse supernovae- from the view of a nuclear theorist
15:50 - 16:10	Coffee break
16:10 - 17:05	*J. Lattimer (II)*: Introduction to Neutron Stars II
17:05 - 18:00	*C. Bertulani (II)*: Two-photon and photonuclear collisions at the Large Hadron Collider at

	CERN
18:00 - 18:15	*A. Saastamoinen*: Study of excited states of ^{35}Ar through β-decay of ^{35}K for nucleosynthesis in novae and X-ray bursts
18:15 - 18:30	*L. Tartaglia* : Interacting supernovae and supernova impostors: evidence of incoming SN explosions?
18:30 - 18:45	*I. Gheorghe*: Absolute photoneutron cross sections of Sm isotopes
18:45 - 19:00	*R. Lica*: Properties of low-lying intruder states in ^{34}Al and ^{34}Si from the beta-decay of ^{34}Mg

Wednesday, July 16th, 2014	
EOS and compact stars **Chair: James M. Lattimer**	
9:00 - 9:55	*F. Gulminelli*: Sub-saturation equation of state for Core-Collapse Supernovae and Neutron Stars
9:55 - 10:50	*A. Fantina*: Neutron-star matter within the energy-density functional theory and neutron-star structure
10:50 - 11:10	Coffee break
11:10 - 12:00	*C. Providência*: The symetry energy: the inner crust and strangeness of neutron stars
12:00 - 12:50	*T. Aumann*: The dipole response and neutron-skin of nuclei and the symmetry energy
13:00 - 15:00	Lunch
Afternoon Session **Chair: Francesca Gulminelli**	
15:00 - 15:50	*I. Vidana*: Hyperons and Neutrons Stars
15:50 - 16:10	Coffee break
16:10 - 17:05	*Ad. Raduta*: Strangeness driven phase transitions in compressed baryonic matter and their relevance for neutron stars and core collapsing supernovae
17:05 - 18:00	*I. Sagert*: Quark matter in compact stars
18:00 - 18:15	*S. Antic*: Relativistic mean-field model with energy dependent self-energies
18:15 - 18:30	*T. Aymard*: Sub-saturation matter in Compact Stars : nuclear modelling in the framework of the Extended Thomas-Fermi theory
18:30 – 18:45	*A. Horvat*: Collective Excitations in Nuclei Away from the Valley of Stability

Thursday, July 17th, 2014	
ELI-NP session **Chair: Nicolae Victor Zamfir**	
9:00 - 9:55	*N.V. Zamfir*: Extreme Light Infrastructure – Nuclear Physics (ELI-NP) Status and Perspectives
9:55 - 10:50	*S. Gales*: Nuclear Science and Applications with next generation of High Power Lasers and Brilliant Low Energy Gamma Beams at ELI-NP
10:50 - 11:10	Coffee break
11:10 - 12:00	*D.L. Balabanski*: Nuclear Physics Experiments at the ELI-NP Facility
12:00 - 12:50	*C.A. Ur*: Gamma Beam System at ELI-NP
13:00 - 15:00	Lunch
Afternoon Session **Chair: Calin A. Ur**	
15:00 - 15:50	*M. Gai*: Physics with Gamma-Beams and Charged Particle Detectors: I Nuclear Structure

15:50 - 16:10	Coffee break
16:10 - 17:05	*M. Gai*: Physics with Gamma-Beams and Charged Particle Detectors: II Nuclear Astrophysics
17:05 - 18:00	*M. Zweidinger*: Contemporary Research with Nuclear Resonance Fluorescence at the S-DALINAC
18:00 - 18:30	*D. Filipescu*: Geant4 simulations on Compton scattering of laser photons on relativistic electrons

Friday, July 18th, 2014	
ELI-NP session **Chair: Sydney Gales**	
9:00 - 9:55	*G. Mourou*: Zepto-Physics at ELI-NP
9:55 - 10:50	*R. Dabu*: Ultrahigh intensity lasers based on chirped pulse amplification technique
10:50 - 11:10	Coffee break
11:10 - 12:00	*R. Dabu*: High Power femtosecond lasers at ELI-NP
12:00 - 12:50	*P.G. Thirolf*: From laser particle acceleration to the synthesis of the extremely neutron rich isotopes via the novel fission-fusion mechanism
13:00 - 14:30	Lunch
Afternoon Session **Chair: Dimiter Balabanski**	
14:30 - 15:20	*P.G. Thirolf*: From laser particle acceleration to the synthesis of the extremely neutron rich isotopes via the novel fission-fusion mechanism
15:20 - 15:50	*E. Turcu*: High Field QED Experiments with ELI-NP 2x10PW Laser
15:50 - 16:10	Coffee break
16:10 - 17:05	*V. Baran*: Mass and Isospin Dependence of the Dipole Response in a Microscopic Transport Model Approach
17:05 - 18:00	*A. Bonasera*: Nuclear Physics Using Lasers
18:00-18:55	*F. Negoita*: Perspectives for neutron and gamma spectroscopy in high power laser driven experiments at ELI-NP

Saturday, July 19th, 2014	
Outreach day **Chair: Michael Wiescher**	
9:00 - 9:55	*A. Haungs (I)*: At the Doorway to Astroparticle Astronomy
9:55 – 10:50	*S. Bishop*: Search for Supernova-produced ^{60}Fe in the Earths Fossil Record
10:50 - 11:10	Coffee break
11:10 - 12:00	*R. Egli*: From supernova to terrestrial dirt: a journey between astrophysics, biology and geophysics
12:00 - 12:30	*K-L Kratz (II)*: Astrophysical, observational and nuclear-structure aspects of r-process nucleosynthesis
12:30 - 13:30	Lunch
13:30 **Round table: CERN at 60.** **And the internationalization of science**	
15:50 - 16:10	Coffee break
16:10 - 17:05	**Round table: continued**
19:00 on	**BANQUET**

Sunday July 20– Excursions: Hiking and bus trip choice; start at 9am

Monday, July 21st, 2014	
Astroparticles **Chair: Marilena Avrigeanu**	
9:00 - 9:50	*A. Haungs (II)*: The Pierre Auger Observatory: highlights and future prospects
10:00 - 10:50	*I. Brâncuş*: Cosmic Muons as Messengers from the Universe
10:50 - 11:10	Coffee break
11:10 - 12:00	*O.Sima*: The KASCADE-Grande Experiment
12:00 - 12:50	*B.Mitrică*: New cosmic rays experiments in the underground laboratory of IFIN-HH from Slănic Prahova, Romania
13:00 - 15:00	Lunch
Exotic decays **Chair: Octavian Sima**	
15:00 - 15:50	*M.Pfutzner*: Charge-particle spectroscopy with the Optical TPC
15:50 - 16:10	Coffee break
16:10 - 17:05	*M.Horoi*: Search for physics beyond the Standard Model in double-beta decay
17:05 - 18:00	*L.V.Grigorenko*: Few-body dynamics on the driplnes
18:00 - 18:15	*N.Arsene*: X^{μ}_{max} vs. N_{μ} from Extensive Air Showers as estimator for the mass of primary UHECR's. Application for the Pierre Auger Observatory
18:15 - 18:30	*A.Gherghel-Lascu*: Refined Lateral Energy Correction Functions for the KASCADE-GRANDE Experiment Based on GEANT4 Simulations
18:30 - 18:45	*M.Niculescu*: Underground cosmic muon detector based on SiPM , optic fibers and plastic scintillators
18:45-19:00	*C.Costache*: RDDS lifetime measurements using the ROSPHERE spectrometer: The case of ^{119}Te

Tuesday, July 22nd, 2014	
Nuclear Reactions **Chair: Thoru Motobayashi**	
9:00 – 9:50	*A.Bonaccorso*: Knockout beyond the dripline
10:00 - 10:50	*T.Uesaka*: Mass measuremen tof r-process nuclei at RIBF
10:50 11:10	Coffee break
11:10 - 12:00	*F.Camera (I)*: New scintillator materials for future and present facilities
2:00 - 12:50	*V.Iacob*: From estimates of the order of magnitude to precise measurements: The superallowed beta decays
13:00 - 15:00	Lunch
Exotic Nuclei **Chair: Vladilen Goldberg**	
15:00 - 15:50	*F.Camera (II)*: New scintillator materials for future and present facilities
15:50 - 16:10	Coffe break
16:10 - 17:05	*F.Carstoiu*: Peripheral reactions with ^{17,18}O at 12MeV/nucleon *M. Avrigeanu*: On reaction mechanism involved in the deuteron-induced surrogate reactions on actinides
17:05 - 17:20	*D.Chesneanu*: Investigating ^{12}C+^{13}C reaction using high resolution gamma ray spectroscopy
17:20 - 17:35	*N.Veselinovic*: CR muon flux measurements at Belgrade shallow underground laboratory

17:35 – 17:50	*O.Sgouros*: Elastic scattering of the system ^{7}Be+^{28}Si at 17.2MeV
18:00 - 18:15	*V.Soukeras*: Elastic scattering of the system ^{6}Li + p at near barrier energies with MAGNEX
18:15 – 18:30	*A.Caruso*: ^{18}F + p at astrophysical energies
18:30 – 18:45	*I.Harca*: Investigation of shell effects in fusion-fission and quasifission processes in the reaction ^{34}S + ^{186}W

Wednesday, July 23rd, 2014	
Morning Session **Chair: Vlad Avrigeanu**	
9:00 - 9:55	*T. Motobayashi*: Nuclear astrophysics studies at RIKEN RIBF
10:00 - 10:50	*A.Parikh*: Important and significant: lies the experimentalist told me
10:50 - 11:10	Coffee break
11:10 - 12:00	*A. Petrovici*: Isospin-symetry-breaking effects in A~70 nuclei within beyond-mean-field approach
12:00 12:50	*M. Petrovici*: Recent results and open questions on collective type phenomena from A+A to p+p collisions
13:00 - 15:00	Lunch
Free afternoon	

Thursday, July 24th, 2014	
Nuclear astrophysics **Chair: Claudio Spitalieri**	
9:00 - 9:50	*M.El Eid*: Heavy Element Synthesis in the Early Galaxy
10:00 - 10:50	*P.Woods*: Measurements for Explosive Nuclear Astrophysics
10:50 - 11:10	Coffee break
11:10 - 12:00	*C.Lederer*: Neutron induced reactions in Nuclear Astrophysics
12:00 - 12:50	*V. Avrigeanu*: Enhanced α-particle optical model potential at low energies for the mass range A~40-209
13:00 - 15:00	Lunch
Afternoon Session: **Chair: Vlad Avrigeanu**	
15:00 - 15:50	*V.Goldberg*: Recently developed approaches to calculate nuclear structure need tests by novel experimental methods
15:50 - 16:10	Coffee break
16:10 – 16:25	*J.S. Bihalowicz*: 3D reconstruction of nuclear reaction using GEM TPC with planar readout
16:25 - 16:40	*B.Chesca*: Ultra-sensitive superconducting detectors of the radiative decay of cosmic background neutrinos
16:40-16:55	*A.Cvetinovic*: Large electron screening effect in ^{1}H(^{7}Li,α)^{4}He and ^{2}H(^{19}F,n)^{20}Ne reactions in different environments
17:05-17:20	*G.M. Halabi*: Effect of ^{12}C+^{12}C Fusion Reaction & Convective Mixing on the Progenitor Mass of ONe White Dwarfs
17:20-17:35	*S.Shibagaki*: Roles of Fission, Neutron Star Mergers and Supernovae in R-Process Nucleosynthesis
17:35-17:50	*S. Balascuta*: The conceptual design of the Electron Spectrometer for the High Field Physics experiments at ELI-NP

17:50-18:05	*S.Sanfillipo*: β-delayed α-decay of ^{16}N and the ^{12}C(α,γ)^{16}O cross-section at astrophysical energies
18:05-18:20	*P.R.Chowdhury*: The Equation of State for Nuclear Matter at Extreme and Compact Star Properties

Friday, July 25th, 2014	
Morning Session **Chair: Mounib El Eid**	
9:00 - 9:50	*C.Spitalieri(I)*: Nuclear Astrophysics with the Trojan Horse Method
10:00 - 10:50	*C.Spitaleri(II)*: Nuclear Astrophysics with the Trojan Horse Method
10:50 - 11:10	Coffee break
11:10 - 12:00	*L.Lamia*: Light elements burning reaction rates at stellar temperatures as deduced by the Trojan Horse measurements
12:00 - 12:50	*A.Best*: LUNA: Underground nuclear astrophysics
13:00 - 15:00	Lunch
Afternoon Session **Chair: Livius Trache**	
15:00 -15:15	*S.Puglia*: Study of the ^{10}B(p,α)^{7}Be reaction through the Trojan Horse Method
15:15-15:30	*M.L. Sergi*: Recent THM determination of the 65 keV resonance strength intervening in the ^{17}O(p,α)^{14}N reaction rate
15:30-15:45	*S.Palmerini*: The RGB and AGB star nucleosynthesis in the light of the recent ^{18}O(p,α)^{15}N and ^{17}O(p,α)^{14}N reaction rate determinations
15:45 - 16:10	Coffee break
16:10-16:25	*C.Oancea*: Reducing the Uncertainties in Particle Therapy
16:25-16:40	*N.Kahledi*: Production and dosimetry of simultaneous therapeutic photons and electrons beam by linear accelerator: a monte carlo study
16:40-16:55	*P.Isar*: Space-atmospheric interactions of ultra-high energy cosmic rays
17:05 - 18:00	Closing

Saturday, July 26th , 2014	9.00 - Departure

Investigating 13 C + 12 C reaction by the activation method. Sensitivity tests

Daniela Chesneanu, L. Trache, R. Margineanu, A. Pantelica, D. Ghita, M. Straticiuc, I. Burducea, A. M. Blebea-Apostu, C. M. Gomoiu, and X. Tang

Citation: AIP Conference Proceedings **1645**, 311 (2015); doi: 10.1063/1.4909592
View online: http://dx.doi.org/10.1063/1.4909592
View Table of Contents: http://scitation.aip.org/content/aip/proceeding/aipcp/1645?ver=pdfcov
Published by the AIP Publishing

Investigating $^{13}C+^{12}C$ Reaction by the Activation Method. Sensitivity Tests

D. Chesneanu[a)], L. Trache, R. Margineanu, A. Pantelica, D. Ghita, M. Straticiuc,

I. Burducea, A.M. Blebea-Apostu, C.M. Gomoiu

[1]*Horia Hulubei National Institute for Physics and Nuclear Engineering, P.O. Box MG-6, 077125 Bucharest-Magurele, Romania*

X. Tang

[2]*Institute of Modern Physics, CAS, 509 NANCHANH ROAD, LANZHOU, GANSU, 730000, China.*

[a)] Corresponding author: chesneanu@nipne.ro

Abstract. We have performed experiments to check the limits of sensitivity of the activation method using the new 3 MV Tandetron accelerator and the low and ultra-low background laboratories of the "Horia Hulubei" National Institute of Physics and Nuclear Engineering (IFIN-HH). We have used the $^{12}C+^{13}C$ reaction at beam energies E_{lab}= 6, 7 and 8 MeV. The knowledge of this fusion cross section at deep sub-barrier energies is of interest for astrophysical applications, as it provides an upper limit for the fusion cross section of $^{12}C+^{12}C$ over a wide energy range. A ^{13}C beam with intensities 0.5-2 particleμA was provided by the accelerator and used to bombard graphite targets, resulting in activation with ^{24}Na from the $^{12}C(^{13}C,p)$ reaction. The 1369 and 2754 keV gamma-rays from ^{24}Na de-activation were clearly observed in the spectra obtained in two different laboratories used for measurements at low and ultralow background: one at the surface and one located underground in the Unirea salt mine from Slanic Prahova, Romania. In the underground laboratory, for E_{lab} = 6 MeV we have measured an activity of 0.085 ± 0.011 Bq, corresponding to cross sections of 1-3 nb. This demonstrates that it is possible to measure ^{12}C targets irradiated at lower energies for at least 10 times lower cross sections than before. β–γ coincidences will lead us another factor of 10 lower, proving that this installations can be successfully used for nuclear astrophysics measurements.

INTRODUCTION

With the final goal of establishing a solid line of research in nuclear astrophysics (NA) at the Bucharest accelerators and laboratories of IFIN-HH, we have performed experiments to check the limits of one method that seems appropriate and for which the institute has or could acquire installations: the activation method. We used for irradiation one of the new tandem accelerators which can provide good intensities for light ions and the low and ultralow background laboratories, situated above ground and underground, respectively, for activation measurements. We have chosen the $^{13}C+^{12}C$ reaction, which leads to an activation appropriate for our tests: ^{24}Na, with a half-life of 15.0 hours, formed by one proton evaporation.

Nuclear astrophysics, or more precisely nuclear physics for astrophysics, is becoming more and more an explicit motivation for nuclear physics research, for European laboratories programs, in the USA, Japan and China, but also for the ones from Romania: through direct measurements (at low energies as in stars) or indirect methods (at the most common energies in nuclear physics laboratories). Direct measurements are very difficult because of the low cross sections involved and require dedicated facilities: proton or alpha particle accelerators of very high intensities at low energies and, if possible, low background and special detection systems. Such a facility did not exist in Romania and therefore, direct measurements were not made in Romania. The use of indirect methods involve typically radioactive beams, which were also not available locally. We wanted to prove that we can do direct measurements now, using newly available installations [1,2].

Exotic Nuclei and Nuclear/Particle Astrophysics (V). From Nuclei to Stars
AIP Conf. Proc. 1645, 311-316 (2015); doi: 10.1063/1.4909592

The reaction $^{12}C + ^{12}C$ in the low energy region is of great interest in astrophysics (see eg [3].) because of its essential role in studying a wide range of burning scenarios in carbon-rich stellar environments. It is important for understanding carbon burning nucleosynthesis that occurs in stars with more than 10 solar masses during late evolutionary periods [4], in intermediate mass stars (8-10 solar masses), which can lead a detonation wave and a supernova explosion [5], in binary systems, where a massive carbon-oxygen white dwarf exceeds the Chandrasekhar mass limit accumulating material from its partner star. The temperatures at which the carbon burnout occurs are found in the range of 0.5-1.2 GK corresponding to the center-of-mass energy range of 1 to 3 MeV. To verify all these scenarios and put constraints on models requires a detailed knowledge of the carbon fusion processes at these energies. Considerable efforts have been made to measure the cross section of $^{12}C + ^{12}C$ reaction at astrophysical energies, involving both the detection of charged particles and gamma-ray spectroscopy. However, previous measurements were made for $E_{c.m} \geq 2.1$ MeV, the upper region of astrophysical interest. Also, as $E_{c.m} = 3.0$ MeV cross sections reported are not consistent and are quite uncertain [6-8]. Moreover, the extrapolation procedure in the case of $^{12}C + ^{12}C$ from current experimental data at ultra-low energies is complicated by the presence of possible resonant structures even in the low energy excitation function. Measurements that could extend to below $E_{c.m} = 2.1$ MeV would be extremely important. It was found, however, that the $^{13}C + ^{12}C$ and $^{13}C + ^{13}C$ reactions do not have such resonances and provide material for understanding fusion at low energies, and ways to determine the maximum cross section for the reaction $^{12}C + ^{12}C$.

A University of Notre Dame group [9] has proposed a $^{13}C + ^{12}C$ experiment in collaboration with us and a group of Lanzhou, China at 3 MV Tandem from IFIN-HH. It is the motivation for our choice of measurements here: irradiations with a ^{13}C beam followed by measurement of activities at both surface and underground laboratory characterized by an ultra-low background radiation.

EXPERIMENTAL METHODS FOR INVESTIGATION OF THE $^{12}C + ^{13}C$ REACTION BY THE ACTIVATION METHOD

The *HVEE Tandetron 3 MV electrostatic accelerator* - recently installed at IFIN-HH is dedicated to:

1) Ion Beam Analysis (IBA) - analytical techniques that use accelerated ion beams: Rutherford backscattering spectrometry (RBS), X-ray emission induced by charged particles (PIXE), nuclear reaction analysis (NRA), etc.

2) Testing the radiation resistance of the materials or implants.

3) Nuclear astrophysics.

For nuclear astrophysics we assess that this facility is suitable for direct measurements of cross sections induced by α particles (He-burning) and light ions (^{6}Li, ^{12}C, ^{13}C, ^{16}O ...), due to relatively low energies and high intensities and its stable functioning, as tested by us last year.

The *GammaSpec laboratory* is an above ground installation in IFIN-HH main campus, in the same location as the tandem accelerators, consisting of a HpGe detector very well shielded, and carefully calibrated with sources and international inter-laboratory comparisons [10, 11].

The *Underground Laboratory in the Unirea salt mine, Slanic Prahova (MicroBequerel or "μBq")*, is located in a salt mine, about 2 hours drive North of Bucharest. Environmental conditions in the salt mine are very stable year round: temperature between 12 and 13° C, humidity 67-70% approximately, area of ~70,000 m^2, height between 52 and 57 m, depth is 208 m below ground (approximately 600 m.w.e), the distance between the walls is between 32 and 36 m, volume is 2.9×10^6 m^3 [12]. In this mine a laboratory was built to perform measurements using gamma-ray spectrometry in ultralow radiation background. The average dose underground was found 1.29 ± 0.30 nSv/h, approximately 70-80 times lower than the dose at the surface. As ambient background radiation comes from: i) natural radioactivity (especially from the decay of ^{238}U, ^{232}Th and ^{222}Rn present in the atmosphere and ^{40}K); ii) cosmic rays (μ, ^{1}H, ^{3}H; ^{7}Be, ^{14}C ...); and iii) neutrons from (α, n) reactions and fission, the i) and iii) sources are particularly low in this mine due to its thick and compact salt walls. Figure 1 compares γ-ray spectra measured above ground and underground. The top spectrum shows that the strongest component of the γ rays spectrum at $E\gamma<3$MeV is associated with the natural environment radioactivity and exhibits intense characteristic lines. At higher energies, the background radiation originates mostly from cosmic rays. The natural radioactivity is significantly reduced for measurements in the underground laboratory (bottom spectrum). From Fig. 1 it can be seen that the measured background radiation (using a protection shield consisting of 15 cm Pb and 5 cm Cu produced by Canberra Ind.) is about 4000 times smaller compared to the background spectrum measured at the surface. This is the major advantage we want to test and use in the current measurements [13, 14].

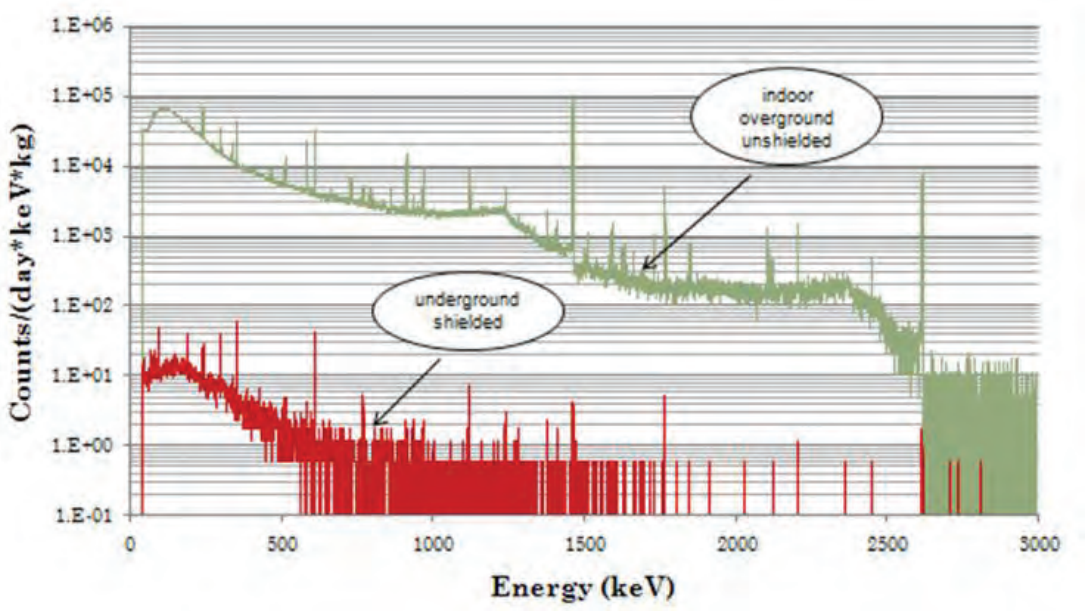

FIGURE 1. Typical spectrum of γ rays measured at the Earth's surface and underground

EXPERIMENTAL RESULTS

In this experimental phase we studied $^{12}C + {}^{13}C$ fusion reaction in the laboratory energy range of 6 to 8 MeV. A $^{13}C^{+3}$ beam with intensity 0.5 μA, at the first irradiation (E_{lab}=8 MeV), and 1.9 μA, for the irradiations at energies E_{lab}= 6 and 7 MeV, provided by the 3 MV Tandetron accelerator, impinged on a 1 mm thick natural carbon (graphite) target. A gas stripper system was used to increase the intensity of the $^{13}C^{+3}$ charge state.

Cross section of the $^{12}C(^{13}C, p)\ ^{24}Na$ reaction can be determined by measuring the γ radiation corresponding to nucleus ^{24}Na ($T_{1/2}$ = 15.00 h), using the activation method. The irradiated carbon targets were measured in the GammaSpec laboratory and in the underground laboratory. The cascading γ rays (1369 and 2754 keV) were detected with germanium detectors. The detection systems have been protected with lead castles to reduce ambient background radiation. The first case studied was a C target irradiated for 15 hours with an 8 MeV beam. γ rays were measured in the underground laboratory 4 times successively, 82.000 s each measurement (comparable to $T_{1/2}$ of ^{24}Na) using a germanium detector with 120% relative efficiency, in a protective castle as described before. We found an activity of 4.44 ± 0.19 Bq and evaluated the minimal detectable activity at 0.048 Bq. In the four the γ-ray spectra we could observe the decreasing activity of the irradiated target and the gradual relative increase of the background radiation.

The following two steps consisted of the activation of C targets at two different beam energies, 6 and 7 MeV, and from measuring them both in the underground laboratory and in the GammaSpec laboratory located at the surface. In this latter laboratory, the spectrometric system is based on an Ortec HPGe detector 30185 GEM, resolution 2.1 keV at 1332 keV of ^{60}Co, and relative efficiency 30% (compared to 3 "x 3" NaI (Tl) standard). This spectrometric system is protected by a lead cylindrical shield (10 cm thick), covered on the inside with tin (1 mm thick) and copper (1.5 mm thick) foils. Thus for γ rays of energies between 20 and 2750 keV in a 24 hours measurement one obtains a count rate of 1.2-1.8 events/sec (depends mainly on the concentration of ^{222}Rn in natural background).

For the target irradiated (23 hours) at E_{lab} = 7 MeV, and measured in the GammaSpec laboratory, the beam intensity was 1.87 μA, yielding an activity at the end of irradiation equal with 5.20 ± 0.40 Bq. This activity was calculated after corrections were made for the efficiency and the time needed to transport the target from the reaction chamber to the GammaSpec laboratory. For measurements made in the underground laboratory another C target was irradiated using the same parameters, but for a longer irradiation time of about 25 hours.

Activity values measured in the two laboratories are shown in Tables 1 and 2; the two sets of measurements gave comparable results, within the evaluated uncertainties. The incident ^{13}C beam energy (E_{lab}) in MeV, beam current (I) in μA, and counting time of the irradiated targets (t_c) in seconds are also given in these tables. Knowing the activated targets activity at the measurement moment and the background rate of accumulation we determined the limit of detection for the evaluation of the $^{12}C + {}^{13}C$ fusion reaction cross sections. The minimum measurable cross section results to be about 3 nb using beam intensity around 0.6 pμA (particleμA, $^{13}C^{+3}$ charge state) , as in these cases. That is an order of magnitude below the lowest value measured until now in other laboratories. Increasing the beam intensity to approximately 6-10 pμA, it is possible to decrease the limit of detection of 10 more times, so we can measure at the energies lower than those now existing in the literature.

Tests conducted at the lowest $E_{lab}(^{13}C)$ = 6 MeV have revealed low activities of the activated targets, but to which the experimental setups are still sensitive. Barely in the surface lab, but clearly in the underground one (see Fig. 2) [15]. Reducing the limit by an order of magnitude is still possible by increasing the beam intensity. There will be, however, limitations on the extent to which the current intensity can be increased without damaging the targets. A high current beam raises problems with sputtering effect (some produced ^{24}Na's are sputtered away from the target surface during irradiation) and with heating effects. In a test at 10 μA we had visible signs of carbon sputtering from the target. For future measurements it will be necessary to construct a target cooling system. But again there is a limitation on how heat can be dissipated in the target.

Another way to improve the signal-to-noise ratio in de-activation measurements is using the β–γ coincidence method. This method allows to suppress the ambient background γ rays from natural radioactive isotopes such as ^{40}K and ^{208}Tl. In the Notre Dame experiment the peaks at 1369 keV and 2754 keV of ^{24}Na could be observed only in the β gated γ-ray spectra. It is obvious that this experimental setup made now at IFIN-HH, will allow decreasing the total fusion cross section from this measurement with another order of magnitude.

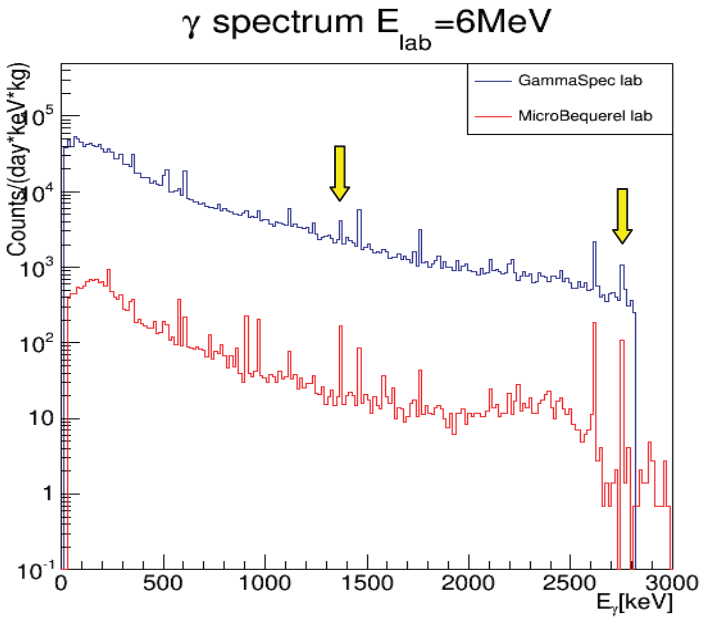

FIGURE 2. Comparison between γ spectra (E_{lab} = 6 MeV) measured in underground laboratory and GammaSpec laboratory (arrows-the cascading γ rays 1369 and 2754 keV)

TABLE 1. Experimental results obtained in GammaSpec laboratory

$E_{lab}(^{13}C)$ (MeV)	I(μA)	t_c(s)	^{24}Na (Bq)
7.0	**1.87**	**81000**	**5.20 ± 0.40**
6.0	**1.90**	**86400**	**0.115 ± 0.018**

TABLE 2. Experimental results obtained in the underground laboratory

$E_{lab}(^{13}C)$ (MeV)	I(μA)	t_c(s)	^{24}Na (Bq)
7.0	**1.87**	**86400**	**5.23 ± 0.043**
6.0	**1.90**	**84480**	**0.085 ± 0.011**

CONCLUSIONS

Study of carbon burning is an open question in nuclear astrophysics. This process represents the third stage of stellar evolution of massive stars with mass greater than 8 stellar masses that continue mainly through $^{12}C + ^{12}C$ fusion processes and to a lesser extent by $^{12}C + ^{16}O$. Direct measurement at the Gamow window energies are therefore essential, but are difficult to carry due to the background from the cosmic rays, terrestrial environment and/or accelerator beams. Major improvements can be achieved by using high intensity accelerators, advanced detection techniques and/or underground measurements. $^{12}C + ^{13}C$ fusion process gives information about the fusion mechanism at low energies and can be studied both in-beam γ spectroscopy and activation method using experimental setups that consists of an accelerator and detectors for γ spectroscopy.

To determine the optimum parameters of this experiment, stability and resolution tests of ^{12}C beam obtained at the 3 MV accelerator of IFIN-HH were conducted last year. Following these tests, it turns out that the accelerator has the characteristics required for nuclear astrophysics measurements, namely: allow the terminal voltage between 0.1-3.2 MV, stable while providing stability of incident beam energy used, the currents are stable over time, allowing precise measurements. In particular, the intensities of the order of 10 pμA obtained for ^{12}C, an order of magnitude higher than those obtained from the University of Notre Dame FN tandem, make possible to carry the proposed experiments in collaboration with the group from there.

We studied the $^{12}C+^{13}C$ fusion reaction in the energy range $E_{c.m}$ = 2.9 - 3.8 MeV using the activation method and gamma-ray spectroscopy. Activities of irradiated targets measured both in the underground and surface laboratories allowed to determine the limit of detection of cross sections of the order of 1-3 nb. By increasing the intensity it is possible to gain a factor of 10 in sensitivity and by using β–γ coincidences, another factor of 10. However, this will imply a good cooling of the graphite targets. We emphasize that the minimum value of the measurable cross sections in general, is dependent on the specific characteristics of the produced isotope and of the γ transition(s) used, but the order of magnitude set here (nanobarns) remains valid, as remains the possibility to reduce it by increasing the intensity and using β–γ coincidences. Calibrations and measurements performed in identical or similar conditions will also allow us to reduce the uncertainties associated with the experimental data corresponding with range $E_{c.m}$ =

2.6-5.0 MeV below 20%, and to determine the cross section for the $^{12}C + ^{13}C$ process at an energy lower than $E_{c.m}$ = 2.6 MeV.

In conclusion, the 3 MV accelerator is suitable for nuclear astrophysics measurements due to energies and intensities provided and stability in operation. Low (DFN) and ultralow ("μBq" Slanic) background laboratories of the institute can be successfully used for measurements by activation with lifetime greater than ten minutes and several hours, respectively, necessary to transport the probes. These facilities have been included recently in a European project proposal Horizon 2020 program, called the European Laboratory Astrophysics Network (ELAN) as TA (Transnational Access facility), in a select group of seven multi-disciplinary laboratories of atomic and molecular spectroscopy or radiation installations and of only two other nuclear astrophysics labs.

ACKNOWLEDGMENTS

This work was supported by the Romanian National Authority for Scientific Research Project No. PN-09-37-01-07 and Project No. PNII-IDEI 27/2013.

REFERENCES

1. D. G. Ghita et al., AIP Conf. Proc. 1525, 208 (2013); doi: 10.1063/1.4802321
2. D. G. Ghita et al., Proceedings of HIAT 2012, Chicago, IL USA
3. G. Wallerstein et. al. Rev. Mod. Phys, 69 998 (1997)
4. F. Kappeler et al., Ann. Rev. Nucl. Part. Sci. 48, 175 (1998).
5. E. Garcia-Berro et al., Astrophys. J. 286, 765 (1997).
6. K. U. Kettner et al., Phys. Rev. Lett. 38, 337 (1977).
7. H.W. Becker et al., Z. Phys. A 303, 305 (1981).
8. T. Spillane et al., Phys. Rev. Lett.98, 122501 (2007).
9. http://www.nipne.ro/facilities/laboratories/english/gamaspec.php
10. A. Pantelica et al., Rad. Prot. Dosim. 97(2) 187-192 (2001).
11. V. Petrescu, "Monografie Slanic Prahova", (2002).
12. R. M. Margineanu et al., Applied Radiation and Isotopes 67 (2009) 759–761
13. R. M. Margineanu et al., J Radioanal Nucl Chem, DOI 10.1007/s10967-013-2545-4
14. D. Chesneanu et al., Carpathian Summer School of Physics 2014, Sinaia, Romania, (2014) (http://www.nipne.ro/indico/getFile.py/access?contribId=73&resId=0&materialId=slides&confId=141).

Fusion cross section of $^{12}C+^{13}C$ at sub-barrier energies

N.T. Zhang[1], X.D. Tang[1], H. Chen[1], D. Chesneanu[2], M. Straticiuc[2], L. Trache[2], K.A. Li[1], Y.J. Li[3], D.G. Ghita[2], I. Burducea[2], R. Margineanu[2], A. Pantelica[2] and C. Gomoiu[2]

[1]*Insitute of Modern Physics, Chinese Academy of Sciences, 730000 Lanzhou, China*
[2]*Horia Hulubei National Institute of Physics and Nuclear Engineering (IFIN-HH), 077125 Bucharest-Magurele, Romania*
[3]*China Institute of Atomic Energy, 102413 Beijing, China*

Abstract. In the recent work at Notre Dame, correlations between three carbon isotope fusion systems have been studied and it is found that the fusion cross sections of $^{12}C+^{13}C$ and $^{13}C+^{13}C$ provide an upper limit on the fusion cross section of the astrophysically important $^{12}C+^{13}C$ reaction. The aim of this work is to continue such research by measuring the fusion cross section of the $^{12}C+^{13}C$ reaction to lower energies. In this experiment, the off-line activity measurement was performed in the ultra-low background laboratory and the fusion cross section for $^{12}C+^{13}C$ has been determined in the energy range of $E_{c.m.}$=2.5-6.8 MeV. Comparison between this work and several models is also presented.

1 Introduction

Heavy-ion fusion reactions between light nuclei such as carbon and oxygen isotopes have been intensively studied because of their importance in a wide variety of stellar burning scenarios. Among them, carbon burning driven by the $^{12}C+^{12}C$ fusion is a crucial process for the formation of white dwarfs, nucleosynthesis in massive stars, and ignition in type Ia supernovae and superbursts [1,2]. The temperatures for the hydrostatic carbon burning process range from 0.8 to 1.2 GK, corresponding to $E_{c.m.}$=1−3 MeV. Unfortunately, because of the very low cross sections, this important energy range is only partially measured at energies above $E_{c.m.}$=2.1 MeV. For the unmeasured energy ranges, one has to rely on extrapolation methods. Moreover, the situation is further complicated by the existence of the strong, relatively narrow resonances in $^{12}C+^{12}C$ reactions. The large resonance reported at energies around $E_{c.m.}$= 2.1 MeV which has not been confirmed by following experiment [3].

In an attempt to learn about the resonance structures of the low-energy $^{12}C+^{12}C$ reaction, the carbon isotope fusion reactions were systematically studied at the University of Notre Dame (UND)[4]. It was found that the cross sections of the $^{12}C+^{12}C$ fusion reaction at resonant energies match with the cross sections in the $^{12}C+^{13}C$ and $^{13}C+^{13}C$ systems within their quoted uncertainties. The observed correlation is explained by the level density differences among the three carbon isotope systems [4, 5]. As a result, the $^{12}C+^{13}C$ and $^{13}C+^{13}C$ systems provide an upper limit for $^{12}C+^{12}C$ in a wide range from $E_{c.m.}$=2.6 MeV up to more than 20 MeV. Since the two carbon fusion cross sections are much easier to be modeled due to their smooth behaviors, such an upper limit could be predicted within the astrophysical energy range. The coupled-channel calculation with the M3Y+Rep potential was used to fit the $^{12}C+^{13}C$ and $^{13}C+^{13}C$ data and constrain the effective nuclear potential, which was then used for the prediction of the $^{12}C+^{12}C$ fusion cross sections [4, 6]. It was found that the coupled-

channel calculation using the constrained M3Y+Rep potential provides an excellent upper limit for almost all the data except for the strong resonance at 2.14 MeV which has not been confirmed [4].

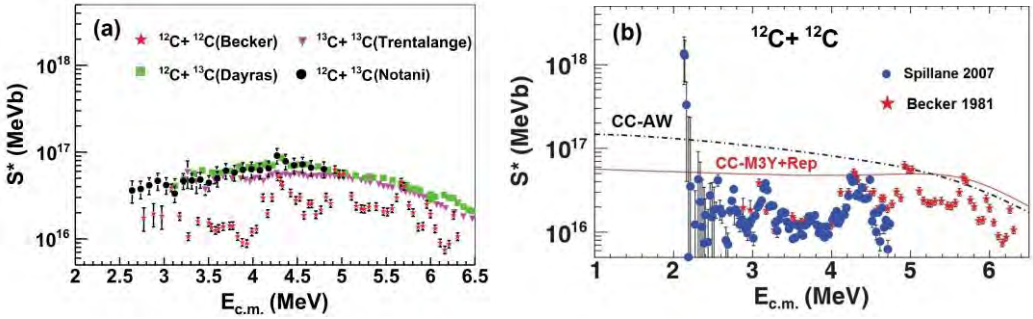

Figure 1. The experimental S*-factors for the carbon isotope fusion reactions: ^{12}C+^{12}C from Ref. [7] (red stars) and Ref. [3] (blue points) and ^{12}C+^{13}C from Ref. [4] (black points) and Ref. [8] (green squares), and ^{13}C+^{13}C [9] (magenta triangles). In Fig. 1(b), two coupled-channels calculations using AW potential (CC-AW, dot-dashed line) and M3Y+Rep potential (CC-M3Y+Rep, red solid line), respectively, are shown for comparison.

Measurement of ^{12}C+^{13}C and ^{13}C+^{13}C at deep sub-barrier energies gives us not only an opportunity to model the resonance strengths in ^{12}C+^{12}C but also a test of the predictive powers of various theoretical models for the carbon fusion cross sections at deep sub-barrier energies. Lacking of experimental data within the energies of astrophysical interest, large discrepancies exist among different nuclear reaction models. Therefore, it is important to push the measurements of the fusion cross sections of ^{12}C+^{13}C and ^{13}C+^{13}C down towards lower energies.

2 ^{12}C+^{13}C experiment at IFIN-HH

We report an experiment to measure the cross section of ^{12}C+^{13}C reaction by detecting the residual nucleus ^{24}Na which β-decays with a half-life of 15.0 h. Similar measurements have been performed by Notani and Dayras [4, 8]. In the present experiment, the ^{13}C beam was produced by a cesium sputter ion source and injected into a HVEE Tandetron 3 MV electrostatic accelerator of IFIN-HH [10]. The ^{13}C beam impinges a natural graphite target with thickness of 1 mm. The reaction has been studied by varying the beam energies between 5.2 and 6.8 MeV in steps of 0.2 MeV. The ^{13}C beam current used in this experiment varies in the range of 2 to 8 pμA.

After each irradiation, the target sample would be quickly transported to an underground counting station (μBq) in the Unirea salt mine for offline γ-ray measurement [11]. This salt mine is located in the vicinity of Slanic-Prahova city, about one hundred kilometers away from the Bucharest. In this salt mine, the μBq underground laboratory is situated at a depth of 208 m below surface (estimated to 560 m water equivalent). The total gamma background spectrum between 40 keV and 3 MeV was 100 times smaller at laboratory level with respect to the same spectrum recorded at surface in open field. In the microBq, a well shielded HPGe detector was used to detect two cascading γ rays (1369- and 2754-keV) emitted from the β decay of ^{24}Na. One typical gamma spectrum was displayed in Fig. 2. In some cases, the measurement was performed in the Low Background Gamma-Ray Spectrometry Laboratory (GAMASPEC) in a basement of IFIN-HH [12]. In this lab, limited by the background γ rays, only target samples irradiated at higher beam energies (>5.8 MeV) could be measured. Furthermore, this measurement was used to cross check the experimental setup in the two laboratories and validate our results.

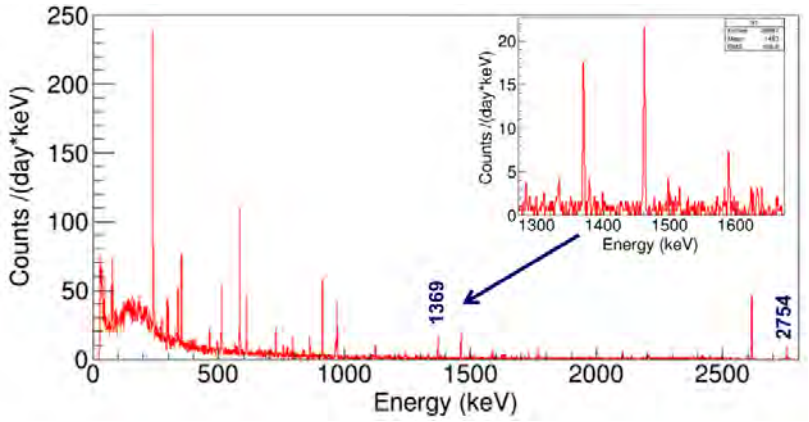

Figure 2. A typical gamma spectrum measured in the underground microBq lab within 46 hours. Beam energy for this spectrum is 5.2 MeV ($E_{c.m.}$=2.5 MeV), which is the lowest energy point in the experiment. The statistical error for 1369-keV γ peak is 11%, much lower than that in the Notani measurement [4].

The thick-target yield (Y) for $^{12}C(^{13}C,p)^{24}Na$ reaction was obtained by normalizing the observed yield to the total incident ^{13}C beam flux. From the thick-target yield excitation function, the differential yield dY/dE are determined and then the corresponding cross sections are calculated using the equation $\sigma(E)=dY/dE*dE/d(\rho X)/N_v$, where N_v is the number of atoms per unit of volume and $dE/d(\rho X)$ is the stopping power in the target material. Finally, the total fusion cross sections of $^{12}C+^{13}C$ are deduced from the proton emission channel using the theoretical branching ratio given by Hauser-Feshbach model [8].

3 Preliminary results and summary

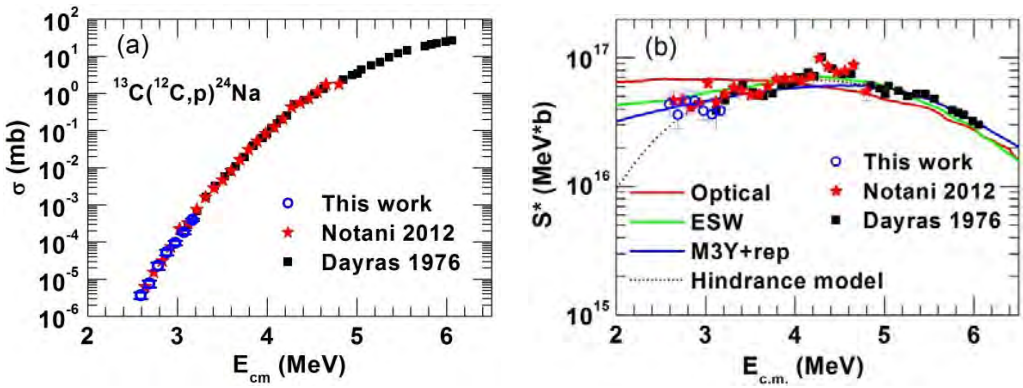

Figure 3. The preliminary fusion cross section of $^{12}C(^{13}C,p)^{24}Na$ reaction obtained from the present work (a) and the deduced S-factors for the $^{12}C+^{13}C$ reaction system (b). The results from the previous experiments are also shown.

The preliminary results are shown in Fig. 3. In this work, the lowest cross section for $^{12}C(^{13}C,p)^{24}Na$ reaction has been measured down to 3 nb as shown in Fig. 3(a), representing the lowest energy reached for this reaction. This is the great advantage of the ultra-low background underground laboratory. Figure 3(b) shows the modified S-factor (S*) deduced from the total fusion cross section. The result agrees with that of the two previous measurements in the energy region from 2.6-3.3 MeV. Limited by the beam time, only one new data point ($E_{c.m.}$=2.5 MeV) is added in our first experiment. It has been observed that the optical model with Woods-Saxon type potential reproduces the experimental data only at energies above 4 MeV. At deep sub-barrier energies, it significantly overestimates the cross section, which is quoted as hindrance effect. The ESW model and coupled-

channels (CC) with M3Y+Rep potential can predict the experimental data very well. The hindrance model prediction obtained by fitting the Dayras data [13] also shows a reasonable agreement to the experimental data above 2.7 MeV, but predicts a much sharper decrease at astrophysical energies. In order to test the predictive power of the extrapolation models, we will continue our measurement towards lower energies.

4 Summary and acknowledgement

In summary, in our first-stage experiment performed in IFIN-HH, $^{12}C+^{13}C$ fusion cross section has been measured down to 2.5 MeV using thick target technique and activation method. It shows the 3 MV accelerator in IFIN-HH is very suitable for nuclear astrophysics measurements because of high beam intensities and stability in operation. Also, the ultralow background underground laboratory of the institute demonstrates a great potential for measurements of ultra-low activity with lifetime several hours. These facilities offer a new opportunity to measure $^{12}C+^{13}C$ fusion cross section at even lower energies.

This work is supported by the National Natural Sciences Foundation of China under Grants No. 11405226 and No. 11475228, the 100 Talents Program of the Chinese Academy of Sciences. ……

References

[1] W. Hillebrandt and J. Niemeyer, Annu. Rev. Astron. Astrophys. **38**, 191 (2000)
[2] L.R. Gasques *et al.*, Phys. Rev. C **76**, 035802 (2007)
[3] T. Spillane *et al.*, M. Romano, J. Schweitzer, Phys. Rev. Lett. **98**, 122501 (2007)
[4] M. Notani *et al.*, Phys. Rev. C **85**, 014607 (2012)
[5] C.L. Jiang, B.B. Back, H. Esbensen, R.V. F. Janssens, K.E. Rehm and R.J. Charity, Phys. Rev. Lett. **110**, 072701 (2013)
[6] H. Esbensen, X. Tang and C.L. Jiang, Phys. Rev. C **84**, 064613 (2011)
[7] H.W. Becker, K.U. Kettner, C. Rolfs, H.P. Trautvetter, Z. Phys. A **303**, 305 (1981)
[8] R.A. Dayras, R.G. Stokstad, Z.E. Switkowski, R.M. Wieland, Nucl. Phys. A **265**, 153 (1976)
[9] S. Trentalange, S.C.Wu, J.L. Osborne, C. A. Barnes, Nucl. Phys. A **483**, 406 (1988)
[10] I. Burducea, M. Straticiuc, D.G. Ghiță, D.V. Moșu, C.I. Călinescu, N.C. Podaru, D.J.W. Mous, I. Ursu and N.V. Zamfir, Nucl. Instr. and Meth. B **359**, 12 (2015)
[11] R. Margineanu, C. Simion, S. Bercea, O.G. Duliu, D. Gheorghiu, A. Stochioiu and M. Matei, Appl. Radiat. Isot. **66**, 1501 (2008)
[12] https://www.nipne.ro/facilities/laboratories/english/gamaspec.php
[13] C.L. Jiang, K.E. Rehm, B.B. Back, and R.V.F. Janssens, Phys. Rev. C **79**, 044601 (2009)

EPJ manuscript No.
(will be inserted by the editor)

Beta-decay of ^{31}Cl: an indirect probe for ^{30}P(p,γ)^{31}S. Present status and future perspectives.

Antti Saastamoinen[1], Anu Kankainen[2a], and Livius Trache[3]

[1] Cyclotron Institute, Texas A&M University, College Station, TX, 77843-3366, USA
[2] University of Edinburgh, Edinburgh EH9 3JZ, United Kingdom
[3] National Institute for Physics and Nuclear Engineering, P.O.Box MG-6, Bucharest-Magurele, Romania

Received: date / Revised version: date

Abstract. β-decay of ^{31}Cl can be used as a selective tool for studying astrophysically relevant states in ^{31}S. In this article we review the present status of the decay data. The implications for the ^{30}P(p,γ)^{31}S reaction rate at novae temperatures, and future experimental ideas are discussed.

PACS. 26.50.+x Nuclear physics aspects of novae, supernovae, and other explosive environments – 23.40.-s β decay; double β decay; electron and muon capture – 27.30.+t $20 \leq A \leq 38$ – 29.30.Ep Charged-particle spectroscopy – 23.20.Lv γ transitions and level energies

1 Introduction

Nova explosions are frequent and bright phenomena resulting from a binary system where a white dwarf accretes hydrogen-rich material from its companion star [1]. Observations from optical, ultraviolet and infrared spectra have given evidence that novae produce enhanced amounts of carbon, nitrogen and oxygen with respect to solar abundances. Heavier so-called ONe novae have shown an enhancement in the abundances of heavier elements. In ONe novae, ^{30}P(p,γ)^{31}S is a bottle-neck reaction, affecting the production of heavier elements. If the reaction is not fast enough, the beta decay of ^{30}P ($T_{1/2} = 2.498(4)$ min [2]) takes over and proton capture fails to produce heavier elements.

At typical nova peak temperatures of about 0.2-0.4 GK, the proton capture reaction ^{30}P(p,γ)^{31}S proceeds mostly via resonant capture through narrow and isolated resonances. For such reactions, the reaction rate can be written

$$N_a \langle \sigma \nu \rangle = 1.5399 \cdot 10^{11} (\mu T_9)^{-3/2} \times \sum_i (\omega\gamma)_i e^{(-11.605 E_i / T_9)}, \quad (1)$$

in units of cm^{3}mol^{-1}s^{-1}, where μ is the reduced mass of the colliding nuclei in units of u, T_9 the temperature in GK, and E_i and $\omega\gamma_i$ are the center of mass energy and the resonance strength of the ith resonance in MeV, respectively [3,4]. Due to the exponential nature of the energy dependence, it is crucial to determine the resonance energies to a reasonably good precision: Uncertainty of few keV is usually enough. However, sometimes better resolution is needed to distinguish densely packed states. In addition, proper identification of the spins and parities, as well as the proton and γ-widths of the states affects the rate directly via the resonance strength $(\omega\gamma)_i$. Typically for low resonance energies when $\Gamma_p << \Gamma_\gamma$, the resonance strength depends only on the proton width, i.e. $\omega\gamma \approx \omega\Gamma_p$.

Given the short half-life of ^{30}P no such targets can be manufactured. So far direct experimental studies of the reaction have not been possible due too low intensities of available ^{30}P radioactive ion beams. On the other hand, ^{31}Cl has a high β-decay Q value ($Q_{EC} = 11976(50)$ keV [5]), allowing it to populate states above the proton separation energy in ^{31}S ($S_p = 6131.3(10)$ keV [5]).

Nuclear β-decay is a very selective process: allowed decays populate only states where the spin changes maximum by one unit, and the parity remains unchanged. If the spin changes by more than one unit, or the parity changes,

[a] *Present address:* Department of Physics, P.O. Box 35 (YFL), FI-40014 University of Jyväskylä, Finland

the decays are strongly suppressed (forbidden decays). Thus β-decay of ^{31}Cl ($J^{\pi}_{g.s.} = \frac{3}{2}^{+}$) populates levels in ^{31}S that have most likely $J^{\pi} = \frac{1}{2}^{+}$, $\frac{3}{2}^{+}$, or $\frac{5}{2}^{+}$.

In the case of ^{30}P(p,γ)^{31}S, the proton is captured by ^{30}P nucleus with $J^{\pi} = 1^{+}$ and thus the s-wave ($l = 0$) captures will go to states with $J^{\pi} = \frac{1}{2}^{+}$ or $\frac{3}{2}^{+}$ which can be populated in the β-decay of ^{31}Cl. As mentioned earlier, allowed β-decay can populate also $J^{\pi}_{g.s.} = \frac{5}{2}^{+}$ states, corresponding to d-wave ($l = 2$) capture.

In this article we review the known experimental data of β-decay of ^{31}Cl, concentrating on the states relevant for the ^{30}P(p,γ)^{31}S reaction: i.e. we focus on the existing data above $S_p(^{31}\mathrm{S})$. Since early 1980s, β-decay of ^{31}Cl has been studied with several different techniques. We group here the experiments by the sample production method used. Experimental setups for experiments where samples were produced with different ISOL (Isotope Separation On-Line) techniques are discussed in Sec. 2, and with samples produced with in-flight technique in Sec. 3. In section 4 we summarize the known β-decay data that is relevant for the ^{30}P(p,γ)^{31}S reaction rate evaluation presented elsewhere in this volume (REF).

2 Samples produced with ISOL techniques

2.1 Studies in Oslo

First studies on the beta decay of ^{31}Cl were performed at the MC-35 cyclotron of the University of Oslo in 1982 [6, 7]. The ^{31}Cl^{+} ions were produced using a 34-MeV proton beam impinging on a ZnS target and transported from the target region via He-jet technique. The ^{31}Cl beam was implanted on an aluminized mylar tape surrounded by a single 31.1-μm-thick surface-barrier detector and a detector telescope consisting of a 10.8-μm, 25-mm^2 ΔE and a 300-μm E, 100-mm^2 E detectors. The two most intense beta-delayed proton groups of ^{31}Cl at 989(10) and 1528(20) keV were observed and a half-life of 150^{+25}_{-20} ms determined based on those groups.

2.2 Studies in Berkeley

The next beta-decay studies on ^{31}Cl were performed at the Lawrence Berkeley Laboratory 88-inch Cyclotron [8] with 45-MeV proton beam on ZnS target. The reaction products were swept away from the target region using the He-jet technique and implanted on a rotating wheel in front of a ΔE (8.3 μm, 50 mm^2)- E (68 μm, 100 mm^2)- E_{rej} (20 μm, 300 mm^2) setup as illustrated in Fig. 1. The E_{rej} detector was used to reject the events due to positrons but also to detect higher energy protons. An overall resolution for protons of 75 keV was achieved with this setup. Altogether eight proton peaks in the energy range of 845 to 2204 keV were observed [8]. ^{31}Cl was restudied at Lawrence Berkeley in 1990s using two gas ΔE (CF_4, 30 μg/cm^2) - gas ΔE (CF_4, 30 μg/cm^2) - E (Si 300 μm, 380 mm^2) detectors. However, this latter experiment suffered from beta-delayed protons of ^{25}Si resulting from the aluminum backing discs of the ZnS target. As a result, only the two strongest proton peaks of [8] were confirmed although the total proton beam charge was 220 mC [9] compared to 90 mC in the previous Berkeley experiment [8] and 15 mC at the Oslo MC-35 cyclotron [7].

2.3 Studies in Jyväskylä

In 2004, the first experiment on ^{31}Cl employing a mass-separator was performed at the IGISOL3 (Ion Guide Isotope Separator On Line) facility [10] at the Accelerator Laboratory of the University of Jyväskylä (JYFL). There, 40 and 45-MeV proton beams impinging on a thin ZnS target at the entrance of the ion guide cell were employed. The reaction products were stopped and thermalized in the helium gas of the ion guide (p = 200 mbar) and extracted from the gas cell via differential pumping system and with the electric field. The ions were acccelerated to $40q$ keV and further mass-separated with a 55° dipole magnet. As a result, a pure beam of $A/q = 31$ reaction products was delivered to the spectroscopy setup. This was an advantage since the previous experiments had to collect data also at lower energy below the ^{31}Cl production threshold in order to distinguish the proton peaks belonging to other reaction products, such as ^{32}Cl. The yield of ^{31}Cl at IGISOL was about around 14 ions/s which was about 1000 times less than the yield of ^{31}S [11].

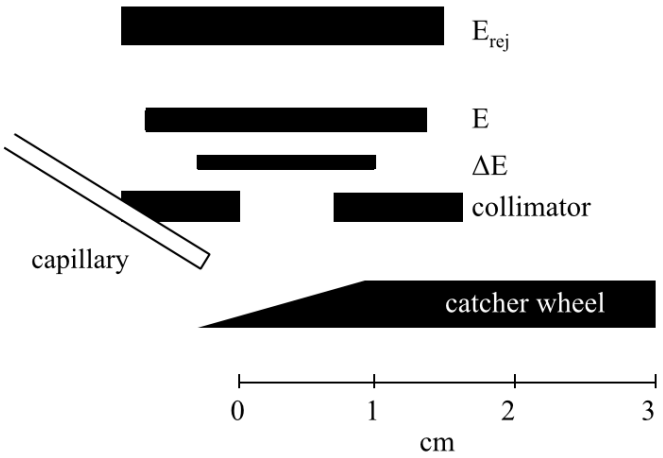

Fig. 1. The experimental setup at Berkeley, adapted from Fig. 1 of Ref. [8].

New double-sided silicon strip detectors (DSSDSs) offering much better energy resolution and reduced summing of the events due to pixelated readout structure became available in the beginning of the millennium [12,13]. At IGISOL, the $31Cl^{+}$ beam was implanted into a 30-μg/cm^2-thick carbon foil surrounded by three DSSSDs and the ISOLDE Silicon Ball detector [14]. The DSSSDs were about 60-μm-thick and had 16 50-mm-long and 3-mm-wide front strips and similar but orthogonal back strips. One of the DSSSDs was a Micron Semiconductor Ltd. (MSL) W1 detector with a dead layer of 600 nm [12] and two others were of a newer design with a dead layer of 100 nm [13]. Each DSSSD was backed with a thick silicon detector in order to detect positrons and higher energy protons. A hemisphere of the ISOLDE Silicon Ball detector [14] consisting of 144 individual 25.5 $\times$ 25.5 mm^2 Si detectors was useful for covering larger solid angle for detecting beta particles. For the first time, a HPGe detetor (70 %) was used to detect beta-delayed gamma-rays from ^{31}Cl. The detector setup of the experiment is shown in Figure 2.

The peaks observed in Ref. [8] were confirmed and 5 new peaks were observed. The experiment suffered from noise at lower energies and no proton peaks below 700 keV could be distinguished. Some of the observed proton peaks were uncertain. This experiment was first to include γ-ray detection in the setup. Total of four γ-lines were attributed to ^{31}Cl decay. One of the lines, at 4045(2) keV, was deduced to originate from the isobaric analogue state (IAS) at 6280(2) keV.

3 Samples produced with in-flight technique

3.1 Studies in Texas A&M

In Texas A&M experiments [15–17], the ^{31}Cl beam was produced by bombarding a 2.5 mg/cm^2-thick liquid-nitrogen-cooled H_2 target at 1.6 atm pressure with a ^{32}S beam at 40 MeV/u. The reaction products from inverse-kinematics reaction ^{1}H(^{32}S,^{31}Cl)2n were separated with the Momentum Achromat Recoil Spectrometer (MARS) [18]. The production method and the energy used allowed for the first time separation of ^{31}Cl from its isobars. The resulting ^{31}Cl beam had intensity of 3000 pps at 90% purity, the major impurity stopped in the setup being ^{29}S. During the implantation into the setup the beam momentum spread was restricted to $\Delta p/p = 0.25$ % and the rate to about 800 pps.

In the first of the experiments, the produced ^{31}Cl ions were implanted into a detector setup consisting of a 65 μm thick MSL W1 type DSSSD with 16+16 3.1 $\times$ 50 mm^2 strips (labeled "p" in Fig. 3), a 1 mm thick Si-pad detector (50 $\times$ 50 mm^2, "β_2" in Fig. 3), and a 70% HPGe detector facing the front side of the Si detector stack [15,16]. In the second experiment, the DSSSD was changed to a 45 μm thick MSL BB2 type detector with 24+24 1 $\times$ 24 mm^2 strips, an additional 300 μm thick Si 50 $\times$ 50 mm^2 detector was added before the DSSSD ("β_1" in Fig. 3), and another 70% HPGe detector was added on the opposite side [17,19]. During the second experiment data was taken also in a configuration consisting only the two HPGe detectors, the thick Si detector, while the other Si detectors were replaced by an 125 μm thick Al plate. This configuration allowed maximum beam to be used for higher statistics of

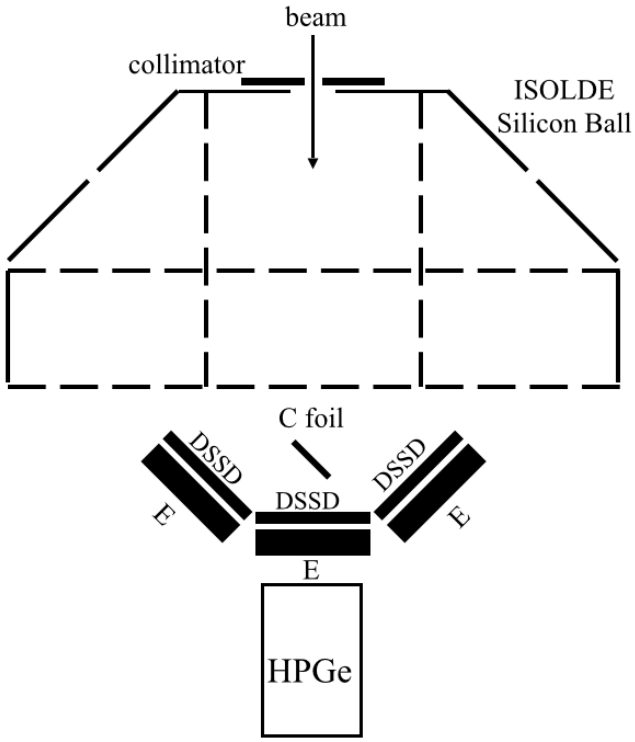

Fig. 2. An illustration of the experimental setup for the beta decay of ^{31}Cl at IGISOL. Not in scale, adapted from Fig. 2 of Ref. [11].

$\beta - \gamma - \gamma$-coincidences. In addition, to measure a more precise half-life, the standard tape transport – gas counter setup for high-precision β-decay half-life measurements was used. See e.g. Ref. [20] and references therein for detailed description of the half-life setup.

The TAMU experiments [15–17] confirmed the results of the JYFL experiment [11] for the proton spectrum up to about 2 MeV, while suffering from ^{29}S impurities and the fact that the higher-energy protons escaped the implantation detector. In addition to proton data, an extensive set of γ-lines was collected. The results include first direct measurement of the IAS through direct four different decay paths, including coincident cascades through the excited states. The comparison of the datasets is discussed further in section 4.

3.2 Studies at NSCL

Very recently, β-decay of ^{31}Cl has been studied at the National Superconducting Cyclotron Laboratory (NSCL) by using coupled K500 and K1200 cyclotrons and the A1900 separator to produce about 88% pure beam of ^{31}Cl. In this experiment, 50-MeV/u ^{31}Cl beam was implanted into a plastic scintillator, surrounded by an array of Yale Clovershare "Clover" type HPGe detectors. At the time of writing this, the resulting $\beta\gamma(\gamma)$-coincidence data are under analysis [21].

4 Summary of the ^{31}Cl β-decay data above $S_p(^{31}S)$

The proton spectra of the experiments in JYFL and in TAMU are compared in Fig.4. It is worth noting that in the JYFL experiment the ^{31}Cl source implanted into a C-foil, whereas the TAMU spectrum has been collected by implanting the ^{31}Cl ions inside the detector. The latter method measures thus, not only the proton energy, but also the energy of the recoiling proton daughter and the preceding β-particle. The TAMU spectrum has several peaks from ^{29}S contamination in the beam implanted. The JYFL data has large background from the whole $A = 31$ isobar present in the beam (mainly ^{31}S). The extracted proton energies of both the aforementioned experiments, along with

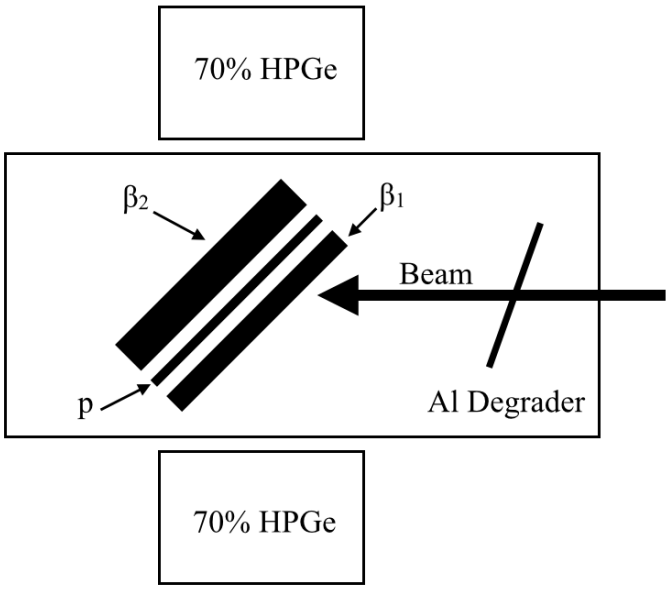

Fig. 3. A schematic presentation of the experimental setup at Texas A&M, not to scale. Label "p" refers to a DSSSD used, "β_1" to Si detector added for the second experiment, and "β_2" for a thick Si-pad detector. In the first experiment, only one HPGe was used. See text for more details.

all other known data are given in table 1. All the known experimental proton energies agree within the uncertainties of each experiment. Table 1 gives these proton energies as ^{31}S excitation energies, assuming that the proton decays populate the ground state of ^{30}P. It is worth noting that there is some evidence for some of these decays populating excited states in ^{30}P as shown in Ref. [17]. However, so far known levels populated by β-delayed proton emission from ^{31}Cl are too high in energy to yield information about the states inside the Gamow window of $^{30}\mathrm{P}(\mathrm{p},\gamma)^{31}\mathrm{S}$ in typical novae temperatures.

Table 1. A comparison of known proton energies from ^{31}Cl decay. All energies are given as E_{lab} in keV. The average value is the weighted average of all the works presented in this table. The corresponding level energy is determined by assuming decay to the ground state of ^{30}P and using the calculated average proton energy with $S_p(^{31}\mathrm{S}) = 6131.3(10)$ keV [5].

Ref. [6]	Ref. [8]	Ref. [9]	Ref. [11]	Ref. [17]	Average	E_{lev}
			762(14)	780(2)	780(2)	6936(2)
	845(30)		853(18)	877(2)	876(2)	7036(2)
989(15)	986(10)	986(10)	978(15)	993(2)	993(2)	7157(2)
	1173(30)		1175(19)	1185(3)	1185(3)	7355(3)
				1345(17)	1345(17)	7521(17)
1528(20)	1520(15)	1524(10)	1521(20)	1520(3)	1521(3)	7702(3)
				1594(17)	1594(17)	7778(17)
	1695(20)		1688(22)	1706(3)	1706(3)	7894(3)
	1827(20)		1825(23)	1830(3)	1830(3)	8022(3)
				1927(17)	1927(17)	8122(17)
	2113(30)		2075(30)	2070(17)	2079(13)	8279(13)
	2204(30)		2217(30)	2224(3)	2224(3)	8429(3)
			2299(30)	2286(17)	2289(15)	8496(15)
			2454(40)	2489(17)	2484(16)	8697(16)
			2601(40)	2641(17)	2635(16)	8854(16)
			2751(40)	2807(17)	2799(16)	9023(16)

The presently known β-delayed γ-data has more information to offer about states inside the Gamow window. Table 2 lists the known β-delayed γ lines beyond the proton threshold, with comparison to other known states that

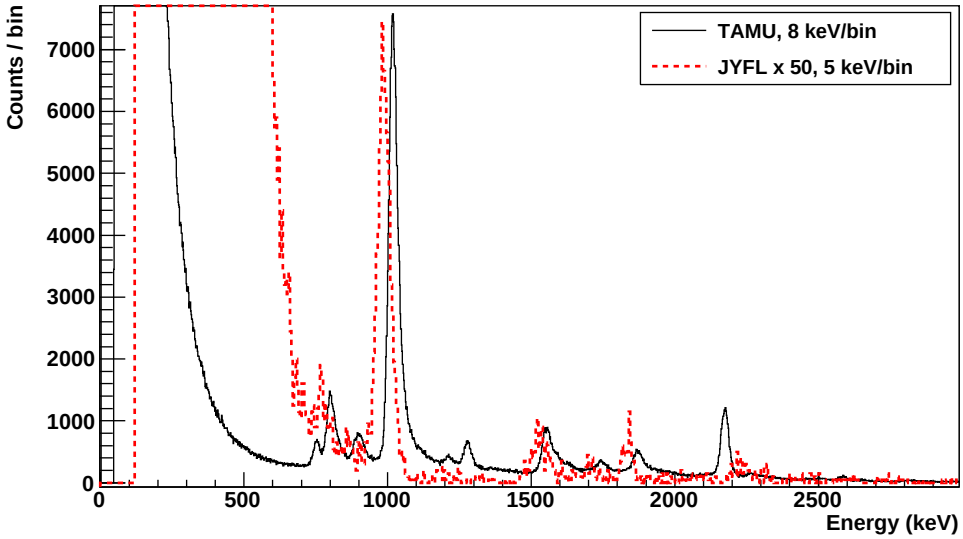

Fig. 4. A comparison between the proton spectra of the experiments in JYFL (red, dashed) and in TAMU (black, solid). The JYFL data has been multiplied by factor of 50 to match the statistics of the 996 keV proton line in TAMU spectrum. Note that in the JYFL experiment the ^{31}Cl source was implanted into a C-foil, whereas the TAMU spectrum has been collected by implanting the ^{31}Cl ions inside the detector. See text for details.

can be populated in β-decay. In the JYFL data, Ref [11], one γ-line was assumed to originate from beyond the proton threshold: the 4045(2) keV was deduced to be transition from the IAS to the 2234 keV second excited state in ^{31}S, and thus level energy of 6280(2) keV was deduced. However, no coincidence data was collected. The TAMU dataset, Ref [15–17], has a direct transition from the IAS, along with three transitions that are in coincidence with γ-lines from the lower levels. One direct transition corresponding to a previously known level at 6259 keV was measured with improved precision. In addition, two transitions without previously known matching levels at 6420 and 7280 keV were observed and tentatively assigned to corresponding levels. Two high energy γ-lines matching previously known 7600(30) and 7660(30) keV levels were observed and tentatively assigned to originate from these levels. None of these four transitions could be attributed to originate any other species in the beam cocktail, nor escape or sum peaks. Their nature needs to be confirmed with an independent measurement. In the TAMU dataset, there is a γ-line at 6389.7(11) keV, but this overlaps with an escape from higher energy γ-ray.

An increased amount of counts at 5030 and 6420 keV were also seen in the JYFL data set, although statistics was not enough to assign them as peaks. In addition, peaks at around 7630 and 7640 keV were observed at IGISOL as seen in Fig. 5. Since they were located at the very end of the gamma-ray energy spectrum, they were treated as possible overflow peaks and not taken into account in the data analysis. However, also a peak located at the position of the first escape peak at around 7130 keV is seen in the JYFL data set supporting that the peaks at around 7630 keV are real. This is supported also by the fact that there are no known γ-rays at these energies originating from any nuclei at $A = 31$, $A = 62$, or $A = 15, 16$ regions.

5 Conclusions and future perspectives

The main contribution of the present β-decay data to the ^{30}P(p,γ)^{31}S rate at nova temperatures are the precise energies of the resonances at 6255.3(5) and 6280.2(3) keV. The latter of these has been observed in two independent β-decay studies [11,17]. These energies are in reasonable agreement with the known energies from other known data as seen in Table 2. There is a few keV discrepancy to some of the known reaction measurements in Refs. [26,22,23, 27], but agreement within the uncertainties of Ref. [25]. The tentative 6420.7(6) keV state of Ref. [17] needs to be confirmed by other study before to be considered. Some of the dataset of Ref. [17] is still under analysis, and the very recent study of Ref. [21] may offer some new insights on some of the states above the proton threshold in ^{31}S. It is worth noting that the improved IAS energy yields a more precise prediction for the ^{31}Cl ground state mass excess

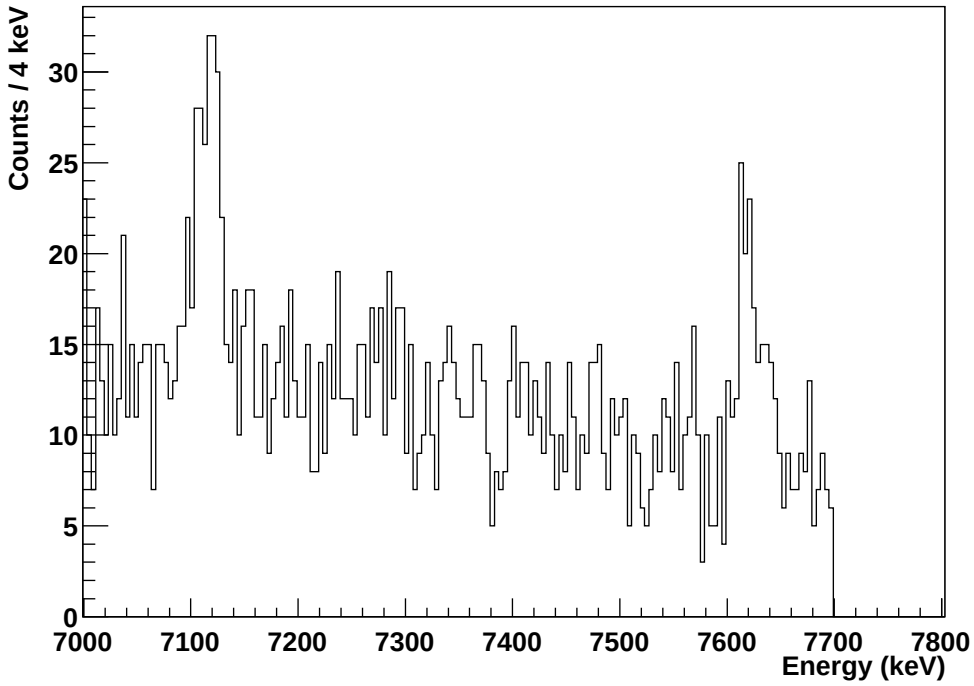

Fig. 5. Previously unpublished high energy part of the γ spectrum from the JYFL experiment. The double peak at around 7630 keV and matching line 511 keV below suggest this being a real transition rather than overflow. See text for more details.

Table 2. The γ transitions from ^{31}Cl decay above $S_p(^{31}\mathrm{S}) = 6131.3(10)$ keV [5]. For comparison, known levels by other techniques from literature. All energies are given in keV.

Ref. [11] E_γ ; E_{final}	Ref.[17] E_γ ; E_{final}	E_{level}	Literature E_{level}; J^π	Remarks
	6254.6(5) ; 0	6255.3(5)	6259(2); $\frac{1}{2}^+, T = \frac{1}{2}$	Ref. [22,23]
	2995.6(2) ; 3284.8(3)	6280.2(3)	6281.2(14); $\frac{3}{2}^+, T = \frac{3}{2}$	Ref. [23]: Average of Refs. [24,25,11,26,23]
4045(2) ; 2235.6(4)	4046.2(2) ; 2234.3(2)			
	5031.5(3) ; 1247.6(3)			
	6279.5(3) ; 0			
	6420.0(6) ; 0	6420.7(6)		
	7279(1) ; 0	7280(1)		
	7415.8(9) ; 0	7416.8(9)		
	7630.8(6) ; 0	7631.8(6)	7600(30)	Ref. [24]
	7643.6(8) ; 0	7644.6(8)	7660(30)	Ref. [24], Ref. [23]: 7641(3), $(\frac{5}{2} - \frac{13}{2})^-$

through the Isobaric Multiplet Mass Equation (IMME). The determined value of -7056.8(3.3) keV agrees with the known value -7070(50) keV [5] and reduces the uncertainties related to the $^{30}\mathrm{S}(\mathrm{p},\gamma)^{31}\mathrm{Cl}$ reaction.

It is clear that so far in-flight methods can provide a cleaner source of ^{31}Cl than ISOL methods. However, if one can acquire high enough production of ^{31}Cl through ISOL methods, then it may be possible to utilize a Penning trap to produce a 100% clean source [28]. In addition, replacing the traditional catcher foil with a Paul trap [29] should allow to reject the effects of catcher foil, making the dead-layer of used Si detectors the only limitation for the low energy. Such configuration would allow also to distinguish the nature of the low energy β-delayed particles, which in principle can be either protons or alphas.

The limitations of silicon detectors make measuring of β-delayed protons of astrophysical interest rather difficult, if not impossible. Even implanting inside of a Si detector, which allows to ignore complications of corrections due to dead-layer or energy deposition into the catcher material, the low energy region is usually dominated by the large background contribution from the betas originating from decay channels without protons, or even worse, from

impurities. In some cases low energy proton peaks can be extracted by using background subtraction [30]. However, recent advances using Micro-MEsh-GAseous-Structures (MicroMEGAS) based detectors are a promising new tool for measuring low energy β-delayed particles essentially background free down to 100 keV or even lower [31]. Using such detector, in combination with efficient γ detection capability, will offer access to the ^{31}Cl β-delayed protons of astrophysical interest.

References

1. J. Jose and M. Hernanz, J. Phys. G **34**, R431 (2007).
2. M. S. Basunia, Nucl. Data Sheets **111**, 2331 (2010).
3. C. Rolfs and W. Rodney, *Cauldrons in the Cosmos* (The University of Chicago Press, Chicago 60637, USA, 1988).
4. C. Iliadis, *Nuclear Physics of Stars* (Wiley-VCH, Weinheim, 2007), ISBN: 978-3-527-40602-9.
5. M. Wang *et al.*, Chin. Phys. C **36**, 1603 (2012).
6. J. Äystö *et al.*, Phys. Lett. B **110**, 437 (1982).
7. J. Äystö *et al.*, Phys. Scr. **T5**, 193 (1983).
8. J. Äystö *et al.*, Phys. Rev. C **32**, 1700 (1985).
9. T. Ognibene *et al.*, Phys. Rev. C **54**, 1098 (1996).
10. P. Karvonen *et al.*, Nucl. Instrum. Meth. in Phys. Res. B **266**, 4454 (2008).
11. A. Kankainen *et al.*, Eur. Phys. J. A **27**, 67 (2006).
12. U. C. Bergmann, H. O. U. Fynbo, and O. Tengblad, Nucl. Instrum. Meth. in Phys. Res. A **515**, 657 (2003).
13. O. Tengblad *et al.*, Nucl. Instrum. Meth. in Phys. Res. A **525**, 458 (2004).
14. L. M. Fraile and J. Äystö, Nucl. Instrum. Meth. in Phys. Res. A **513**, 287 (2003).
15. L. Trache *et al.*, PoS(NIC X) 163 (2008).
16. A. Saastamoinen *et al.*, AIP Conf. Proc. **1409**, 71 (2011).
17. A. Saastamoinen, Ph.D. thesis, University of Jyväskylä, 2011.
18. R. Tribble *et al.*, Nucl. Phys. A **701**, 278 (2002).
19. M. McCleskey *et al.*, Nucl. Instrum. Meth. in Phys. Res. A **700**, 124 (2013).
20. V. E. Iacob *et al.*, Phys. Rev. C **82**, 035502 (2010).
21. M. Bennet and C. Wrede, Private communication.
22. C. Wrede *et al.*, Phys. Rev. C **76**, 052802(R) (2007).
23. C. Wrede *et al.*, Phys. Rev. C **79**, 045803 (2009).
24. P. Endt, Nucl. Phys. A **633**, 1 (1998).
25. J. Vernotte *et al.*, Nucl. Phys. A **655**, 415 (1999).
26. Z. Ma *et al.*, Phys. Rev. C **76**, 015803 (2007).
27. A. Parikh *et al.*, Phys. Rev. C **83**, 045806 (2011).
28. T. Eronen *et al.*, Eur. Phys. J. A **48**, 46 (2012).
29. N. Scielzo *et al.*, Nucl. Instrum. Meth. in Phys. Res. A **681**, 94 (2012).
30. A. Saastamoinen *et al.*, Phys. Rev. C **83**, 045808 (2011).
31. E. Pollacco *et al.*, Nucl. Instrum. Meth. in Phys. Res. A **723**, 102 (2013).

New generation of experiments for the investigation of stellar (p,γ) reaction rates using SAMURAI *

V. Panin[1], K. Yoneda[1] M. Kurokawa[1], J. Blackmon[2] Z. Elekes[3] D. Kim[4] T. Motobayashi[1]
H. Otsu[1] B. C. Rasco[2] A. Saastamoinen[5] L. Sobotka[6] L. Trache[7] T. Uesaka[1]

1. *RIKEN Nishina Center, 2-1 Hirosawa, Wako, Saitama 351-0198, Japan;*
2. *Louisiana State University, 211-A Nicholson Hal, Tower Dr., Baton Rouge, LA 708030-4001, USA;*
3. *MTA Atomki, Bem tér 18/c H-4026 Debrecen, Hungary;*
4. *Ewha Womans University, Seoul, South Korea;*
5. *Texas A&M University, USA;*
6. *Department of Chemistry, Washington University, Saint Louis, MO, 63130, USA;*
7. *IFIN-HH, str. Reactorului 30, Bucharest-Magurele RO-77125, Romania;*

Abstract

The future experimental campaign with the SAMURAI setup at RIKEN will explore a wide range of neutron-deficient nuclei with a particular focus on the most critical (p,γ) reaction rates relevant to the astrophysical *rp*-process in type I X-ray bursts (XRB). Intense radioactive-ion (RI) beams at an energy of a few hundred MeV/nucleon will be deployed to populate proton-unbound states in the nuclei of interest through the Coulomb excitation or nucleon-removal processes. The decay of these states into a proton and a heavy residue will be measured using complete kinematics and the information about time reversal proton-capture process will be obtained. This method will provide the vital experimental data on the resonances, which dominate the stellar (p,γ) reaction rates, as well as on the direct proton-capture process for some other cases. The experimental setup will utilize for the first time the High-Resolution 90°-mode of the SAMURAI spectrometer in combination with the existing detection systems, including custom-designed Si-strip detectors for simultaneous detection and tracking of heavy ions and protons emitted from the target. The details of the experimental method and the utilized apparatus are discussed in this paper.

Key words: type I X-ray bursts, *rp*-process, (p,γ) reaction rates, neutron-deficient RI beams

1 Subject and Motivation

Explosive hydrogen burning at extreme temperature and density conditions is one of the most fascinating topics in modern nuclear astrophysics, which only in the last decades became accessible for detailed experimental studies due to availability of intense neutron-deficient RI beams. Such exotic nuclear species in the proximity of the proton drip-line play an important role in the astrophysical *rp*-process - a dominating nucleosynthesis path in type-I X-ray bursts (XRB) which are often referred as the most frequent type of thermonuclear explosions in the Galaxy [1–3]

XRBs are recurrent events originating from close binary star systems due to thermonuclear runaway at the surface of a neutron star which accretes H/He-rich matter from an adjacent low-mass donor star [1]. When

Received date: **Revised date:**

∗ **Foundation item:** This work is supported by the OTKA project number 114454.

Biography: Valerii Panin (1985), male (Ukraine), Alchevsk, PhD, Experimental Nuclear Physics; E-mail: valerii.panin@riken.jp

critical temperature (T≈1-2 GK) and density ($\rho \approx 10^6$ g/cm^3) are reached in the hot envelope of the neutron star, the explosive process is triggered by 3α-reaction followed by a sequence of (p,γ) and (α,p) reactions (αp-process) promoting the burning material into the A=40 region [4]. After that, a rapid sequence of (p,γ) reactions and β-decays occurs (rp-process), thus processing the abundance flow further along the proton dripline with an extension all the way into A≈100 region [5, 6] where the nucleosynthesis is believed to stop in the closed SnSbTe cycle due to disintegration of α-unbound isotopes $^{106-108}$Te. The entire process lasts typically 10-100 s and results in an excessive yield (factor of about 10) of X-ray photons emanated from the neutron star's surface. This phenomenon is usually observed as a fast X-ray flash with a characteristic shape of the light curve. A wealth of information about properties of a neutron star such as mass, radius, spinning frequency etc., can be extracted from the XRB light curves [3, 7], if the underlying nuclear process is correctly described in the framework of an accurate fluid dynamics model.

The main difficulty in studying XRB nucleosynthesis arises from its complexity - several hundreds isotopes and thousands nuclear interactions can be involved in a single XRB event. However, experimental information is very scare for most of them and theoretical calculations may yield uncertainties of a factor of 10-100 for some reaction rates that, in turn, leads to significant discrepancies in the predicted XRB properties such as energy generation rates, light curves and resulting final chemical abundances [8, 9]. The final chemical abundances can be essential, in particular, for the cooling of the neutron star surface as well as for the consecutive bursts which develop on the preceding nuclear ashes [10]. It was found in the recent state-of-the-art sensitivity studies [3, 8, 9], based on large (over 600 isotopes) network calculations and on various hydrodynamic models with different XRB conditions (accreation rate, temperature and density profiles, etc.), that about less than 50 reactions may have any significant effect on the XRB properties such as overall energy output and final chemical yields. Such reactions can be identified in the vicinity of the so called waiting point (WP) nuclei (^{30}S, ^{60}Zn, ^{64}Ge, ^{68}Se, etc.) for which successive adding of another proton is inhibited by negative or very low proton-capture Q-values (a few hundreds keV). In such case (p,γ) reactions are hampered by either proton decay or reverse photodisintegration (γ,p) establishing (p,γ)-(γ,p) equilibrium. In both situations the process must "wait" until the relatively slow β^+ decay to process towards heavier nuclei via adjacent isotonic chains. This may lead to accumulation of the material in the region of the WP-nucleus (Z,N) and thus define the resulting composition of the burned ashes as well as nuclear energy generation rates and profiles of the XRB light curves. Investigation of the identified most critical (p,γ) reaction rates is of primary importance for the experimental studies in the next years. It will also become the main focus of the future experimental campaign with the large-acceptance spectrometer SAMURAI, taking advantage of the most intense RI-beams in the world available at RI-beam Factory in RIKEN [11]

2 Reactions in focus and the experimental method

Based on the previous theoretical sensitivity studies and XRB model predictions, the following set of reactions has been selected for future experiments at SAMURAI.

2.1 Breakout from WP-nuclei ^{64}Ge and ^{56}Ni

- **^{65}As$(p,\gamma)^{66}$Se**

  The reaction rate is found amongst the most influential for the final chemical yields of XRB [3, 9]. This is mainly due to its bridging effect on WP-nuclei ^{64}Ge , which, in most of the studied models, is a starting points towards production of heavier elements but is also a limiting factor of the rp-process due to its

β-decay life-time of 92 s being comparable to the typical time scale of the entire XRB process. A possible breakout can occur at certain density and temperature conditions even through the proton unbound nucleus ^{65}As due to its finite lifetime. Hence, sequential two-proton capture on the WP-nucleus can be much faster than the associated β-decay [12]. In this case, decay constant of the ^{64}Ge via two-proton capture can be expressed as follows [3]:

$$\lambda_{^{64}Ge\longrightarrow^{65}As\longrightarrow^{66}Se} = F(N_p,T,j_i,G_i)\times\exp\left(\frac{Q_{^{64}Ge\longrightarrow^{65}As}}{kT}\right)\times\lambda_{^{65}As\rightarrow^{66}Se} \quad (1)$$

where $F(N_p,T,j_i,G_i)$ is a function depending on proton density N_p, temperature T, nuclear spins j_i and normalized partition functions G_i (for i = ^{64}Ge, ^{65}As and proton); $Q_{^{64}Ge\longrightarrow^{65}As}$ is a Q value for proton capture on ^{64}Ge and $\lambda_{^{65}As\rightarrow^{66}Se}$ is a decay constant of ^{65}As with respect to subsequent proton capture. It can be seen that the breakout is not governed by the rate of ^{64}Ge$(p,\gamma)^{65}$As reaction, but by its Q-value, and by the rate of ^{65}As$(p,\gamma)^{66}$Se reaction.

- **^{57}Cu$(p,\gamma)^{58}$Zn**

  Similarly to the previous case, the reaction can lead to the breakout from doubly-magic WP-nucleus ^{56}Ni via sequential proton capture [13]. Early network calculations assumed that the rp-process stops at ^{56}Ni due to its low proton capture Q-value of 695 keV and comparatively long β-decay lifetime ($\tau = 2.3\times10^4$ s). However, later calculations [4, 14] employing larger networks show that the rp-process may process well beyond ^{56}Ni region. Influence of this reaction rate on the final chemical yelds, nuclear enegy generation rates and on the XBR light curves is also discussed in the recent state-of-the-art sensitivity studies [3, 9]

In the experiment, proton unbound states of ^{66}Se and ^{58}Zn will be populated by neutron removal reactions from ^{67}Se and ^{59}Zn beams, respectively, incident on the Be target at an energy 250 MeV/u. Proton decay spectroscopy of these states will be performed in-flight using the SAMURAI setup as explained in section 3.

2.2 Resonant reaction rates around WP-nucleus ^{34}Ar

- **^{34}Ar$(p,\gamma)^{35}$K**

  Together with ^{30}S, the WP-nucleus ^{34}Ar was theoretically linked to the phenomenon of the multiple-peaked structure observed in some X-ray bursts [15]. Since the rates near the proton drip line can be significantly affected by isolated resonances [16], the identification of these states are important together with the determination of resonance energies (E_R) and strengths ($\omega\gamma$), which are the only nuclear physics inputs into the resonant part of thermonuclear reaction rate. There is no experimental information on the resonance strengths, only shell model calculations are available to evaluate this reaction rate.

- **^{35}Ar$(p,\gamma)^{36}$K**

  When varied by a factor greater than 3, the reaction rate was found to significantly affect the calculated nuclear energy generation rate in the theoretical models [17]. The dramatic impact of ^{35}Ar$(p,\gamma)^{36}$K rate on XRB light curves had also been previously demonstrated by Thielemann [18]. Resonance strengths are not measured for this reaction yet.

- **^{35}K$(p,\gamma)^{36}$Ca**

  The reaction rate was identified by Amthor [19] as one of the 12 proton capture rates with an impact on predicted light curves. This rate was also found to affect predicted nuclear energy generation rates in the study of [17]. Presently, only the energy of one excited state is known in ^{36}Ca [20], and this state with tentative spin-parity assignment is the sole input considered in rate evaluations to date. so far.

The above three reactions will studied via coulomb dissociation of ^{35}K, ^{36}K and ^{36}Ca beams inside lead target at 200 MeV/u beam energy. One- and two-proton decays in-flight of these nuclei will be measured to extract energies and strengths of the resonances relevant to the rp-process.

2.3 Direct proton capture reaction rates ^{27}P$(p,\gamma)^{28}$S and ^{31}Cl$(p,\gamma)^{32}$Ar

These reactions are predicted to be among 10 most important reaction [19] with the strong influence on the calculated XRB light curves. Both reactions rates are expected to be dominated by a direct proton capture, because no excited states at astrophysically relevant energies are known for ^{32}Ar and ^{28}S. Coulomb dissociation cross section of time-reversal processes ^{32}Ar$\rightarrow^{31}$Cl+p and ^{28}S$\rightarrow^{27}$P+p will be measured with lead target and 250 Mev/u beam energies to extract direct-capture components of the reaction rates. Complementary measurements of proton-removal reactions in the nuclear field (e. g. using ^{12}C target) will be additionally performed to extract Asymptotic Normalization Coefficients, which can be directly related to the direct-capture cross section. Combining the information from the both type of measurements would help to constrain the model uncertainties and to determine the reaction rates with higher accuracy

2.4 Direct proton capture reaction rate ^{8}B$(p,\gamma)^{9}$C

The current knowledge of the rate of the ^{8}B$(p,\gamma)^{9}$C reaction in stellar conditions is contradictory at the best and there is no hope to determine it by other means than by indirect methods. This reaction gives a possible path to the hot pp chain pp-IV at high temperatures and away from it toward a rapid alpha process *rap* I at high temperatures and densities and therefore is important in understanding nucleosynthesis in super-massive hot stars in the early universe, including possible bypasses of the 3α-process [21]. Similar to the method described in subsection 2.3, breakup in nuclear and Coulomb fields at a beam energy of 300 MeV/u will be employed to estimate the direct-capture reaction rate.

3 Experimental appratus

3.1 SAMURAI setup

An overview of the intended experimental setup is shown in Fig.1. Radioactive secondary beams will be produced by the fragmentation of primary stable beams (e. g. ^{78}Kr, ^{40}Ca or ^{16}O) at a few hundreds MeV/u energy in beryllium target and separated by BigRIPS fragment separator [11]. The particle identification of the beam will be then performed event-by-event using the Bρ-ΔE-ToF method. A secondary reaction target will be placed at the target position of the Superconducting Analyzer for MUlti-particles from RAdioIsotope Beams (SAMURAI) [22] and the incident beam will be focused on the target via superconducting quadrupole magnet STQ. Incident secondary beams will be measured in the tracking systems before the target with two scintillating detectors, SBT1 and SBT2, for time-of-flight measurements. The position of hit on the target and incoming angle of the secondary beams will be measured by two drift chambers (BDC1,2) placed upstream of the target. An ionization chamber ICB will be used for charge identification of the incident ions. After traversing this pre-

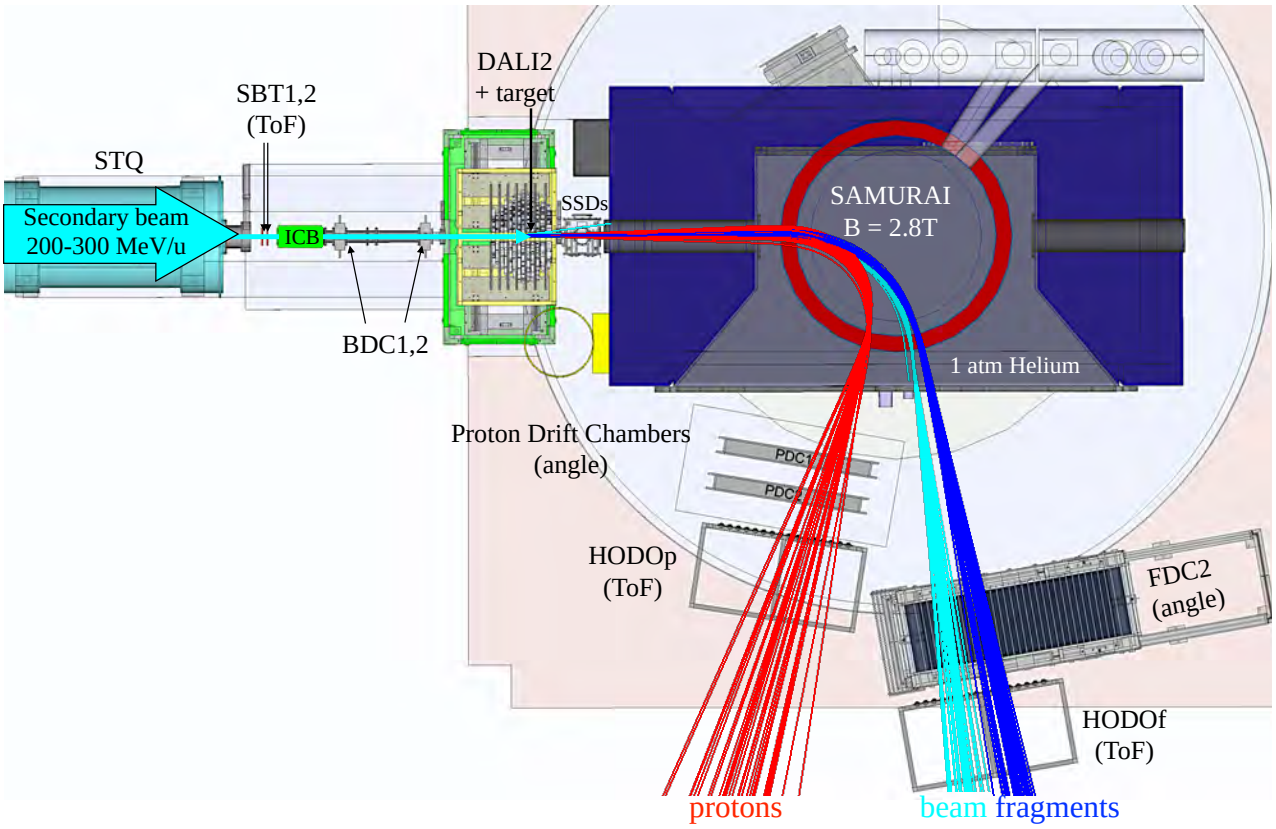

Fig. 1 High-Resolution (90°) mode of the SAMURAI setup will be used to measure heavy-ion-proton breakup reactions. Shown particle trajectories were simulated with Geant4 for the case of ^{28}S→^{27}P+p breakup. See text for more details.

target section the beam is incident on the reaction target (beryllium, carbon or lead) inside the DALI2 γ-ray detector that will measure gamma-rays in coincidence with charged fragments. Directly after the target an array of Silicon Strip Detectors (SSDs) will be used to measure trajectories of outgoing protons and fragments. Due to the wide dynamic range of these detectors ($\sim 10^4$), simultaneous detection and tracking of a proton and a heavy ion is possible. The SSDs will provide vital information about relative angles between the fragment and the proton with a resolution of a few mrad, which determines to a large extent the invariant mass reconstruction and the corresponding relative energy resolution. Next, the SAMURAI spectrometer, rotated 90 degrees with respect to the beam (High-Resolution mode) will separate the unreacted beam, breakup fragments and protons. The magnetic field will be set at around 2.8 Tesla in the center of the spectrometer filled with helium gas at 1 atmosphere pressure. After the magnet, the protons are tracked by the two proton drift chambers, PDC1 and PDC2. The heavy fragments and the unreacted beam are measured in a separate drift chamber, FDC2. The time of flight and ΔE of the decay products are measured in two hodoscopes, labeled HODP and HODF, for the protons and the heavy fragments, respectively. Hence, identification and momentum measurement of every traversing particle will be performed and the invariant-mass analysis of the reaction products will be applied to reconstruct the decay energy of the initial system.

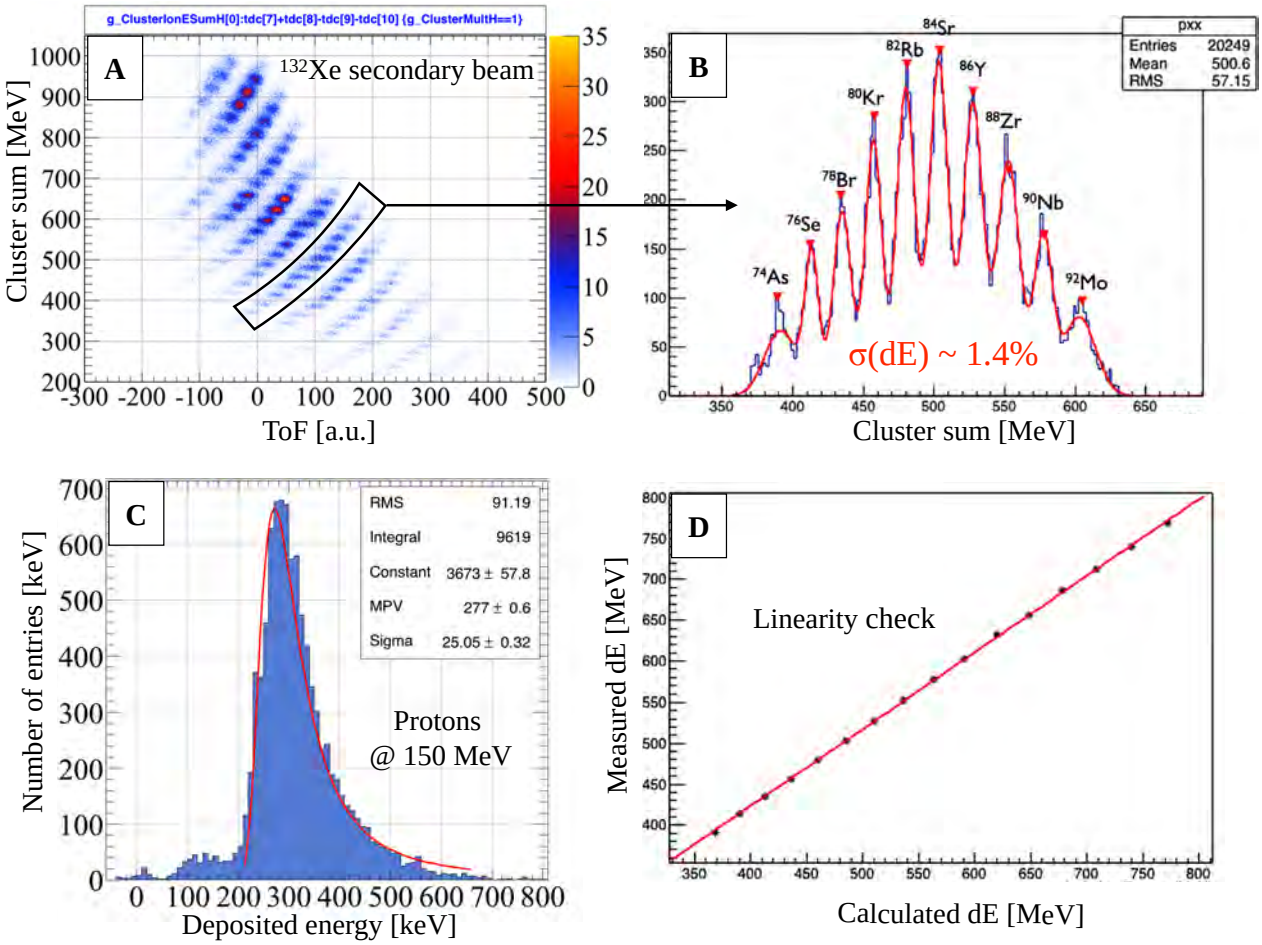

Fig. 2 Results of the performance test of the SSDs. Figure A shows the particle identification of ^{132}Xe secondary beam, using the deposited energy (strip-cluster sum) measured by low-gain readout of the SSD as a function of the ToF. Figure B shows the energy response in the SSD with the graphical cut indicated in Figure A, while Figure D displays the linearity check for this energy range by plotting measured energies against the calculated ones. A signal form 150 MeV proton in high-gain readout of the same SSD is shown in Figure C together with the Landau function fit.

3.2 Silicon Strip Detectors

An essential component of the setup will be an array of GLAST-type [23] single-sided Silicon Strip Detectors (SSDs) situated downstream of the target. Each detector is 325 μm thick and has dimensions of 87.6×87.6 cm^2 with 864 μm readout pitch size. Outgoing protons and heavy residues will be measured in the SSDs in order to reconstruct their relative angles with the precision of a few mrad. A key feature of the detectors is their wide dynamic range, which allows for simultaneous detection of protons and heavy ions, depositing in a single SSD a few hundred keV and up to 1 GeV energy, respectively. This is achieved via custom-designed ASIC dual-gain preamplifiers coupled to the high-density processing circuit HINP [24].

A performance test of the SSDs was conducted at the HIMAC facility in Japan, using irradiation of the detectors by proton beams at different energies (from 150 to 230 MeV/u) as well as by heavy-ion beams at a few hundred MeV/u in order to confirm the designed dynamic range. The results of the performance test are summarized in Fig.2. Good linearity of the low-gain readout was observed together with the deposited-energy (dE) resolution of $\sim 1.4\%$. The performance of the high-gain readout with respect to proton beams

was also confirmed, yielding a proton-detection efficiency of >97% and the cross-talk ratio of ∼1%. Thus, it was confirmed that the dynamic range of the SSDs spans from ∼100keV up to ∼ 1 GeV, which would allow simultaneous detection of protons and Z≈50 heavy ions in SAMURAI experiments.

3.3 Parameters of the experimental setup

Based on detailed Geant4 simulations of the particle transmission through the magnetic field of the SAMURAI spectrometer, and taking into account realistic detector responses, the following parameters of the setup can be estimated:

- Momentum resolutions: $P/\sigma_P \approx 1300$ for heavy ions and $P/\sigma_P \approx 500$ for protons;
- Angular resolutions: ∼3 mrad for protons and ∼2 mrad for heavy ions;
- Total detection efficincy: ∼100% for heavy ions and ∼20% for protons at relative energy E_{rel}=1 MeV;
- E_{rel} resolution ∼100 keV (sigma) at E_{rel}=1 MeV.

4 Summary and Outlook

The future experimental setup using SAMURAI spectrometer will serve as a powerful tool for systematic experimental studies of the most important (p,γ) reactions in the region of the astrophysical interest, using inverse and complete kinematics measurements of the heavy-ion-proton breakup reactions at relativistic energies. With the combination of the SAMURAI tracking detectors and the newly designed SSD trackers, possessing an extremely wide dynamic range, several neutron-deficient nuclei up to ^{100}Sn region can be potentially studied. The first experimental campaign will be ready to run in 2016, focusing on the proton decay of such exotic species as ^{66}Se, ^{58}Zn, ^{35}K, ^{36}K, ^{36}Ca, ^{28}S, ^{32}Ar and ^{9}C.

References

[1] W. H. G. Lewin, J. van Paradijs, and R. E. Taam, Space Science Rev., 1993, **62**:223.

[2] S. E.Woosley and R. E. Taam, Nature, 1976 **263**:101.

[3] A. Parikh, J. Jose, G. Sala, and C. Iliadis, Prog. Part. Nucl. Phys., 2013, **69**:225.

[4] H. Schatz et al, Phys. Rep., 1998, **294**:167.

[5] H. Schatz et al., Phys. Rev. Lett., 2001, **86**:3471.

[6] O. Koike et al., Astrophys. Jour., 2004, **603**:242.

[7] W. H. G. Lewin et al., Cambridge Univ. Press,1995, p. 175.

[8] A. Parikh et al., Phys. Rev. C, 2009, **79**:045802.

[9] A. Parikh et al., New Astron. Rev., 2008, **52**:409.

[10] H. Schatz, Int. Symp. Nucl. Astrophys., Nuclei in the Cosmos IX, 2006.

[11] http://www.nishina.riken.jp/RIBF/

[12] J. Görres, M. Wiescher, and F.-K. Thielemann, Phys. Rev. C, 1995, **51**:392.

[13] O. Forstner, H. Herndl, H. Oberhummer, H. Schatz, and B. A. Brown, Phys. Rev. C, 2001, **64**:045801.

[14] L. van Wormer, J. Gorres, C. Iliadis, M. Wiescher, and F.-K. Thielemann, Astrophys. Jour., 1994, **432**:326.

[15] J. L. Fisker et al. Astr. J., 2004 **608**:L61.

[16] H. Schatz et al. Nucl. Phys. A, 1999, **654**:924c.

[17] A. Parikh et al. Astr. J. Suppl., 2008, **178**:110.

[18] F. K. Thielemann et al. Prog. Part. Nucl. Phys., 2001, **46**:5.

[19] A. M. Amthor. PhD thesis, Michigan State University, 2008.

[20] A. Bürger et al. Phys. Rev. C, 2012, **86**:064609.

[21] M. Weischer et al., Astrophys. Jour., 1989, **343**:352

[22] T. Kobayashi et al., Nucl. Instr. Meth. Phys. Res., 2013 **B317**:294

[23] R. Bellazzini, Nucl. Instr. Meth. Phys. Res., 2003 **A512**:136.

[24] G. L. Engel, Nucl. Instr. Meth. Phys. Res., 2007, **A573**:418.

Peripheral elastic and inelastic scattering of 17,18 O on light targets at 12 MeV/nucleon

F. Carstoiu, T. Al-Abdullah, C. A. Gagliardi, and L. Trache

Citation: AIP Conference Proceedings **1645**, 39 (2015); doi: 10.1063/1.4909558
View online: http://dx.doi.org/10.1063/1.4909558
View Table of Contents: http://scitation.aip.org/content/aip/proceeding/aipcp/1645?ver=pdfcov
Published by the AIP Publishing

Peripheral elastic and inelastic scattering of ^{17,18}O on light targets at 12 MeV/nucleon

F. Carstoiu[*], T. Al-Abdullah[†], C.A. Gagliardi[**] and L. Trache[**]

[*]*National Institute for Physics and Nuclear Engineering Horia Hulubei, Bucharest, Romania*
[†]*Physics Department, The Hashemite University. Zarqa, Jordan*
[**]*Cyclotron Institute, Texas A&M University, College Station, Texas 77843, USA*

Abstract. The elastic and inelastic scattering of ^{17,18}O with light targets has been undertaken at 12 MeV/nucleon in order to determine the optical potentials needed for the transfer reaction ^{13}C(^{17}O,^{18}O)^{12}C. Optical potentials in both incoming and outgoing channels have been determined in a single experiment. This transfer reaction was used to infer the direct capture rate to the ^{17}F(p,γ)^{18}Ne which is essential to estimate the production of ^{18}F at stellar energies in ONe novae. We demonstrate the stability of the ANC method and OMP results using good quality elastic and inelastic scattering data with stable beams. The peripherality of our reaction is inferred from a semiclassical decomposition of the total scattering amplitude into barrier and internal barrier components. Comparison between elastic scattering of ^{17}O, ^{18}O and ^{16}O projectiles is made.

Keywords: Woods-Saxon potential, folding potentials, WKB.
PACS: 25.70.Bc, 25.70.Hi, 24.10.Ht.

INTRODUCTION

The ^{17}F(p,γ)^{18}Ne reaction is important for understanding nucleosynthesis in novae and plays a role in determining if radioactive nuclei with characteristic gamma-ray signature are produced in sufficient yield to be observed by gamma-ray satellites. The reaction rate is expected to be dominated by direct-capture cross section at nova temperatures and influences the abundances of ^{15}O, ^{17}F, ^{18}F and ^{18}Ne [1]. The rate also determines the ^{17}O/^{18}O ratio that is produced and explains the transition sequence from the HCNO cycle to the *rp*-process [2]. The primary goal of the experiment was the measurement of the peripheral neutron transfer reaction ^{13}C(^{17}O,^{18}O)^{12}C. Optical potentials in the incoming and outgoing channels have been obtained by measuring elastic scattering angular distributions ^{17}O+ ^{13}C and ^{18}O+ ^{12}C at 12 MeV/nucleon incident energy. The quality of the obtained potentials has been also checked from inelastic scattering to selected states in ^{17}O* and ^{18}O*. Since the ANC method assumes the peripherality of the reaction mechanism, we discuss here rather extensively this issue by decomposing semiclassically the total scattering amplitude into barrier and internal barrier subcomponents. We show that the internal barrier subcomponent, which corresponds to the flux penetrating the barrier, gives negligible small contribution to the total cross section, and thus the reaction is peripheral. The elastic scattering ^{17}O+^{13}C includes a weakly bound target.

Previously, ^{18}O+^{12}C elastic scattering at barrier energies was measured by Robertson *et al.*[3], by Szilner *et al.*[4] and Rudchik *et al.*[5] at some 5-7 MeV/nucleon. Fresnel scattering of ^{18}O on ^{28}Si was measured by Mermaz *et al.*[6] at 56 MeV. For the ^{17}O+ ^{13}C reaction the data are rather scarce, we identified a single fusion study and poor elastic angular distributions at barrier energies [7]. The main conclusion of these studies was that the interaction of ^{17,18}O nuclei with light targets is slightly more absorptive compared with that of the closed shell nucleus ^{16}O and that no significant effects due to the neutron excess were identified.

In Sec. II we give a short description of the experiment. Elastic scattering data and the derivation of the OM potentials are discussed in Sec. III. The semiclassical (WKB) method is used in Sec IV to decompose the total scattering amplitude into barrier and internal barrier components. Inelastic angular distributions to selected states in ^{18}O* and ^{17}O* are discussed in Sec. V. Our conclusions are summarized in Sec. VI.

THE EXPERIMENT

The experiment was carried out with two separate ^{17}O and ^{18}O beams from K500 superconducting cyclotron at Texas A&M University. Each beam was transported through the beam analysis system to the scattering chamber of the

Exotic Nuclei and Nuclear/Particle Astrophysics (V). From Nuclei to Stars
AIP Conf. Proc. 1645, 39-51 (2015); doi: 10.1063/1.4909558

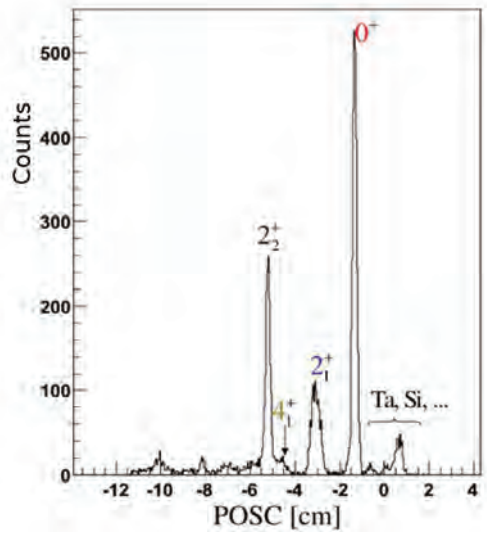

FIGURE 1. (Color online) Low-lying spectrum of ^{18}O versus the particle position in the focal plane, measured at the spectrometer angle of 4°. The peaks at the right of the elastic peak are due to Si and Ta contaminants in the target.

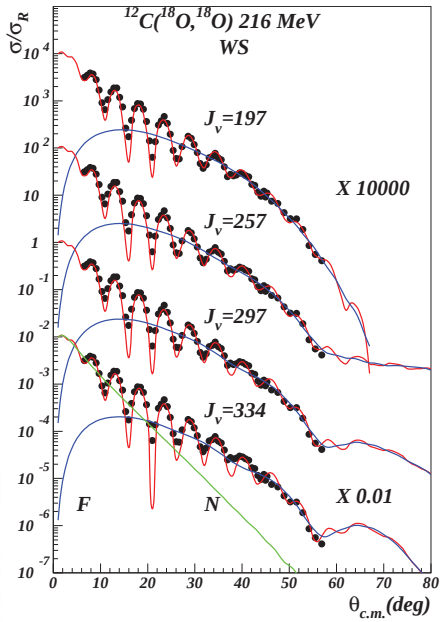

FIGURE 2. (Color online) Cross section and far side/near side (F/N) decomposition of the scattering amplitude for WS potentials in Table 1. Each calculation is identified by its real volume integral J_V and shifted by factors X to increase the visibility.

multipole-dipole-multipole (MDM) magnetic spectrometer [8], where it interacted with 100 μg/cm^2 self-supporting targets.

First, the ^{17}O beam impinged on ^{13}C target enriched up to 99%. We continuously monitored the excitation of the 4.44 MeV state in ^{12}Cin order to estimate the carbon deposition during the exposure and found negligible small contribution. The elastic scattering angular distribution was measured for the spectrometer angles 4°-25° in the laboratory system. Fine tuned RAYTRACE [9] calculations were used to reconstruct the position of particles in the focal plane and the scattering angle at the target. A 4° × 1° wide-opening mask and an angle mask consisting of five narrow ($\Delta\theta$ = 0.1°) slits were used for each spectrometer angle to double-check the absolute values of the cross section and the quality of the angle calibration. The instrumental setup, including the focal plane detector, and processes for energy and angle calibrations, are identical to that described in Ref. [10]. Second, the ^{12}C target was bombarded by ^{18}O beam with 216 MeV total laboratory energy. The elastic scattering cross section was measured at 4°-22° spectrometer angles.

ELASTIC SCATTERING

Woods-Saxon formfactors

The measured elastic scattering data at E_{lab}=216 and 204 MeV are shown in Figs. 2 and 3. The data are first analyzed using optical potentials with conventional Woods-Saxon (WS) form factors for the nuclear term, supplemented with a Coulomb potential generated by a uniform charge distribution with a reduced radius fixed to r_c=1 fm. No preference has been found for volume or surface localized absorption and throughout the paper only volume absorption is considered. In the absence of any spin dependent observables, spin-orbit or tensor interactions have been ignored. Ground state reorientation couplings have been neglected also. The potential is defined by six parameters specifying the depth and geometry of the real and imaginary terms, with the standard notations, the same as used in Ref. [11]. The number of data points N is quite large, and consequently the usual goodness of fit criteria (χ^2) normalized to N has been used.

Using the strength of the real component of the optical potential as a control parameter, a grid search procedure

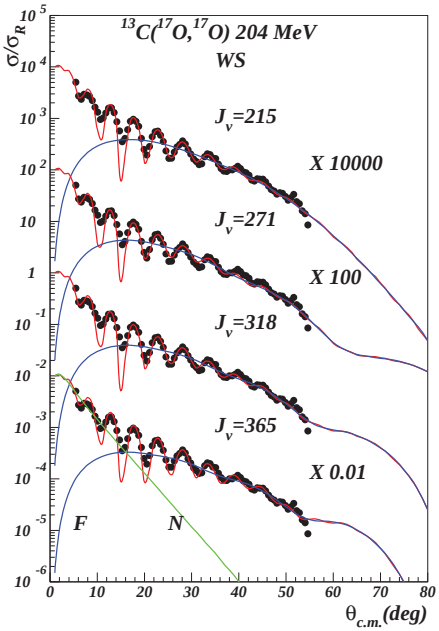

FIGURE 3. (Color online) Cross sections and F/N decomposition for the WS potentials Table 1. The far side component shows Airy oscillation which moves to forward angles with increased value of the real volume integral.

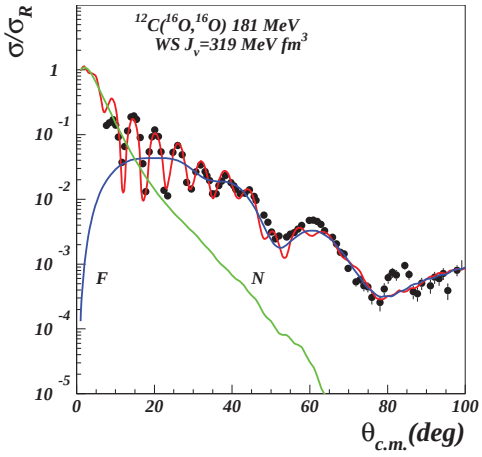

FIGURE 4. (Color online) Elastic scattering $^{16}O+^{12}C$ at 11.3 MeV/nucleon. The real part of the WS optical potential is much stronger and the far side component shows several deep Airy oscillations. Experimental data are taken from [12].

TABLE 1. Discrete solutions obtained with WS form factors for $^{18}O+^{12}C$ at 216 MeV and $^{17}O+^{13}C$ at 204 MeV. The line labeled PP9 is a WS phase equivalent of the JLM1 solution.

pot	V MeV	W MeV	r_V fm	r_W fm	a_V fm	a_W fm	χ^2	σ_R mb	J_V MeV fm^3	R_V fm	J_W MeV fm^3	R_W fm
$^{18}O+^{12}C$ at 216 MeV												
PP5	89.18	25.24	0.88	1.16	0.88	0.68	5.12	1712	197	4.69	103	5.09
PP6	195.40	25.59	0.68	1.16	0.96	0.67	6.39	1702	257	4.40	104	5.07
PP7	295.82	26.00	0.60	1.16	0.95	0.67	7.54	1696	297	4.20	106	5.06
PP8	374.41	26.19	0.58	1.16	0.90	0.68	9.78	1695	334	4.01	107	5.06
PP9	75.68	26.16	0.89	1.15	0.93	0.66	5.31	1677	178	4.85	104	5.02
$^{17}O+^{13}C$ at 204 MeV												
T1	94.69	26.91	.91	1.13	.84	.67	4.47	1659	215	4.67	99	4.96
T2	188.40	24.95	.72	1.12	.94	.69	4.62	1667	271	4.44	92	4.99
T3	248.75	26.36	.69	1.13	.90	.66	4.53	1659	318	4.27	99	4.97
T4	275.49	25.63	.73	1.15	.81	.65	5.90	1660	365	4.11	100	5.00

revealed a number of discrete solutions. Their parameters are presented in Table 1. The ambiguity in the optical potential has two main sources: the limited range of the measured angles and the strong absorption. When the strong absorption dominates the reaction mechanism, then the interaction is sensitive only to the surface and several phase equivalent optical potentials will appear. The patterns shown in Figs 2 and 3 show rapid oscillation at forward angles followed by a smooth fall-off at intermediate angles. Assuming pure Fraunhofer scattering at forward angles, we extract a grazing angular momentum $\ell_g \approx 36$ from the angular spacing $\Delta\theta = \pi/(\ell_g + 1/2)$. The corresponding grazing distance is quite large, $R_g \approx 7$ fm, much larger than the distance of touching configuration. We systematically find diffuse real potentials ($a_V \approx 0.9$ fm). This effect may be tentatively attributable to the neutron excess. We find also quite constant volume integrals and *rms* radii for the imaginary component. As a consequence the total reaction cross section seems to be a well defined observable. Weighted average values from Table 1 and Table 2 are $\sigma_R = 1713 \pm 35$ mb and

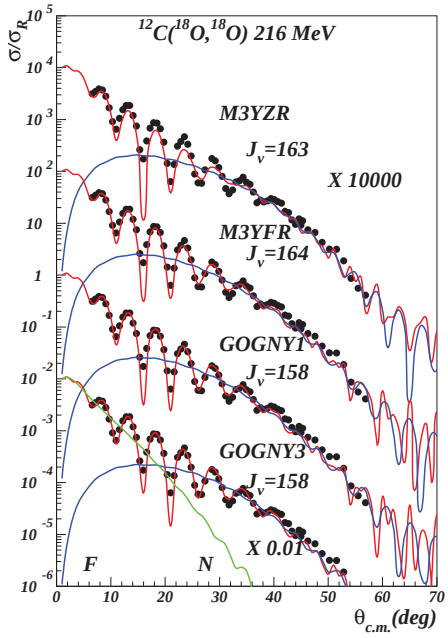

FIGURE 5. (Color online) Cross section calculated with folding form factors using the M3Y and GOGNY models. The real volume integral is indicated on each curve. The far side/near side components of the cross section are denoted by F/N. Experimental data and calculation have been shifted by factor X to increase visibility.

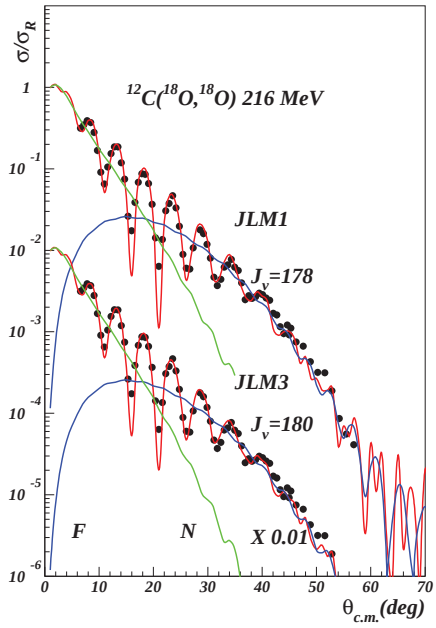

FIGURE 6. (Color online) The same as in Fig.5 but for the JLM model.

$\sigma_R = 1699 \pm 36$ mb for ^{18}O+^{12}C and ^{17}O+^{13}C reactions respectively. For the largest real volume integral an Airy oscillation forward to a primary rainbow becomes apparent. Usually, the dominance of the far-side component beyond the Fraunhofer crossover is interpreted as a signature of refractive effects due to a strongly attractive real potential and weak absorption. We will show bellow that the strong absorption is still the dominant reaction mechanism.

A comparison with the scattering of the tightly bound nucleus ^{16}O is in order. Experimental data [12] and our calculation for ^{16}O+^{12}C at 11.3 MeV/nucleon are displayed in Fig. 4. We did not find any reasonable WS solution with $J_V < 300$ MeV fm^3 and so the solution with the lowest acceptable real volume integral is plotted. Since the potential is strong, the far-side component of the cross section is much more structured. While the Fraunhofer (diffractive) part at forward angles is similar to our reactions, strong refractive effects appear at $\theta > 40^\circ$ as deep Airy oscillations.

Folding formfactors

In the following we discuss the ability of the folding model to describe our data. We start by a quite simple model in which the spin-isospin independent formfactor of the OMP is given by the double folding integral,

$$V_{fold}(R) = \int d\vec{r}_1 d\vec{r}_2 \rho_1(r_1)\rho_2(r_2) v_{M3Y}(s) \tag{1}$$

where v_{M3Y} is the M3Y parametrization of the G-matrix obtained from the Paris NN interaction [13], and $\vec{s} = \vec{r}_1 + \vec{R} - \vec{r}_2$ is the NN separation distance. For the reaction ^{17}O+^{13}C we add the small isovector component arising from the nonnegligible neutron skin present in both interacting partners. The Coulomb component of the optical potential is calculated by replacing the nuclear s.p. densities with proton densities and using $v_{coul}(s) = e^2/s$ as effective interaction. The small effect arising from finite proton size is ignored. In the simplest version of this model, dubbed here as

TABLE 2. Unique solutions obtained with folding form factors for ^{18}O+^{12}C at 216 MeV and ^{17}O+^{13}C at 204 MeV.

pot	N_V	N_W	t_V	t_W	χ^2	σ_R mb	J_V MeV fm^3	R_V fm	J_W MeV fm^3	R_W fm
^{18}O+^{12}C at 216 MeV										
M3YZR	0.37	0.20	0.88	0.80	10.72	1812	163	4.60	86	5.06
M3YFR	0.33	0.21	0.88	0.86	8.15	1737	164	4.68	103	4.83
GOGNY1	0.28	0.18	0.89	0.87	7.27	1707	158	4.70	103	4.83
GOGNY3	0.37	0.21	0.91	0.84	7.39	1767	158	4.69	89	5.08
JLM1	0.33	0.93	0.87	0.86	6.87	1675	178	4.55	109	4.80
JLM3	0.36	1.02	0.86	0.85	6.75	1708	180	4.56	102	4.85
^{17}O+^{13}C at 204 MeV										
M3YZR	0.46	0.22	0.91	0.85	5.24	1742	203	4.48	95	4.80
M3YFR	0.38	0.18	0.93	0.86	5.16	1738	196	4.52	94	4.87
GOGNY1	0.32	0.15	0.94	0.85	5.74	1748	188	4.53	88	4.99
GOGNY3	0.41	0.20	0.95	0.87	6.03	1729	186	4.53	88	4.97
JLM1	0.35	0.72	0.89	0.84	6.06	1691	196	4.47	84	4.96
JLM3	0.37	0.80	0.88	0.83	5.63	1719	192	4.49	81	5.00

M3YZR, the knockon exchange component is simulated by a zero range potential with a slightly energy dependent strength,

$$J_{00}(E) = -276(1 - 0.005E/A) \tag{2}$$

We keep the number of fitting parameters at the minimum level and take the OMP in the form,

$$U(R) = N_V V(R, t_V) + iN_W V(R, t_W) \tag{3}$$

where $N_{V,W}$ are normalization constants and $t_{V,W}$ are range parameters defined by the scaling transformation,

$$V(R,t) \rightarrow t^3 V_{fold}(tR) \tag{4}$$

This transformation conserves the volume integral of the folding potential and modifies the radius as,

$$< R^2 >_V = \frac{1}{t^2} < R^2 >_{fold} \tag{5}$$

Thus the strength of the formfactor is controlled by the parameters $N_{V,W}$. Note that the transformation in Eq. (4) ensures that only the *rms* radius of the bare folding potential is changed. Based on Eq. (5) one may estimate in an average way the importance of the dynamic polarization potential (DPP) and finite range effects. Throughout this paper we use single particle densities obtained from a spherical Hartree-Fock (HF+BCS) calculation based on the density functional of Beiner and Lombard [15]. The obtained *rms* charge radii are very close to the experimental values [16] and the model predicts a neutron skin $\Delta r = r_n - r_p$ of 0.1, 0.18 and 0.1 fm for ^{13}C, ^{18}O, ^{17}O respectively. The calculated neutron *rms* radii are 2.84 and 2.76 fm for ^{18}O, ^{17}O in good agreement with the values extracted by Khoa *et al.*[17] from high energy interaction cross section. Note that for the weakly bound ^{13}C ($S_n = 4.9$ MeV) this model predicts a small occupation probability for the neutron $2s_{1/2}$ level of $v^2_{2s_{1/2}} = 0.0016$ but this has a small influence on the tail of the s.p. density. A more elaborate calculation leads to a nonlocal knockon exchange kernel [18],

$$\begin{aligned} U_{ex}(\vec{R}^+, \vec{R}^-) = \mu^3 v_{ex}(\mu R^-) \int d\vec{X}_1 \rho_1(X_1) \hat{j}_1(k_{f1}(X_1) \frac{(A_1-1)A_2}{A_1+A_2} R^-) \\ \times \rho_2(|\vec{R}^+ - \vec{X}_1|) \hat{j}_1(k_{f2}(|\vec{R}^+ - \vec{X}_1|) \frac{(A_2-1)A_1}{A_1+A_2} R^-) \end{aligned} \tag{6}$$

where $A_{1,2}$ are mass numbers, μ is the reduced mass of the system, $k_{f1,2}$ are Fermi momenta, $R^{+,-}$ are the usual nonlocal coordinates and v_{ex} is the exchange component of the interaction including the long range OPEP tail.

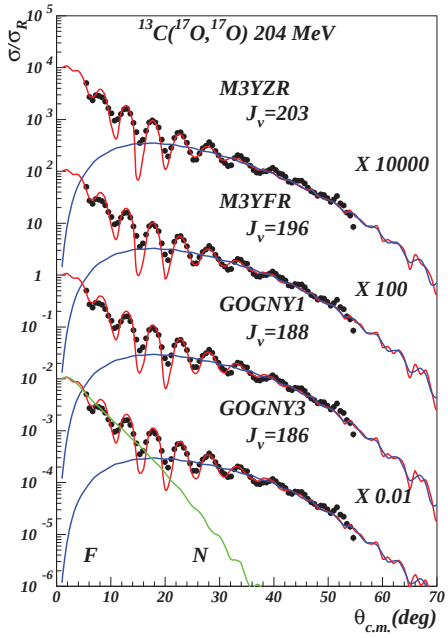

FIGURE 7. (Color online) Cross section and F/N decomposition with folding form factors. Parameters are taken from Table 2.

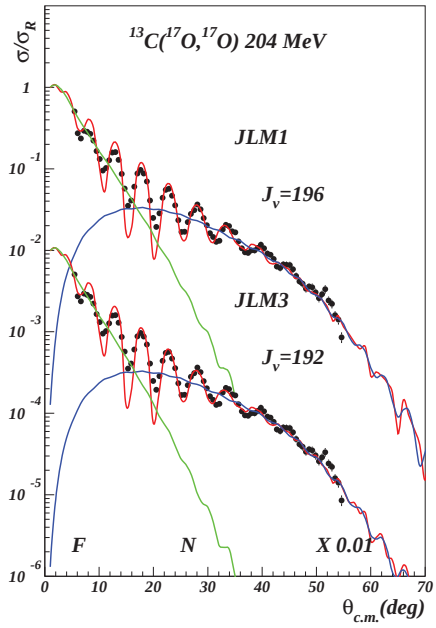

FIGURE 8. (Color online) Cross section and F/N decomposition using the JLM form factors

Eq. (6) already shows that the nonlocality is small and behaves as $\sim \mu^{-1}$. In the lowest order of the Perey-Saxon approximation, the local equivalent of the nonlocal kernel is obtained by solving the nonlinear equation,

$$U_L(R) = 4\pi \int d\vec{r}_1 d\vec{r}_2 \rho_1(r_1)\rho_2(r_2) \int s^2 ds v_{ex}(s) \hat{j}_1(k_{f1}(r_1)\beta_1 s) \hat{j}_1(k_{f2}(r_1)\beta_2 s) j_0(\frac{1}{\mu} K(R)s) \delta(\vec{r}_2 - \vec{r}_1 + \vec{R}) \quad (7)$$

Above $\beta_i = (A_i - 1)/A_i$ are recoil corrections, $\hat{j}_1(x) = 3j_1(x)/x$ and $j_{0,1}$ are spherical Bessel functions. The local Fermi momenta k_f are evaluated in an extended Thomas-Fermi approximation [19]. The local momentum for the relative motion is given by,

$$K^2(R) = \frac{2\mu}{\hbar^2}(E_{c.m.} - U_D(R) - U_L(R)) \quad (8)$$

where U_D is the total direct component of the potential including the Coulomb term. In Eq. (8) we assumed a purely real local momentum of the relative motion since the absorptive component of the OMP is small compared with the real part. The effective mass correction [21], $\frac{\mu^\star}{\mu} = 1 - \frac{\partial U}{\partial E}$ is of the order of a few percent for our systems and is absorbed in the renormalization parameter N_W. Calculations with finite range model are dubbed M3YFR.

Neglecting the spin-orbit component, the Gogny NN effective interaction can be expressed as a sum of a central, finite range term and a zero range density dependent term,

$$v(\vec{r}_{12}) = \sum_{i=1}^{2} (W_i + B_i P_\sigma - H_i P_\tau - M_i P_\sigma P_\tau) e^{-\frac{r_{12}^2}{\mu_i^2}} + t_3(1 + P_\sigma)\rho^\alpha(\vec{R}_{12})\delta(\vec{r}_{12}) \quad (9)$$

where $\vec{r}_{12} = \vec{r}_1 - \vec{r}_2$, $\vec{R}_{12} = (\vec{r}_1 + \vec{r}_2)/2$ and standard notations have been used for parameter strengths and spin-isospin exchange operators. The strengths parameters and the ranges are taken from [22]. Antisymmetrization of the density

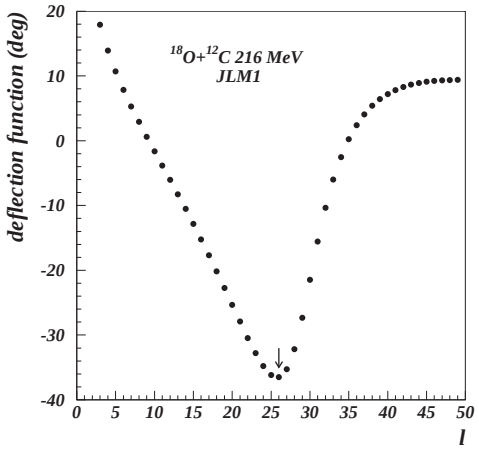

FIGURE 9. Classical deflection function for the WS potential equivalent to JLM1. The rainbow angle is $\theta_R = 36°$. The entire measured angular range is illuminated.

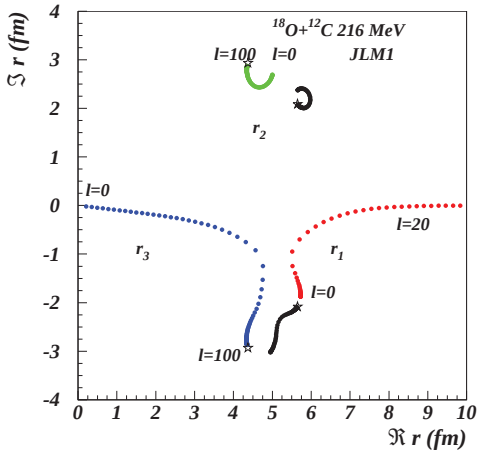

FIGURE 10. (Color online) Complex turning points for the WS potential equivalent to JLM1. The stars denote the complex poles of the potential.

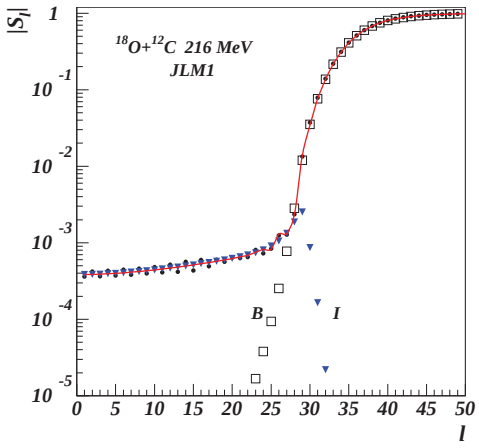

FIGURE 11. (Color online) Semiclassical absorption profile for the WS potential equivalent to JLM1. The barrier and internal barrier components of the S-matrix are shown by open squares and triangles respectively. The barrier component is typical for strong absorption. The black dots denote the exact quantum result for the same potential and the line is a spline interpolation of the WKB S-matrix.

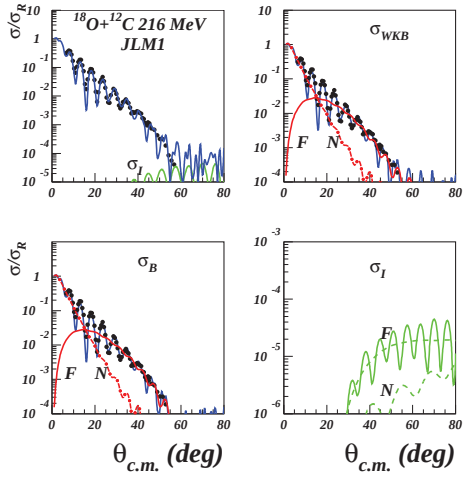

FIGURE 12. (Color online) Semiclassical calculation of the cross section based on the WS potential equivalent to JLM1. The WKB scattering amplitude is further decomposed into barrier (σ_B) and internal barrier (σ_I) components. The internal barrier component is negligible small in the measured angular range. The reaction is peripheral.

dependent term is trivial, so that the sum of direct and exchange term reads,

$$v_D^\rho(r_{12}) + v_{ex}^\rho(r_{12}) = \frac{3t_3}{4}\rho^\alpha \delta(\vec{r}_{12}) \tag{10}$$

The local equivalent of the finite range knockon exchange is calculated with Eq. (7). Two approximations were used for the overlap density,

$$\rho = (\rho_1(r_1)\rho_2(r_2))^{1/2} \tag{11}$$

and

$$\rho = \frac{1}{2}(\rho_1(r_1) + \rho_2(r_2)) \tag{12}$$

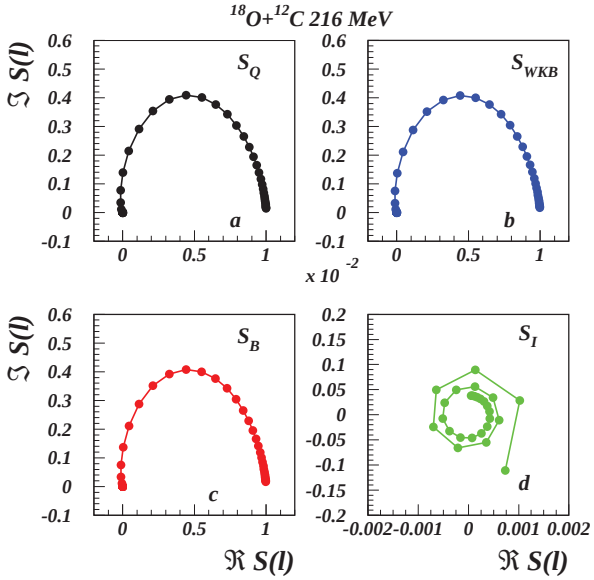

FIGURE 13. (Color online) Argand diagram for the semiclassical S-matrix based on the WS potential equivalent to JLM1. The barrier trajectory (panel c) is identical to the exact quantum result (panel a). The small internal barrier component (panel d) shows a hint of an orbiting effect or the presence of Regge poles, but these are too far from the real axis to have noticeable effect in the total cross section.

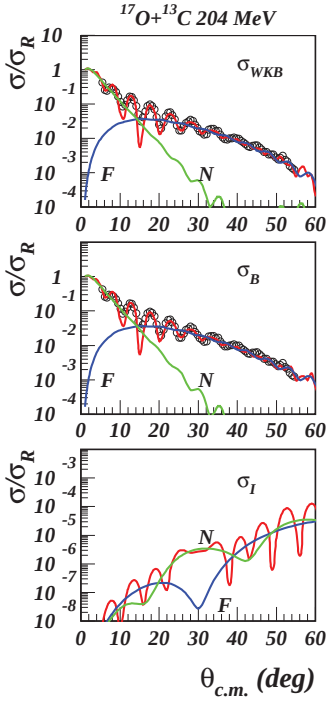

FIGURE 14. Semiclassical (WKB) calculation of the cross section based on the T1 potential Table 1. The barrier component match perfectly the data in the entire angular range, while the internal barrier component is negligibly small.

The calculated OM potentials are dubbed GOGNY1 and GOGNY3 respectively. Both definitions represent crude approximations of the overlap density but are widely used in the estimation of the density dependence effects in the folding model.

We further examine the density dependence effects by using the nuclear matter approach of Jeukenne, Lejeune and Mahaux (JLM) [14] which incorporates a complex, energy and density dependent parametrization of the NN effective interaction obtained in a Brueckner Hartree-Fock approximation from the Reid soft core NN potential. The systematic study [11] of the elastic scattering between *p*-shell nuclei at energies around 10 MeV/nucleon leads to the surprising result that on average, the imaginary part of the folded JLM potential was perfectly adequate to describe such reactions and did not need any renormalization ($N_W = 1.00 \pm 0.09$), while the real component needed a substantial renormalization, in line with other effective interactions used in folding models. We examine here to which extent this feature is conserved for tightly bound nuclei in the *d* shell in the presence of a small neutron excess. Exchange effects are included in this model at the level of N-target interaction. Calculations with this model are dubbed JLM1 and JLM3, depending on which definition we use for the overlap density (Eqs.(11) and (12) respectively).

A grid search on the real volume integral reveals a unique solution for all six versions of the effective interaction, see Table 2 and Figs 5, 6, 7 and 8. The folding model validates only the solution with the lowest real volume integral found with the WS parametrization. Averaging over all six folding calculations, we find $J_V = 167 \pm 9$ MeV fm^3 for ^{18}O and $J_V = 194 \pm 5$ MeV fm^3 for ^{17}O and so the interaction of ^{17}O is slightly more refractive. Again imaginary volume integrals are quite small pointing to a some transparency of the potential. Correction due to the finite range effects are quite large, of the order of $\Delta R \approx 0.5$ fm for the real potential and much larger for the imaginary potential. The folding calculation reproduces perfectly the diffractive pattern at forward angles and the Fraunhofer F/N crossover produces always an interference maximum. Beyond the cross-over the far-side component decays quite smoothly and shows some glory effects at $\theta > 60^\circ$.

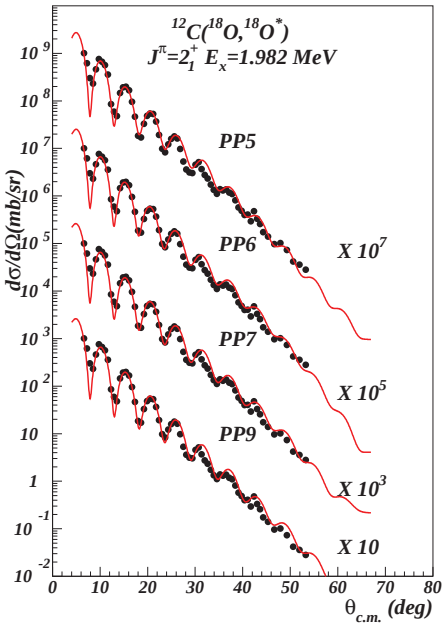

FIGURE 15. (Color online) Inelastic cross section to 2_1^+ (1.982 MeV) state in ^{18}O. The DWBA calculation is based on the potentials in Table 1.

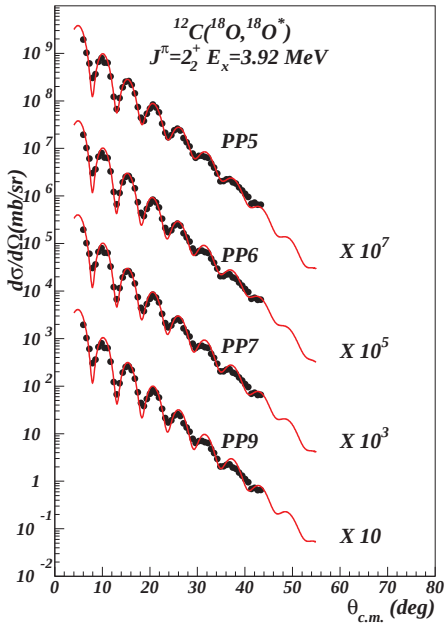

FIGURE 16. (Color online) Inelastic cross section to 2_2^+ (3.92 MeV) state in ^{18}O. The DWBA calculation is based on the potentials in Table 1.

A close examination of the results in Table 2 shows that we have obtained consistent results for all effective interactions used in the folding model. Our results confirm the conjecture that one can extract from the elastic scattering at best only the low momenta of the interaction (volume integrals and *rms* radii). Corrections in the range parameters are large especially for the imaginary component of the optical potential. We found substantial renormalization for the real part of the optical potential, on average $N_V = 0.36 \pm 0.05$ in line with the previous study [11]. This can be easily understood: the bare folding formfactor has a volume integral around $J_V \approx 450$ MeV fm^3, while the data requires precise values around 160-190 MeV fm^3. Noteworthy, the renormalization of the imaginary component in the JLM model is again quite close to unity. Although the density dependence in the GOGNY and JLM effective interactions is very different, one cannot disentangle between the two models for the overlap density based on the present data, since both of them give identical results.

SEMICLASSICAL BARRIER AND INTERNAL BARRIER AMPLITUDES

Once we have established the main features of the average OM potential, we turn now to study the reaction mechanism using semiclassical methods.

The semiclassical uniform approximation for the scattering amplitude of Brink and Takigawa [26] is well adapted to describe situations in which the scattering is controlled by at most three active, isolated, complex turning points. An approximate multireflection series expansion of the scattering function can be obtained, the terms of which have the same simple physical meaning as in the exact Debye expansion for the scattering of light on a spherical well. The major interest in this theory comes from the fact that it can give precious information on the response of a nuclear system to the nuclear interior.

We take as an example the potential PP9 in Table 1 which is a WS phase equivalent to the JLM1 optical potential. We discard the absorptive term and define the effective potential as,

$$V_{eff}(r) = V(r) + \frac{\hbar^2}{2\mu}\frac{\lambda^2}{r^2}, \quad \lambda = \ell + \frac{1}{2} \tag{13}$$

where the Langer prescription has been used for the centrifugal term. This guarantees the correct behavior of the semiclassical wave function at the origin. Then we calculate the deflection function,

$$\Theta(\lambda) = \pi - 2\int_{r_1}^{\infty} \frac{\sqrt{\frac{\hbar^2}{2\mu}}\lambda dr}{r^2\sqrt{E_{c.m.} - V_{eff}}} \tag{14}$$

where r_1 is the outer zero of the square root, i.e. the radius of closest approach to the scatterer and μ is the reduced mass. Note that with the replacement $\hbar\lambda = b\sqrt{2\mu E}$, Eq. 14 becomes identical with the classical deflection function $\Theta(b)$, where b is the impact parameter. The result is shown in Fig. 9. The behavior of $\Theta(\lambda)$ is the one expected for an attractive nuclear potential. The nuclear rainbow angle is $\theta_R \approx 36^\circ$. All the measured angular range is classically illuminated and only a few points were measured in the dark side. This explains partially the ambiguities found with the WS formfactors.

However this simple calculation does not provide too much information about the interference effects of the corresponding semiclassical trajectories. Going into the complex r-plane we search for complex turning points, i.e. the complex roots of the quantity $E_{c.m.} - V_{eff} - iW$. This is an intricate numerical problem, because, for a WS optical potential, the turning points are located near the potential singularities and there are an infinite number of such poles. The situation for integer angular momenta is depicted in Fig. 10. Active turning points are located near the poles of the real formfactor. Inactive turning points are located quite far from the real axis and give negligible small contribution to the total S-matrix. We observe an ideal situation with three, well isolated, turning points for each partial wave. The multireflection expansion of the scattering function in the Brink-Takigawa approach reads,

$$S_{WKB}(\ell) = \sum_{q=0}^{\infty} S_q(\ell) \tag{15}$$

where,

$$S_0(\ell) = \frac{\exp(2i\delta_1^\ell)}{N(S_{21}/\pi)} \tag{16}$$

and for $q \neq 0$,

$$S_q(\ell) = (-)^{q+1}\frac{\exp[2i(qS_{32} + S_{21} + \delta_1^\ell)]}{N^{q+1}(S_{21}/\pi)} \tag{17}$$

In these equations δ_1^ℓ is the WKB (complex) phase shift corresponding to the turning point r_1, $N(z)$ is the barrier penetrability factor,

$$N(z) = \frac{\sqrt{2\pi}}{\Gamma(z+\frac{1}{2})}\exp(z\ln z - z) \tag{18}$$

and S_{ij} is the action integral calculated between turning points r_i and r_j,

$$S_{ij} = \int_{r_i}^{r_j} dr\{\frac{2\mu}{\hbar^2}[E_{c.m.} - V_{eff} - iW]\}^{1/2} \tag{19}$$

S_{21} and S_{32} are independent of the integration path provided they lie on the first Riemann sheet and collision with potential poles is avoided. Each term in Eq. 15 has a simple physical interpretation. The first term (the barrier term, denoted also S_B) retains contributions from trajectories reflected at the barrier, not penetrating the internal region. The qth term corresponds to trajectories refracted q times in the nuclear interior with q-1 reflections at the barrier turning point r_2. Summation of terms $q \geq 1$ can be recast into a single term,

$$S_I = \frac{\exp[2i(S_{32} + S_{21} + \delta_1^\ell)]}{N(S_{21}/\pi)^2}\frac{1}{1 + \exp[2iS_{32}]/N(S_{21}/\pi)} \tag{20}$$

and is known as the internal barrier scattering function. The last factor in Eq. 20, the enhancement factor, is responsible for the multiple reflections of the wave within the potential pocket. When the absorption in the nuclear interior is large, the enhancement factor reduces to unity. Since the semiclassical scattering function is decomposed additively, $S_{WKB} = S_B + S_I$, the corresponding total scattering amplitude is decomposed likewise as $f_{WKB} = f_B + f_I$ and conveniently the

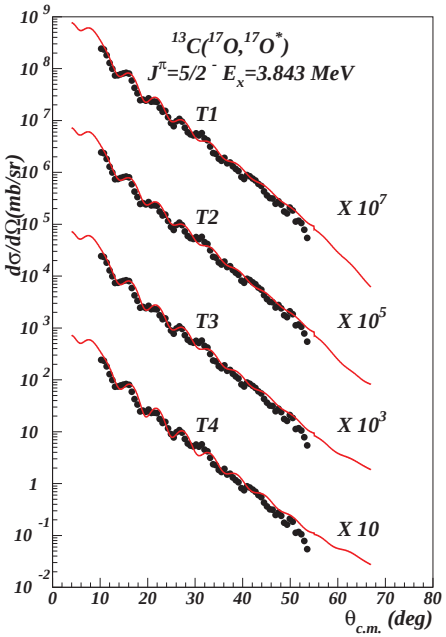

FIGURE 17. (Color online) Inelastic cross section to $5/2^-$ (3.84 MeV) state in ^{17}O. The DWBA calculation is based on the potentials in Table 1.

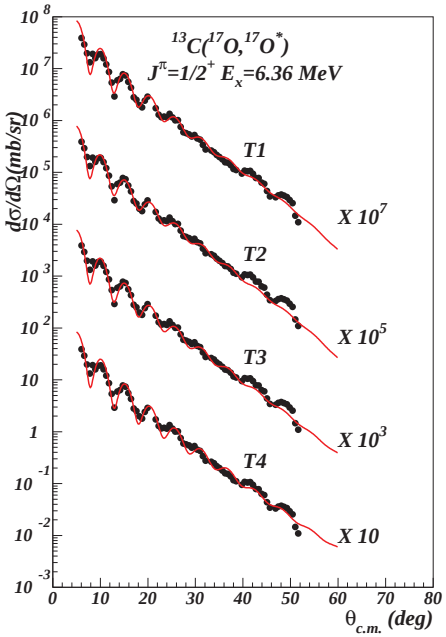

FIGURE 18. (Color online) Inelastic cross section to $1/2^+$ (6.36 MeV) state in ^{17}O. The DWBA calculation is based on the potentials in Table 1.

corresponding barrier and internal barrier angular distributions are calculated as $\sigma_{B,I} = |f_{B,I}|^2$, using the usual angular momentum expansion of the amplitudes.

The poles of the semiclassical S-matrix are given by,

$$N(i\varepsilon) + e^{2iS_{32}} = 0 \;\; ; \;\; \varepsilon = -\frac{i}{\pi} S_{21} \tag{21}$$

Semiclassical Regge poles of Eq. 21 are too far from the real axis to have a noticeable influence on the total cross section. The accuracy of the semiclassical calculation has been checked by comparing the barrier and internal barrier absorption profiles with the exact quantum-mechanical result in Fig. 11. One observes that the semiclassical B/I expansion is an *exact* decomposition of the quantum result. They are virtually identical at the scale of the figure. The internal component gets significant values up to the grazing angular momentum (ℓ_g=36) and is negligible small beyond this value. The barrier component resembles a strong absorption profile and this justifies the interpretation that it corresponds to that part of the flux not penetrating into the nuclear interior. Second, the B/I components are almost decoupled in the angular momentum space and therefore they will contribute in different angular ranges.

Semiclassical cross sections are compared with the data in Fig. 12. Better insight into this technique is obtained by further decomposing the B/I components into far and near (BF/BN and IF/IN) subcomponents. Clearly, the barrier component dominates the entire measured angular range. Fraunhofer diffractive oscillations appear as the result of BF and BN interference. At large angles, the internal contribution is negligible and the reaction is peripheral.

The Argand diagrams corresponding to the B/I decomposition is displayed in Fig. 13. The barrier amplitude (panel c) is almost identical with the exact quantum result (panel a) while the internal barrier component shows a nice orbiting effect, but the corresponding dynamical content ($S_I(\ell)$ is too small to have any sizeable effect in the total cross section.

A similar analysis was performed for the reaction ^{17}O+^{13}C based on the WS potential, parameter set T1 Table 1. Again we find that the WKB cross section is identical with the exact quantum result based on the same potential. The barrier component match perfectly the data in the entire angular range, while the internal barrier component gives negligible contribution, see Fig.14. Thus the peripherality character of our reactions is completely demonstrated.

INELASTIC TRANSITIONS

TABLE 3. Average deformation obtained from inelastic scattering.

Nucleus	J^π	β_λ
^{17}O	$5/2^-$	0.66 ± 0.03
^{17}O	$1/2^+$	0.19 ± 0.01
^{18}O	2_1^+	0.38 ± 0.04
^{18}O	2_2^+	0.52 ± 0.05

We examine in this section the ability of our optical potentials to describe the measured data for inelastic transitions to selected states in ^{18}O ($J^\pi = 2_1^+, E_x = 1.982$ MeV, Fig. 15 and $J^\pi = 2_2^+, E_x = 3.92$ MeV, Fig. 16) and two transitions in ^{17}O ($J^\pi = \frac{5}{2}^-, E_x = 3.843$ MeV, Fig. 17 and $J^\pi = \frac{1}{2}^+, E_x = 6.36$ MeV, Fig. 18).

The pattern of our data shows a clear diffractive character since they obey fairly well to the Blair phase rule [27] and therefore a standard DWBA should be an appropriate approach. The deformation table [28] indicates a quadrupole deformation $\beta_2 = 0.107$ for ^{18}O. The systematic by Raman *et al.*[29] gives a value of 0.355(8). Since the DWBA cross section scales with β_2^2, we execute a number of calculations using $\beta_2 = 0.015 - 0.6$, chosen rather arbitrary in the range of suggested values. DWUCK4 and FRESCO give identical shapes for these values using the usual formfactor for inelastic transitions $V_\lambda = -\frac{\delta_\lambda}{\sqrt{4\pi}} \frac{dU}{dr}$ where δ_λ is the deformation length and U is the potential. Optimum deformation parameters were obtained by averaging over various optical potentials and different angular ranges in the angular distributions. The scaled calculations that match the data are shown in Fig. 15 and Fig. 16 and the optimum deformation parameters are given in Table 3.

The shape of the calculated cross section is virtually identical for all the potentials at the scale of the figure. This proves once again that our potentials are almost phase equivalent, small differences appearing only at large angles much beyond the measured angular range. Remarkably, the calculation with the PP9 parameter set, which is a WS potential phase equivalent to JLM1 folding potential describes the data as well as the other parameter sets. The situation is similar for the other folding potentials. Thus we have obtained a consistent description of both elastic and inelastic cross section using a large palette of optical potentials.

The pattern of the measured transitions in ^{17}O is quite different. The cross section decays almost exponentially at large angles with small amplitude wiggles. The experimental study by Cunsolo *et al.*[30] using three particle transfer reaction showed that the low-lying negative parity state in ^{17}O, $J^\pi = \frac{5}{2}^-, E_x = 3.843$ MeV is a member of ^{16}O K^+ α-rotational band coupled to $p_{1/2}$ neutron, and thus has a pure $4p-3h$ configuration. The state $J^\pi = \frac{1}{2}^+, E_x = 6.36$ MeV, located only 3 keV bellow the α threshold in ^{17}O is weakly populated in the reaction ^{13}C(^{6}Li,d)^{17}O [31]. This state is astrophysically important since it is considered the main source of the ^{13}C(α,n)^{16}O reaction rate uncertainty. According to Cunsolo *et al.*[32] this state has a dominant $3p-2h$ structure and belongs to a $(sd)^3$,T=1/2 ^{17}O rotational band. Repeating the procedure used for ^{18}O, we obtain a satisfactory description of our data with the deformation parameters given in Table III, see Figs. 17 and 18.

CONCLUSIONS

We have measured elastic scattering cross sections for ^{18}O+^{12}C and ^{17}O+^{13}C at 12 MeV/nucleon as well as inelastic transition to selected states in ^{18}O* and ^{17}O* in order to determine the optical potentials needed to study the one neutron pickup reaction ^{13}C(^{17}O,^{18}O)^{12}C. Optical potentials in both incoming and outgoing channels were extracted from a standard analysis using Woods-Saxon formfactors. Analysis in terms of semimicroscopic double folding formfactors, using six different approximations for the NN effective interactions helped us to eliminate the ambiguities found with WS potentials. Thus a unique solution emerged from the analysis, which is quite surprising when the reaction mechanism is dominated by strong absorption. We found that the neutron excess over the closed *d* shell leads to a less refractive interaction as compared with the closed shell nucleus ^{16}O. We found that the absorptive component of the JLM is adequate for the *d* shell heavy ion interaction. The well known Gogny effective interaction, designed mainly for HFB calculations gives excellent results for scattering provided that the knockon exchange and isovector components are properly included. A detailed semiclassical analysis in terms of barrier and internal barrier amplitudes

of Brink and Takigawa demonstrated that the flux penetrating the barrier has negligible contribution to the total cross section, and thus the reactions are peripheral. This provides a complete justification for the use of ANC method to extract spectroscopic information from the transfer reaction.

ACKNOWLEDGMENTS

This work was supported by CNCSIS (Romania) Grant PN-II-PCE-55/2011 . T. A-A. thanks the Hashemite University for support. We thanks V. Balanica for technical support and to dr. Vlad Avrigeanu for correspondence.

REFERENCES

1. A. Garcia. E. G. Adelberger, P. V. Magnus, D. M. Markoff, K. B. Swartz, M. S. Smith, K. I. Hahn, N. Bateman and P. D. Parker, Phys. Rev. **C43**, 2012 (1991).
2. R. K. Wallace and S. E. Woosley, Astrophys. J. Suppl. Ser. **45**, 389 (1981).
3. B. C. Robertson, J. T. Sample, D. R. Goosman, K. Nagatani and K. W. Jones, Phys. Rev. **C4**, 2176 (1971).
4. S. Szilner, M. P. Nicoli, Z. Basrak, R. M. Freeman, F. Haas, A. Morsad, M. E. Brandan, and G. R. Satchler, Phys. Rev. **C64**, 064614 (2001).
5. A. T. Rudchik *et al.*, Eur. Phys. J. **A44**, 221 (2010).
6. M. C. Mermaz, M. A. G. Fernandes, A. Greiner, B. T. Kim and N. Lisbona, Phys. Rev. **C19**, 794 (1979).
7. B. Heusch, C. Beck, J. P. Coffin, P. Engelstein, R. M. Freeman, G. Guillaume, F. Haas, and P. Wagner, Phys. Rev. **C26**, 542 (1982).
8. D. M. Pringle, W. N. Catford, J. S. Winfield, D. G. Lewis, N. A. Jelley, K. W. Allen and J. H. Coupland, Nucl. Instrum. Methods Phys. Res. **A245**, 230 (1986).
9. S. Kowalski and H. A. Enge, computer code RAYTRACE (unpublished), University of Oxford, England, UK, 1986.
10. A. M. Mukhamedzhanov, V. Burjan, F. Carstoiu, J. Cejpek, H. L. Clark, C. A. Gagliardi, Y.-W. Lui, V. Kroha, L. Trache, R. E. Tribble, H. M. Xu and X. G. Zhou, Phys. Rev. **C56**, 1302 (1997).
11. L. Trache, A. Azhari, H. L. Clark, C. A. Gagliardi, Y.-W. Lui, A. M. Mukhamedzhanov, X. Tang, N. Timofeyuk, R. E. Tribble and F. Carstoiu, Phys. Rev. **C61**, 024612 (2000).
12. Yu. A. Glukhov, S. A. Goncharov, A. S. Dem'yanova, A. A. Ogloblin, M. V. Rozhkov, V. P. Rudakov, V. Trashka, J. Izv. Ross. Akad. Nauk, Ser. Fiz. **65**, 647 (2001).
13. N. Anantaraman, H. Toki and G. F. Bertsch, Nucl. Phys. **A398**, 269 (1983).
14. J. P. Jeukenne, A. Lejeune and C. Mahaux, Phys. Rev. **C16**, 80 (1977).
15. M. Beiner and R. J. Lombard, Ann. Phys. (N.Y.) **86**, 262 (1974).
16. I. Angeli, Heavy Ion Physics, **8**, 23 (1998).
17. Dao T. Khoa, Hoang Sy Than, Tran Hoai Nam, Marcella Grasso, and Nguyen Van Giai Phys. Rev. **C 69**, 044605 (2004).
18. F. Carstoiu and M. Lassaut, Nucl. Phys. **597**, 269 (1996).
19. Dao T. Khoa, Phys. Rev. **C63**, 034007 (2001).
20. X. Campi and A. Bouyssy, Phys. Lett. **73B**, 263 (1978).
21. J. W. Negele and K. Yazaki, Phys. Rev. Lett. **47**, 71 (1981).
22. D. Gogny, *Proc. Int. Conf. on Nucl. Physics, Munich 1973, eds J. de Boer and H. J. Mang, Vol. 1, p. 48.*
23. D. H. Youngblood, H. L. Clark and Y.-W. Lui, Phys. Rev. Lett. **82**, 691 (1999).
24. G. Colo, N. Van Giai, P. F. Bortignon and M. R. Quaglia, Phys. Lett. **B485**, 362 (2000).
25. J. P. Auger and R. J. Lombard, Phys. Lett. **90B**, 200 (1980).
26. D. M. Brink and N. Takigawa, Nucl. Phys. **A279**, 159 (1977).
27. J. S. Blair, Phys. Rev. **115**, 928 (1959).
28. P. Möller, J. R. Nix, W. D. Myers and W. J. Swiatecki, At. Data Nucl. Data Tables **59**, 185 (1995).
29. S. Raman, C. W. Nestor, Jr. and P. Tikkanen, Atomic Data and Nuclear Data Tables **78**, 1 (2001).
30. A. Cunsolo, A. Foti, G. Immé, G. Pappalardo, G. Raciti, N. Saunier, Phys. Rev. **C24**, 2127 (1981).
31. S. Kubono, K. Abe, S. Kato, T. Teranishi, M. Kurokawa, X. Liu, N. Imai, K. Kumagai, P. Strasser, M. H. Tanaka, Y. Fuchi, C. S. Lee, Y. K. Kwon, L. Lee, J. H. Ha and Y. K. Kim, Phys. Rev. Lett. **90**, 062501 (2003).
32. A. Cunsolo, A. Foti, G. Immé, G. Pappalardo and G. Raciti, Phys. Lett. **124B**, 439 (1983).

HEAVY ION ORBITING AND REGGE POLES

F. Carstoiu[1], M. Lassaut[2], L. Trache[1] and V. Balanica[1]
[1] National Institute for Nuclear Physics and Engineering,
P.O.Box MG-6, RO-077125 Bucharest-Magurele, Romania
[2] Institut de Physique Nucléaire, CNRS-IN2P3, Univ. Paris-Sud,
Université Paris-Saclay, 91406 Orsay Cedex, France

(Received November 23, 2015)

Abstract

We review the semiclassical theory for heavy ion orbiting insisting on the connection with Regge poles and barrier-top resonances. Although the physical content of the phenomenon is well understood semiclassically, a clear signature is hard to be found because the relation between the observation angle and the deflection angle is not one to one.

Key words: Heavy ion orbiting, barrier-top resonances, Regge poles.

1 Introduction

We have a long-term program to understand and describe nucleus-nucleus collisions in terms of one body interaction potential, the optical model potential (OMP). A good understanding of all phenomena occurring in the elastic nucleus-nucleus scattering, which are used typically to extract OMP, and the interpretation of the origin of different aspects, including the well know potential ambiguities, are of crucial importance for finding and justifying the procedures used for predicting nucleus-nucleus OMP in the era of radioactive nuclear beams (RNB), including ours based on double folding [1]. The reliability of these potentials is crucial in the correct description of a number of reactions involving RNBs, from elastic to transfer and breakup, at energies ranging from a few to a few hundred MeV/nucleon. Of particular interest for us is to support the absolute values of the calculated cross sections for reactions used in indirect methods for nuclear astrophysics, see [2] and [3] for the most recent results. In this framework, we treat here the case of heavy ion orbiting, one of the phenomena found over the years to occur is special cases

of elastic scattering, well understood semi-classically, but not well documented by specific examples.

The anomalous large-angle scattering of α-particles at moderate energies from elements throughout the periodic table has been a subject of considerable experimental study and has evoked a wide range of novel theoretical explanations [4, 5]. The conventional nuclear optical potential can explain much, if not all, of the anomalous scattering. The dominant physical parameter determining back-angle scattering is the strength, W, of the imaginary part of the optical potential. Lowering of W by a modest factor of two or three lead to changes in back-angle scattering by several orders of magnitude. This effect was dubbed in literature improperly as incomplete absorption. This severe sensitivity of back-angle scattering to the imaginary strength of the optical potential was explained as a sudden emergence of the giant resonances of the high-partial-wave strength functions, as W decreases[6]. A more popular explanation is the interference between the wave reflected at the internal angular momentum barrier with the wave reflected at the nuclear radius.

Analysis of several heavy ion elastic scattering angular distribution in the energy range of 4-10 MeV/A conclude that backward-angle structures are caused by very few partial waves close to grazing collision value $\ell = kR$. Consequently, all theoretical approaches have to strengthen the contribution from these partial waves relative to the normal optical or diffraction model. Cowley and Heymann [7] and McVoy [8] parametrize the scattering amplitude by a Regge pole expansion in angular momentum. The explanation in terms of a sequence of Regge poles suggests that the physical mechanism behind the large angle structures could be heavy ion orbiting.

Orbiting could be understood simply in terms of the classical equation of motion. Let a particle m in a strong attractive potential $V(r)$. Then the motion is given by

$$\frac{1}{2}m\dot{r}^2 + \frac{1}{2}\frac{L^2}{mr^2} + V(r) = E \tag{1}$$

Let the effective interaction $U(r, L) = \frac{1}{2}\frac{L^2}{mr^2} + V(r)$ and assume that for a certain angular momentum $L = L_o$ the effective interaction has a maximum U_{max} and $U_{max} = E$. If this condition is satisfied then the radial velocity $\dot{r} = 0$ and the particle is orbiting indefinitely with a radius corresponding to the maximum. For E close to the critical energy the particle remains a finite time in this state.

In this paper we review the semiclassical theory of Brink and Takigawa [9] in relation with heavy ion orbiting, barrier-top resonances and Regge poles. In a second part of the paper we examine the ability of the double folding model of the optical potential to describe orbiting.

2 Orbiting and Regge poles

We start from the radial Schrödinger equation for a real spherical potential

$$-\frac{\hbar^2}{2\mu}\left(\frac{\partial}{\partial r^2}-\frac{\ell(\ell+1)}{r^2}\right)\Psi+V(r)\Psi=E\Psi \tag{2}$$

and assume that the effective potential

$$V_{\text{eff}}(r)=V(r)+\frac{\hbar^2}{2\mu}\frac{\ell(\ell+1)}{r^2} \tag{3}$$

has a barrier at a finite radius say $r=r_B$. Then close to the barrier we may write:

$$V_{\text{eff}}(r)\approx V_B-\frac{1}{2}\mu\omega_B^2(r-r_B)^2 \tag{4}$$

$$-\frac{\hbar^2}{2\mu}\frac{\partial^2\Psi}{\partial r^2}-\frac{1}{2}\mu\omega_B^2(r-r_B)^2\Psi=(E-V_B)\Psi \tag{5}$$

In fact a Taylor series expansion of V_{eff} gives:

$$V_{\text{eff}}(r)=V_{\text{eff}}(r_B)+\frac{1}{2}(r-r_B)^2V''_{\text{eff}}\Big|_{r_B} \tag{6}$$

$$V_B=V_{\text{eff}}(r_B) \tag{7}$$

$$\omega_B=\sqrt{-\frac{V''_{\text{eff}}(r_B)}{\mu}} \tag{8}$$

In Eq.(5) we change the variable

$$x=\sqrt{\frac{\mu\omega_B}{\hbar}}(r-r_B) \tag{9}$$

and Eq.(5) becomes

$$\begin{aligned}&\frac{\partial^2\Psi}{\partial x^2}+x^2\Psi+2\varepsilon\Psi=0\\&\text{with}\quad \varepsilon=\tfrac{E-V_B}{\hbar\omega_B}\end{aligned} \tag{10}$$

Friedman and Goebel [10] have shown that resonances (poles in complex energy plane) emerge when

$$\varepsilon_n=-\left(n+\frac{1}{2}\right)i \tag{11}$$

which is just the quantization of the inverted harmonic oscillator well. It results that

$$E_n=V_B-i\left(n+\frac{1}{2}\right)\hbar\omega_B \tag{12}$$

These are poles for fixed angular momentum in complex energy plane. The orbiting angular momentum is defined by

$$V_B(\ell_{\rm orb}(E)) = E \tag{13}$$

From Eq.(14) to Eq.(24) ℓ_0 has been replaced by $\ell_{\rm orb}$
For ℓ close to $\ell_{\rm orb}$ we expand to first order

$$V_B(\ell) = V_B(\ell_{\rm orb}) + \frac{\partial V_B}{\partial \ell}(\ell - \ell_{\rm orb}) = E + \hbar\omega_{\rm orb}(\ell - \ell_{\rm orb}) \tag{14}$$

where

$$\begin{aligned} \hbar\omega_{\rm orb} &= \left.\frac{\partial V_B}{\partial \ell}\right|_{\ell=\ell_{\rm orb}} = \frac{\partial}{\partial \ell}\left[\frac{\hbar^2}{2\mu}\frac{\ell(\ell+1)}{r_B^2}\right]\Bigg|_{\ell=\ell_{\rm orb}} \\ &= \left.\frac{\hbar^2}{2\mu r_B^2}\frac{\partial}{\partial \ell}(\ell^2 + l)\right|_{\ell=\ell_{\rm orb}} = \frac{\hbar^2}{2\mu r_B^2}(2\ell_{\rm orb} + 1) \end{aligned} \tag{15}$$

The orbiting frequency at the top of the barrier reads :

$$\omega_{\rm orb} = \frac{\hbar}{\mu r_B^2}\left(\ell_{\rm orb} + \frac{1}{2}\right) \tag{16}$$

We can write Eq.(14) in the form

$$E - V_B(\ell) = -\hbar\omega_{\rm orb}(\ell - \ell_{\rm orb}) \tag{17}$$

and continue with Eq.(10)

$$E - V_B(\ell) = \hbar\omega_B\varepsilon = -\hbar\omega_{\rm orb}(\ell - \ell_{\rm orb}) \tag{18}$$

The reduced momentum reads

$$\frac{E - V_B(\ell)}{\hbar\omega_B} = -\frac{\hbar\omega_{\rm orb}}{\hbar\omega_B}(\ell - \ell_{\rm orb}) \equiv -\lambda \tag{19}$$

Therefore we have $\lambda = -\varepsilon$ and the barrier-top resonances translate into Regge poles at

$$\lambda_n = \left(n + \frac{1}{2}\right) i \tag{20}$$

or

$$(\ell_n - \ell_{\rm orb})\frac{\omega_{\rm orb}}{\omega_B} = \left(n + \frac{1}{2}\right) i \tag{21}$$

We get

$$\ell_n = \ell_{\rm orb} + \frac{\omega_B}{\omega_{\rm orb}}\left(n + \frac{1}{2}\right) i \tag{22}$$

or

$$\ell_n = \ell_{\rm orb} + \Gamma_\ell \left(n + \frac{1}{2} \right) i \tag{23}$$

so the lowest pole is exactly at $\ell_0 = \ell_{\rm orb} + i\frac{\Gamma_\ell}{2}$ with $\Gamma_\ell = \frac{\omega_B}{\omega_{\rm orb}}$. Note that Γ_ℓ depends on $\ell_{\rm orb}$ through relation (16)

$$\Gamma_\ell = \frac{\omega_B}{\omega_{\rm orb}} = \frac{\sqrt{-\frac{V''_{\rm eff}(r_B)}{\mu}}}{\frac{\hbar}{\mu r_B^2}\left(\ell_{\rm orb} + \frac{1}{2}\right)} \tag{24}$$

where in Eq.(24) the primes denote the derivative with respect to r_B. We have

$$V_{\rm eff}(r_B) = V(r_B) + \frac{\hbar^2}{2\mu}\frac{\ell(\ell+1)}{r_B^2} \tag{25}$$

$$V'_{\rm eff}(r_B) = V'(r_B) - \frac{\hbar^2}{2\mu}\ell(\ell+1)\frac{2}{r_B^3} = V'(r_B) - \frac{\hbar^2}{\mu}\frac{\ell(\ell+1)}{r_B^3} \tag{26}$$

$$V''_{\rm eff}(r_B) = V''(r_B) + \frac{\hbar^2}{\mu}\frac{3\ell(\ell+1)}{r_B^4} \tag{27}$$

In the presence of absorption, Friedman and Goebel [10] conjectured that the pole will be shifted by the quantity

$$\Delta\ell_n = i\frac{\omega(r_B)}{\omega_{\rm orb}} \tag{28}$$

3 Semiclassical orbiting

We turn now to study the reaction mechanism governing orbiting using semiclassical methods. The far-side dominance observed in some heavy ion elastic scattering angular distributions is not able to explain the behavior of the S-matrix elements at low angular momentum. The reason is of course that the far/near (F/N) decomposition method does not perform a dynamic decomposition of the scattering function, but merely decomposes the scattering amplitude into traveling waves. The intermediate angle structures, have been repeatedly interpreted as arising from the interference of two ranges in angular momenta, $\ell_<$ and $\ell_>$, contributing to the same negative deflection angle. However, the corresponding cross sections, $\sigma_{F<}$ and $\sigma_{F>}$, cannot be isolated because their dynamic content (S-matrix) is not accessible.

The semiclassical uniform approximation for the scattering amplitude of Brink and Takigawa [9] is well adapted to describe situations in which the scattering is controlled by at most three active, isolated, complex turning points. An approximate multireflection series expansion of the scattering function can

be obtained, the terms of which have the same simple physical meaning as in the exact Debye expansion for the scattering of light on a spherical well. The major interest in this theory comes from the fact that it can give precious information on the response of a nuclear system to the nuclear interior. An application [11] of this technique helped to clarify the controversial problem of the "Airy oscillation" seen in low energy ^{16}O+^{12}C scattering [13].

We discard the absorptive term in the optical potential and define the effective potential as,

$$V_{\rm eff}(r) = V(r) + \frac{\hbar^2}{2\mu}\frac{\lambda^2}{r^2}, \quad \lambda = \ell + \frac{1}{2} \tag{29}$$

where the Langer prescription has been used for the centrifugal term. This guarantees the correct behavior of the semiclassical wave function at the origin [14]. Then we calculate the deflection function,

$$\Theta(\lambda) = \pi - 2\int_{r_1}^{\infty} \frac{\sqrt{\frac{\hbar^2}{2\mu}}\lambda dr}{r^2\sqrt{E_{\rm c.m.} - V_{\rm eff}(r)}} \tag{30}$$

where r_1 is the outer zero of the square root, i.e. the radius of closest approach to the scatterer and μ is the reduced mass. Note that with the replacement $\hbar\lambda = b\sqrt{2\mu E}$, Eq.(30) becomes identical with the classical deflection function $\Theta(b)$, where b is the impact parameter. The behavior of $\Theta(\lambda)$ is the one expected for a strong nuclear potential in a *near orbiting* kinematical situation in which the c.m. energy approximately equals that of the top of the barrier for some specific angular momentum. All the measured angular range is classically illuminated. The deflection function exhibit no genuine minima, but rather a pronounced cusp close to an orbiting logarithmic singularity. Therefore any interpretation of structures in angular distributions in terms of Airy oscillations can be discarded. Rather we need an interpretation appropriate for orbiting, a well documented situation in classical physics [15]. We identify the cusp angular momentum as orbiting momentum ($\lambda_{\rm orb}$) since this is related to the coalescence of two (barrier) turning points and the innermost turning point given by the centrifugal barrier becomes classically accessible. There are two branches that can be distinguished, an internal branch for low active momenta $\lambda < \lambda_{\rm orb}$ related to semiclassical trajectories which penetrate into the nuclear pocket and a less developed external (barrier) branch ($\lambda > \lambda_{\rm orb}$) related to trajectories deflected at the diffuse edge of the potential.

However this simple calculation cannot determine the relative importance of these branches and provides no information about the interference effects of the corresponding semiclassical trajectories. To clarify these points it is best to go into the complex r-plane and look for complex turning points, i.e. the complex roots of the quantity $E_{\rm c.m.} - V_{\rm eff} - iW$. This is an intricate numerical

problem, because, for a WS optical potential, the turning points are located near the potential singularities and there are an infinite number of such poles. We consider an ideal situation with three, well isolated, turning points for each partial wave.

The multireflection expansion of the scattering function in the Brink-Takigawa approach reads,

$$S_{WKB}(\ell) = \sum_{q=0}^{\infty} S_q(\ell) \tag{31}$$

where,

$$S_0(\ell) = \frac{\exp(2i\delta_1^\ell)}{N(-i\varepsilon)} \tag{32}$$

and for $q \neq 0$,

$$S_q(\ell) = (-)^{q+1} \frac{\exp\left[2i(qS_{32} + S_{21} + \delta_1^\ell)\right]}{N^{q+1}(-i\varepsilon)} \tag{33}$$

In these equations, $\varepsilon = S_{21}/\pi$ and δ_1^ℓ is the WKB (complex) phase-shift corresponding to the turning point r_1, $N(z)$ is the barrier penetrability factor,

$$N(z) = \frac{\sqrt{2\pi}}{\Gamma\left(z + \frac{1}{2}\right)} \exp\left(z \ln z - z\right) \tag{34}$$

and S_{ij} is the action integral calculated between turning points r_i and r_j,

$$S_{ij} = \int_{r_i}^{r_j} dr \left\{ \frac{2\mu}{\hbar^2} [E_{\text{c.m.}} - V_{\text{eff}}(r) - iW(r)] \right\}^{1/2} \tag{35}$$

S_{21} and S_{32} are independent of the integration path provided they lie on the first Riemann sheet and collision with potential poles is avoided. Each term in Eq.(31) has a simple physical interpretation. The first term (the barrier term, denoted also S_B) retains contributions from trajectories reflected at the barrier, not penetrating the internal region. The qth term corresponds to trajectories refracted q times in the nuclear interior with q-1 reflections at the barrier turning point r_2. Summation of terms $q \geq 1$ can be recast into a single term,

$$S_I = \frac{\exp\left[2i(S_{32} + S_{21} + \delta_1^\ell)\right]}{N(-iS_{21}/\pi)^2} \frac{1}{1 + \exp\left[2iS_{32}\right]/N(-iS_{21}/\pi)} \tag{36}$$

and is known as the internal barrier scattering function. When the absorption in the nuclear interior is large, the second factor in the above equation reduces to one and we are left with the expression used in [16]. Since the semiclassical

scattering function is decomposed additively, $S_{\rm WKB} = S_B + S_I$, the corresponding total scattering amplitude is decomposed likewise as $f_{\rm WKB} = f_B + f_I$ and conveniently the corresponding barrier and internal barrier angular distributions are calculated as $\sigma_{B,I} = |f_{B,I}|^2$, using the usual angular momentum expansion of the amplitudes.

The accuracy of the semiclassical calculation is usually checked by comparing the barrier and internal barrier absorption profiles with the exact quantum-mechanical result. When the action integrals are calculated accurately, the semiclassical B/I expansion is an *exact* decomposition of the quantum result. The internal component gets significant values up to the grazing angular momentum ℓ_g and is negligibly small beyond this value. The barrier component resembles a strong absorption profile and this justifies the interpretation that it corresponds to that part of the flux not penetrating into the nuclear interior. For values near the orbiting angular momentum $\ell_{\rm orb}$, the two components interfere and a downward spike appears in the total profile, in complete agreement with the quantum result. This is the famous Grühn-Wall spike [17] introduced phenomenologically to explain ALAS for α-particle scattering, and appears here as a strong interference between barrier and internal barrier amplitudes. Second, the B/I components are almost decoupled in the angular momentum space and therefore they will contribute in different angular ranges.

A better insight into this technique is obtained by further decomposing the B/I components into far and near (BF/BN and IF/IN) subcomponents. The barrier component dominates the forward angle region. Fraunhofer diffractive oscillations appear as the result of BF and BN interference. At large angles, the internal contribution accounts for the full cross section.

Thus, the intermediate angle exotic structure in angular distributions for the elastic scattering of ^{6}Li on ^{16}O [18] can be understood as a result of coherent interference of two far-side subamplitudes generated by different terms in the uniform multireflection expansion of the scattering function (terms q=0 and q=1 in Eq.(31)), corresponding to the scattering at the barrier and the internal barrier. This interference effect appears as a signature of a surprisingly transparent interaction potential for loosely bound nucleus ^{6}Li at this low energy which allows part of the incident flux to penetrate the nuclear interior and reemerge with significant probability.

The multireflection series (31) is the uniform approximation analogue of the Debye expansion of the scattering function. Anni [11] used Eq.(31) to interpret ^{16}O+^{12}C scattering data at 132 MeV assuming a surface transparent optical potentials and convincingly showed that medium angle structures are given by interference effects of the barrier/internal amplitudes and more precisely by interference between saddles appearing in the first and second term of multireflection expansion and therefore cannot be interpreted as a manifes-

tation as a nuclear rainbow and associated Airy oscillation.
In the following we will provide a third interpretation by using explicitly the orbiting conditions and explicitly calculating Sommerfeld poles near the real axis.

We will made a totally different assumption on the physical nature of the phenomenon: the absorption is negligible near the barrier but strong in the nuclear interior. In such conditions, the scattering amplitude is described by the barrier component alone modified slightly by the barrier penetration factor :

$$S_n \approx \frac{e^{2i\delta_1(\lambda)}}{N(-i\frac{S_{21}}{\pi})} \tag{37}$$

which is slightly changed compared with the original Brink-Takigawa formulation. Since δ_1 describes trajectories reflected at outer turning point, the scattering amplitude $S \sim e^{2i\delta_1}$ will be very much similar to that given by the strong absorption model
The action S_{21} is given by

$$S_{21} = \int_{r_2}^{r_1} \left[\frac{2\mu}{\hbar^2}(E - V_{\rm eff}(r))\right]^{\frac{1}{2}} dr \tag{38}$$

with

$$V_{\rm eff}(r) = V(r) + V_c(r) + \frac{\hbar^2}{2\mu}\frac{\lambda^2}{r^2} \quad , \qquad \lambda = \ell + \frac{1}{2} \tag{39}$$

where V_c is the Coulomb potential. Near the barrier, the absorption is small and the effective potential is almost real and

$$V_{\rm eff}(r) = V_B + \frac{1}{2}\mu\omega_B^2(r - r_B)^2 \tag{40}$$

with

$$\omega_B = \sqrt{-\frac{V''_{\rm eff}(r)}{\mu}}\Big|_{r=r_B} \tag{41}$$

where in Eq.(41) the prime denote the derivative with respect to r. Eq.(38) becomes:

$$S_{21} = \int_{r_2}^{r_1} \left[\frac{2\mu}{\hbar^2}(E - V_B - \frac{1}{2}\mu\omega_B^2(r - r_B)^2\right]^{\frac{1}{2}} dr \tag{42}$$

With the variable change,

$$r - r_B = \frac{\hbar x}{\mu\omega_B}, \quad x = \frac{\mu\omega_B}{\hbar}(r - r_B), \quad dx = \frac{\mu\omega_B}{\hbar}dr \tag{43}$$

$$S_{21} = \frac{\hbar}{\mu\omega_B}\int_{x_2}^{x_1}\left[\frac{2\mu}{\hbar^2}(E-V_B)-x^2\right]^{\frac{1}{2}}dx \tag{44}$$

$$x_2 = \frac{\mu\omega_B}{\hbar}(r_2-r_B), \qquad x_1 = \frac{\mu\omega_B}{\hbar}(r_1-r_B) \tag{45}$$

the action integral S_{21} can be calculated exactly as,

$$S_{21} = \pi\frac{E-V_B}{\hbar\omega_B} \tag{46}$$

So that ε entering Eq.(32) is

$$\varepsilon = \frac{E-V_B}{\hbar\omega_B} \tag{47}$$

Eqs.(32) and (34) show that the poles in S-matrix are given by the poles of the Gamma function [12]. Taking $z = -i\varepsilon$ in Eq.(34)

$$\frac{1}{2} - i\varepsilon_n = -n \tag{48}$$

$$\varepsilon_n = -i\left(n+\frac{1}{2}\right) \tag{49}$$

$$\frac{E_n - V_B}{\hbar\omega} = -i\left(n+\frac{1}{2}\right) \tag{50}$$

$$E_n = V_B - i\hbar\omega_B\left(n+\frac{1}{2}\right) \tag{51}$$

Eq.(51) represents the Bohr-Sommerfeld quantization for the inverted oscillator well. These are precisely the barrier-top resonances (Regge poles) of Friedman and Goebel [10].
Now we use the orbiting condition

$$V_B\left(\ell_{\mathrm{orb}(E)}\right) = E \tag{52}$$

to obtain poles in angular momentum. For ℓ close to orbiting momentum we expand the potential to first order

$$V_B(\ell) = V_B(\ell_{\mathrm{orb}}) + \frac{\partial V_B}{\partial\ell}(\ell-\ell_{\mathrm{orb}}) \equiv E + \hbar\omega_{\mathrm{orb}}(\ell-\ell_{\mathrm{orb}}) \tag{53}$$

where the orbiting frequency is

$$\hbar\omega_{\mathrm{orb}} = \left.\frac{\partial V_B}{\partial\ell}\right|_{\ell_{\mathrm{orb}}} = \frac{\hbar^2}{\mu r_B^2}\left(\ell_{\mathrm{orb}}+\frac{1}{2}\right) \tag{54}$$

Taking in (53) $E = E_n$ and $\ell = \ell_n$ and then combining with (51) we obtain

$$\left\{ \begin{array}{rcl} V_B - E_n & = & \hbar\omega_{\rm orb}(\ell_n - \ell_{\rm orb}) \\ V_B - E_n & = & i\hbar\omega_B \left(n + \frac{1}{2}\right) \end{array} \right. \tag{55}$$

We get

$$\hbar\omega_{\rm orb}(\ell_n - \ell_{\rm orb}) = i\hbar\omega_B \left(n + \frac{1}{2}\right) \tag{56}$$

so on

$$\ell_n = \ell_{\rm orb} + i\frac{\omega_B}{\omega_{\rm orb}} \left(n + \frac{1}{2}\right) \tag{57}$$

These are the barrier-top poles in angular momentum space. Eq.(57) shows that the nearest pole to real axis has a real part given precisely by the orbiting momentum and a width:

$$\Gamma_\ell = \frac{\omega_B}{\omega_{\rm orb}} \Rightarrow \ell_n = \ell_{\rm orb} + i\Gamma_\ell \left(n + \frac{1}{2}\right) \tag{58}$$

Going back to the amplitude (37), the phase shift reads :

$$2i\widetilde{\delta_1}(\lambda) = 2i\delta_1(\lambda) + \ln\left[\Gamma\left(\frac{1}{2} - i\varepsilon\right)\right] - \frac{1}{2}\ln(2\pi) + (z - z\ln z)|_{z=-i\varepsilon} \tag{59}$$

Taking into account the equations (47,55) or (18) we have

$$\varepsilon_n = -\frac{\hbar\omega_{\rm orb}}{\hbar\omega_B}(\ell_n - \ell_{\rm orb}) = -\frac{\hbar\omega_{\rm orb}}{\hbar\omega_B}(\lambda_n - \lambda_{\rm orb}), \quad \lambda = \ell + \frac{1}{2} \tag{60}$$

At the vicinity of $\lambda = \lambda_{\rm orb}$, where ε_0 is close to zero, the equation (59) is separated in a smooth part labeled $g(\lambda)$ and a part including the logarithmic singularity, namely :

$$2\widetilde{\delta_1}(\lambda) = g(\lambda) + (\varepsilon_0 \ln(-i\varepsilon_0) - \varepsilon_0) \tag{61}$$

Here ln denotes the principal determination of the complex Logarithm. We have

$$\begin{array}{rcll} \ln(-i\varepsilon_0) & = & \ln|\varepsilon_0| - i\frac{\pi}{2} & \varepsilon_0 > 0 \\ \ln(-i\varepsilon_0) & = & \ln|\varepsilon_0| + i\frac{\pi}{2} & \varepsilon_0 < 0 \end{array}$$

which implies that the imaginary part of $\varepsilon_0 \ln(-i\varepsilon_0) - \varepsilon_0$ has the same sign regardless of whether ε_0 is positive or negative. This smooth part of the singularity, namely $-i\frac{\pi}{2}|\lambda - \lambda_{\rm orb}|$, is included in the function g and we are left with :

$$2\widetilde{\delta_1}(\lambda) = g(\lambda) + (\varepsilon_0 \ln(|\varepsilon_0|) - \varepsilon_0) \tag{62}$$

Using Eq.(62) and the fact that

$$\frac{d}{d\varepsilon_0}(\varepsilon_0 \ln(|\varepsilon_0|) - \varepsilon_0) = \ln(|\varepsilon_0|) \tag{63}$$

we obtain the following semiclassical deflection function

$$\Theta(\lambda) = 2\widetilde{\delta}_1'(\lambda) = g'(\lambda) + \frac{\omega_{\rm orb}}{\omega_B} \ln\left[\frac{\omega_{\rm orb}}{\omega_B}|\lambda - \lambda_{\rm orb}|\right] \tag{64}$$

(the prime being taken with respect to λ) which displays the normal logarithmic singularity near the orbiting on angular momentum. Thus the main signature of the heavy ion orbiting will be a logarithmic singularity in the semiclassical deflection function.

The Equation (64) is valid for every $\lambda - \lambda_{\rm orb}$ positive or negative. Note that we have neglected the weak dependence of orbiting frequency on angular momentum (54).

4 Regge poles

A long standing problem in the α-nucleus scattering at energies above the Coulomb barrier is the so called ALAS, a strong increase of the cross section at large angles. It was observed by Grühn and Wall [17] that a downward narrow spike superimposed on the smooth-cut-off model for ℓ values near grazing $\ell = kR$ aided materially to explain ALAS. The Grühn and Wall dip is explained semiclassically as a strong destructive interference between the internal barrier and barrier components of the scattering amplitude near the orbiting momentum. Alternatively, the dip is explained as an interference pole-background components of the scattering amplitude for highly transparent potentials, such that the low absorption is not able to suppress the resonant effects in the low partial waves. Semiclassically, these effects appear as a consequence of multiple reflections of the internal amplitude between the most internal complex turning points of the potential. In fact a common property of the WS potentials which describe well the data, is that they possess several narrow shape (molecular) resonances located in the most active waves . In this section we examine this effect in terms of a purely phenomenological Regge pole approximation.

For this purpose we adopt the "product" representation of the S-matrix [8],

$$S(\ell) = S_{bkg}(\ell) S_{pole}(\ell) \tag{65}$$

where the background (bkg) component is borrowed from the strong absorption model of Ericson [19],

$$S_{bkg} = \left[1 + \beta \exp(-i\alpha) \exp\left(\frac{L-l}{\Delta}\right)\right]^{-1} \tag{66}$$

We note that an alternative description in terms of additive pole-background components is possible [7]. For the pole term we adopt the expression,

$$S_{pole}(\ell) = \prod_{j=1}^{2} \left[1 + i \frac{D_j(\ell)}{l - L_j - i\hat{\Gamma}_j(\ell)/2} \right] \tag{67}$$

This term describes resonances in ℓ centered at L_j with total width $\hat{\Gamma}_j$. In line with McVoy [8] we assume the zeros and the widths slowly ℓ dependent and vanishing exponentially as $\ell \to \infty$,

$$D_j(\ell) = \frac{D_j}{1 + \exp(\frac{l-L}{\Delta_j})} \tag{68}$$

$$\hat{\Gamma}_j(\ell) = \frac{\Gamma_j}{1 + \exp(\frac{l-L}{\Delta_j})} \tag{69}$$

Clearly, D measures the distance between the pole ($p = 1/2\Gamma$) and the zero($z = 1/2\Gamma - D$). The model has 12 parameters, twice as much as the WS model. The reason is that we were not able to find a single pole unitary solution for both background and pole components. Since the problem is highly nonlinear there is no guarantee for the uniqueness of the solution. We used a Monte Carlo procedure to generate input parameters and then minimized the usual χ^2 objective function.

5 Conclusions

We have reviewed the semiclassical theory of Brink and Takigawa [9] in connection with heavy ion orbiting. The phenomenon is quite frequent for α-particle scattering on light targets in the energy range 5-10 MeV/A where significant increase in the cross section at large angles is found. A possible signature will be to find a logarithmic singularity is the semiclassical deflection function associate with a downward spike in the absorption profile near the grazing angular momentum $\ell = kR$.

Acknowledgements

This work was partly supported by CNCSIS Romania, under program PN-II-PCE-55/2011 and PN-II-ID-PCE-0299/2012, and partly by IN2P3, France.

References

[1] L. Trache, A. Azhari, H. L. Clark, C. A. Gagliardi, Y.-W. Lui, A. M. Mukhamedzhanov, R. E. Tribble, F. Carstoiu Phys. Rev. C **61**, 024612(2000).

[2] T. Al-Abdullah, F. Carstoiu, X. Chen, H. L. Clarke, C. A. Gagliardi, Y.-W. Lui, A. Mukhamedzhanov, G. Tabacaru, Y. Takimoto, L. Trache, R.E.Tribble, Y. Zhai Phys. Rev. C **89**, 025809 (2014).

[3] T. Al-Abdullah, F. Carstoiu, C. A. Gagliardi, G. Tabacaru, L. Trache and R. E. Tribble. Phys. Rev. C **89**, 064602 (2014).

[4] G. Gaul, H. Lüdecke, R. Santo, H. Schmeing and R. Stock, Nucl. Phys. **A137**, 177 (1969).

[5] H. Oeschler, H. Schröter, H. Fuchs, L. Baum, G.Gaul, H. Ludeke, R.Santo and R. Stock, Phys. Rev. Lett. **28**, 694 (1972).

[6] D. M. Brink, J. Grotowski and E. Vogt, Nucl. Phys. **A309** 359(1978).

[7] A. A.Cowley and G. Heymann, Nucl. Phys. **A146**, 465 (1970).

[8] K. W. McVoy, Phys. Rev. C **3**, 1104 (1971).

[9] D. M. Brink and N. Takigawa, Nucl. Phys. **A279**, 159 (1977).

[10] W. A. Friedman and C. J. Goebel, Ann. Phys. **104**, 145 (1977).

[11] R. Anni, Phys. Rev. C **63**, 031601R (2001).

[12] A. Erdélyi, W. Magnus, F. Oberhettinger and F.G. Tricomi : Higher Transcendental Functions vol II. McGraw-Hill, New York (1953)

[13] A. A. Ogloblin *et al.*, Phys. Rev. C **62**, 044601 (2000).

[14] P. Fröbrich and R. Lipperheide, *Theory of Nuclear Reactions*, Clarendon Press, Oxford, 1996.

[15] K. W. Ford and J. A. Wheeler, Ann. Phys. (N. Y.) **7**, 259 (1959).

[16] F. Michel, G. Reidemeister and S. Ohkubo, Phys. Rev. Lett. **89**, 152701 (2002);ibidem, Phys. Rev. C **63**, 034620 (2001).

[17] C. R. Grühn and N. S. Wall, Nucl. Phys. **81**, 161 (1966).

[18] F. Carstoiu and L. Trache , Phys. Rev. **C85**, 054606 (2012).

[19] T. E. O. Ericson, Preludes in Theoretical Physics, eds, A. de-Shalit, L. Van Hove and H. Feshbach, North Holland, 1965.

HEAVY ION ORBITING AND REGGE POLES (II)

F. Carstoiu[1], M. Lassaut[2], L. Trache[1] and V. Balanica[1]
[1] National Institute for Nuclear Physics and Engineering,
P.O.Box MG-6, RO-077125 Bucharest-Magurele, Romania
[2] Institut de Physique Nucléaire
IN2P3-CNRS, Université Paris-Sud 11
F-91406 Orsay Cedex, France

. (Received November 24, 2015)

Abstract

We discuss two specific examples of heavy ion orbiting. A first example, α+^{16}O at 54.1 MeV reaction dominated by strong optical potentials shows all characteristics of a strongly refractive scattering: Fraunhofer cross over at very forward angles, deep Airy oscillation, rainbow bump, significant increase of the cross section at large angles. We demonstrate semiclassically that this in fact is a typical orbiting reaction. In a second example, α+^{28}Si at 18.0 MeV, we describe a special king of heavy ion orbiting-butterfly scattering, with diffractive oscillations in the entire physical angular range, determined by Regge pole dominance.

Key words: G-matrix effective interactions, folding potentials, WKB, Regge poles.

1 Introduction

We have a long-term program to understand and describe nucleus-nucleus collisions in terms of one body interaction potential, the optical model potential (OMP). A good understanding of all phenomena occurring in the elastic nucleus-nucleus scattering, which are used typically to extract OMP, and the interpretation of the origin of different aspects, including the well know potential ambiguities, are of crucial importance for finding and justifying the procedures used for predicting nucleus-nucleus OMP in the era of radioactive nuclear beams (RNB), including ours based on double folding [23]. The reliability of these potentials is crucial for the correct description of a number of reactions involving RNBs, from elastic to transfer and breakup, at energies

ranging from a few to a few hundred MeV/nucleon. Of particular interest for us is to support the absolute values of the calculated cross sections for reactions used in indirect methods for nuclear astrophysics, see [31] and [32] for the most recent results. In this framework, we treat here the case of heavy ion orbiting, one of the phenomena found over the years to occur is special cases of elastic scattering, well understood semi-classically, but not well documented by specific examples.

2 Folding formfactors

In the following we discuss the ability of the folding model to describe orbiting/resonant elastic scattering. We start by a quite simple model in which the spin-isospin independent formfactor of the OMP is given by the double folding integral,

$$V_{fold}(R) = \int d\vec{r}_1 d\vec{r}_2 \rho_1(r_1)\rho_2(r_2)v_{M3Y}(s) \tag{1}$$

where v_{M3Y} is the M3Y parametrization of the G-matrix obtained from the Paris NN interaction [10], and $\vec{s} = \vec{r}_1 + \vec{R} - \vec{r}_2$ is the NN separation distance. A small isovector component arising from a nonnegligible neutron skin is added if necessary. The Coulomb component of the optical potential is calculated by replacing the nuclear s.p. densities with proton densities and using $v_{coul}(s) = e^2/s$ as effective interaction. The small effect arising from finite proton size is ignored. In the simplest version of this model, dubbed here as M3YZR, the knockon exchange component is simulated by a zero range potential with a slightly energy dependent strength,

$$J_{00}(E) = -276(1 - 0.005E/A) \tag{2}$$

We keep the number of fitting parameters at the minimum level and take the OMP in the form,

$$U(R) = N_V V(R, t_V) + iN_W V(R, t_W) \tag{3}$$

where $N_{V,W}$ are normalization constants and $t_{V,W}$ are range parameters defined by the scaling transformation,

$$V(R, t) \rightarrow t^3 V_{fold}(tR) \tag{4}$$

This transformation conserves the volume integral of the folding potential and modifies the radius as,

$$< R^2 >_V = \frac{1}{t^2} < R^2 >_{fold} \tag{5}$$

Thus the strength of the formfactor is controlled by the parameters $N_{V,W}$. Note that the transformation in Eq. (4) ensures that only the rms radius of the bare folding potential is changed. This is in line with the original prescription of [11] which proposed a smearing procedure in terms of a normalized Gaussian function. We found that the transformation in Eq. (4) is more efficient and less time consuming. Based on Eq. (5) one may estimate in an average way the importance of the dynamic polarization potential (DPP) and finite range effects. Throughout this paper we use single particle densities obtained from a spherical Hartree-Fock (HF+BCS) calculation based on the density functional of Beiner and Lombard [12]. The obtained rms charge radii are very close to the experimental values [13]. A more elaborate calculation leads to a nonlocal knockon exchange kernel [15],

$$U_{ex}(\vec{R}^+,\vec{R}^-) = \mu^3 v_{ex}(\mu R^-)\int d\vec{X}_1\rho_1(X_1)\hat{j}_1(k_{f1}(X_1)\frac{(A_1-1)A_2}{A_1+A_2}R^-) \qquad (6)$$
$$\times\rho_2(|\vec{R}^+-\vec{X}_1|)\hat{j}_1(k_{f2}(|\vec{R}^+-\vec{X}_1|)\frac{(A_2-1)A_1}{A_1+A_2}R^-)$$

where $A_{1,2}$ are mass numbers, μ is the reduced mass of the system, $k_{f1,2}$ are Fermi momenta, $R^{+,-}$ are the usual nonlocal coordinates and v_{ex} is the exchange component of the interaction including the long range OPEP tail. Eq. (6) already shows that the nonlocality is small and behaves as $\sim\mu^{-1}$. In the lowest order of the Perey-Saxon approximation, the local equivalent of the nonlocal kernel is obtained by solving the nonlinear equation,

$$U_L(R) = 4\pi\int d\vec{r}_1 d\vec{r}_2\rho_1(r_1)\rho_2(r_2)$$
$$\times\int s^2 ds v_{ex}(s)\hat{j}_1(k_{f1}(r_1)\beta_1 s)\hat{j}_1(k_{f2}(r_1)\beta_2 s)$$
$$\times j_0(\frac{1}{\mu}K(R)s)\delta(\vec{r}_2-\vec{r}_1+\vec{R}) \qquad (7)$$

Above $\beta_i=(A_i-1)/A_i$ are recoil corrections, $\hat{j}_1(x)=3j_1(x)/x$ and $j_{0,1}$ are spherical Bessel functions. The local Fermi momenta k_f are evaluated in an extended Thomas-Fermi approximation [16]. We have explored also the extended Slater approximation for the mixed densities of Campi and Bouyssy [17] but did not obtained substantial improvements over the usual Slater approximation. The local momentum for the relative motion is given by,

$$K^2(R) = \frac{2\mu}{\hbar^2}(E_{c.m.}-U_D(R)-U_L(R)) \qquad (8)$$

where U_D is the total direct component of the potential including the Coulomb term. In Eq. (8) we assumed a purely real local momentum of the relative motion since the absorptive component of the OMP is small compared with the real part. The effective mass correction [18], $\frac{\mu^\star}{\mu} = 1 - \frac{\partial U}{\partial E}$ is of the order of a few percent for our systems and is absorbed in the renormalization parameter N_W. Some tens of iterations are needed to solve the coupled Eq. (7) and (8) in order to obtain a precision of 10^{-7} in the entire radial range ($R_{max} = 25$ fm). We start the iteration process by using $U_L^{(0)} = U_D$ Calculations with finite range model are dubbed M3YFR.

Neglecting the spin-orbit component, the Gogny NN effective interaction can be expressed as a sum of a central, finite range term and a zero range density dependent term,

$$v(\vec{r}_{12}) = \sum_{i=1}^{2}(W_i + B_i P_\sigma - H_i P_\tau - M_i P_\sigma P_\tau) e^{-\frac{r_{12}^2}{\mu_i^2}} + t_3(1 + P_\sigma)\rho^\alpha(\vec{R}_{12})\delta(\vec{r}_{12}) \tag{9}$$

where $\vec{r}_{12} = \vec{r}_1 - \vec{r}_2$, $\vec{R}_{12} = (\vec{r}_1 + \vec{r}_2)/2$ and standard notations have been used for parameter strengths and spin-isospin exchange operators. The strengths parameters and the ranges are taken from [19]. The isoscalar and isovector components of the effective interaction are constructed in the standard way. The interest in this interaction resides in its excellent description (at the HF level) of the saturation properties of the nuclear matter in line with modern estimation from the isoscalar giant monopole [20] or dipole resonance [21] studies. Antisymmetrization of the density dependent term is trivial, so that the sum of direct and exchange term reads,

$$v_D^\rho(r_{12}) + v_{ex}^\rho(r_{12}) = \frac{3t_3}{4}\rho^\alpha\delta(\vec{r}_{12}) \tag{10}$$

The local equivalent of the finite range knockon exchange is calculated with Eq. (7). Two approximations were used for the overlap density,

$$\rho = (\rho_1(r_1)\rho_2(r_2))^{1/2} \tag{11}$$

and

$$\rho = \frac{1}{2}(\rho_1(r_1) + \rho_2(r_2)) \tag{12}$$

The first approximation Eq. (11) has the merit that the overlap density goes to zero when one of the interacting nucleons is far from the bulk. In Eq. (12) a factor 1/2 was introduced such as the overlap density does not exceeds the equilibrium density for normal nuclear matter. At large density overlaps, the fusion and other inelastic processes are dominant and the elastic scattering amplitude is negligible small. The calculated OM potentials are dubbed

GOGNY1 (11) and GOGNY3 (12). Both definitions represent crude approximations of the overlap density but are widely used in the estimation of the density dependence effects in the folding model.

We further examine the density dependence effects by using the nuclear matter approach of Jeukenne, Lejeune and Mahaux (JLM) [11] which incorporates a complex, energy and density dependent parametrization of the NN effective interaction obtained in a Brueckner Hartree-Fock approximation from the Reid soft core NN potential. The systematic study [23] of the elastic scattering between p-shell nuclei at energies around 10 MeV/nucleon leads to the surprising result that on average, the imaginary part of the folded JLM potential was perfectly adequate to describe such reactions and did not need any renormalization ($N_W = 1.00 \pm 0.09$), while the real component needed a substantial renormalization, in line with other effective interactions used in folding models. We examine here to which extent this feature is conserved for tightly bound nuclei . Exchange effects are included in this model at the level of N-target interaction. Calculations with this model are dubbed JLM1 and JLM3, depending on which definition we use for the overlap density (Eqs.(11) and (12) respectively).

3 ^{4}He+^{16}O at 54.1 MeV

The reaction ^{4}He+^{16}O at E_{lab}= 54.1 MeV was measured by Abele et al. [24] and discussed extensively within the folding model in [25]. An optical potential description of both α+^{16}O elastic scattering and α-cluster states in ^{20}Ne was given by Michel et al. [28]. The corresponding global potential α+^{16}O gives a reasonable description of the α-structure in ^{20}Ne. However such a global approach cannot be used to reveal a delicate phenomenon such as orbiting. A more detailed analysis is necessary.

A grid search using standard WS[1] formfactors for the optical potential revealed a number of discrete solutions, see Table 1 and Figure 1. Although almost all physical angular range was measured the data are not able to fix uniquely the potential of a WS shape. The members of the potential family are very strong , reaching high values of the normalized real volume integral. The rms radii of the real and imaginary component get smaller as the potential is stronger. However the reaction cross section is almost constant which suggests that the members of the potential sequence are almost phase equivalent. Examination of the Figure 3 shows quite similar cross section with the exception of the solution with $J_v = 399$ MeV fm^3 which show a very deep Airy oscillation near $\theta = 60^\circ$ just at the end of the Fraunhofer sector. This structure which is followed by a wide bump together with the far side dominance is usually interpreted a a strong refractive effect of a quite transparent potential

. This picture has been already challenged by Anni [3] for the simple reason that the far side amplitude has never been decomposed into subamplitudes which would explain the interference.

A subsequent analysis in terms of WS^2 formfactors (squared WS) revealed a single solution in the range $J_v < 1000$ MeV fm^3, see Table 2 and Figure 2. The uniqueness of the solution cannot be guaranteed by our search procedure. Remarkably, the WS^2 solution and the first WS^1 solution in Table 1 have almost identical bulk average parameters (volume integrals, rms radii and reaction cross section) which suggests that this is the physical solution.The far and near side (F and N) amplitudes have the same structure with a deep Airy oscillation carried entirely by the far side component. We shall use later this solution for our semiclassical analysis.

In the folding model we use three different effective interactions, namely the density independent M3Y, and two density dependent GOGNY and JLM in six different versions. A grid search using the strength N_v as a control parameter revealed a unique solution for all model interactions. We have obtained an almost unique shape for the function $\chi^2(J_v)$ see Table 3 and Figure 5. The folding solutions are fully consistent with the WS model. The average real volume integral is $J_v = 392 \pm 18$ MeV fm^3 and the real rms radius $R_v = 3.65 \pm 0.02$ fm. The normalization for the real component ranges from $N_v \approx 0.7$ to $N_v \approx 0.9$ strengthen once again the conjecture that the true physical parameter is the volume integral and not the normalization parameter. A standard far side/near side decomposition is plotted in Figures 6 and 7 showing the same far side dominance and an Airy minimum forward to a "rainbow" bump. There are some glories at very large angles due to a strong F/N interference since both amplitudes become large in this sector.

We start a WKB analysis [8] by searching the turning point trajectories in the complex r plane. We use the WS^1 potential with real volume integral $J_v = 399$ MeV fm^3. We observe an ideal situation with three active well separated turning points close to the real axis, Figure 8. The active points, which give the essential contribution to the action integrals are correlated with the poles of the real component of the optical potential (left hand stars in the figure). The inactive turning points are correlated with the poles of the imaginary potential and give negligible small contribution to the action integrals. The semiclassical deflection function is shown in Figure 9. There are at most 20 partial waves which contribute significantly to the scattering. The Coulomb rainbow is embedded in the Fraunhofer sector. Clearly there is a logarithmic singularity near $l_{orb} = 12$ and therefore the reaction is dominated by orbiting. The semiclassical absorption profile (modulus of the scattering amplitude as a function of the angular momentum) is shown in Figure 10. The semiclassical profile (curve) is identical with the exact quantum-mechanically result (black dots) which strengthen the conjecture that the WKB decomposition of the

scattering amplitude is exact, at least for this reaction. The internal barrier component (I) is quite large, characteristic for strongly refractive reactions [29] and is negligibly small beyond the orbiting momentum. The barrier (B) and internal barrier (I) components of the scattering amplitude interfere destructively giving rise to a shallow Grühn-Wall dip near the orbiting momentum. The semiclassical (WKB), barrier(B) and internal barrier (I) cross sections as well as their far side/near side subcomponents are shown in Figures 11 and 12. The barrier component (left lower panel) is responsible for the diffractive Fraunhofer sector and becomes again significant near $\theta = 180^\circ$. The internal barrier component (right lower panel) is significat at all intermediate angles and the destructive interference with the barrier component explains the Airy minimum near $\theta = 60^\circ$. The internal barrier cross section is exceptionally large near $\theta = 180^\circ$ where $\sigma^I/\sigma_R = 20$. Finally, the Argand diagram for the semiclassical (WKB) S-matrix is shown in Figure 13. The exact quantum result (Q) is shown for comparison. The WKB S-matrix is decomposed into barrier (B) and internal barrier (I) components. The orbiting/resonant effect is evident in the low partial waves sector. The barrier component is free for resonances. The entire resonant effect is isolated into the internal barrier component (right lower panel) where the S-matrix rotates anti-clockwise several times around the origin. These are resonances /Regge poles of the orbiting mechanism.

V	W	r_V	r_W	r_c	a_V	a_W	χ^2	σ_R	J_V	R_V	J_W	R_W
135.	10.57	0.7231	1.0741	1.0	0.8022	0.6867	8.72	1050.	399.	3.7646	74.	4.2654
160.	18.17	0.8773	0.9618	1.0	0.5993	0.5083	7.87	999.	624.	3.5712	85.	3.5963
214.	24.42	0.9104	0.9553	1.0	0.5066	0.1188	7.72	986.	865.	3.4548	97.	3.0712

Table 1: Discrete solutions with WS[1] form factors for the reaction ^{4}He+^{16}O at 54.1 MeV

V	W	r_V	r_W	r_c	a_V	a_W	χ^2	σ_R	J_V	R_V	J_W	R_W
155.	14.75	0.9088	1.1628	1.0	1.2026	1.0812	4.19	1028.	393.	3.6687	75.	4.0902

Table 2: Unique solution with WS[2] form factors for the reaction ^{4}He+^{16}O at 54.1 MeV

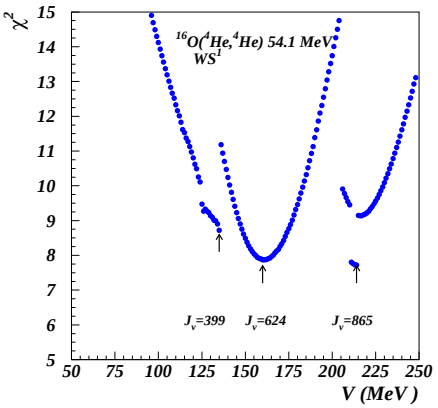

Figure 1: (Color online) Grid search with WS^1 form factors for the reaction ^{4}He+^{16}O at 54.1 MeV, Table 1.

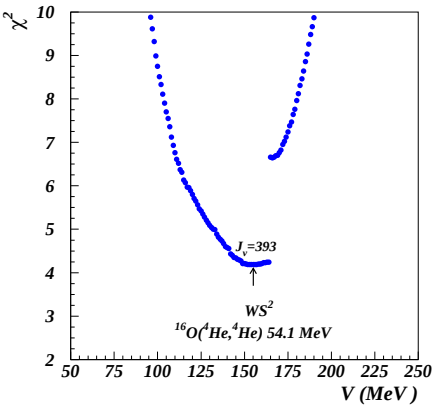

Figure 2: (Color online) Grid search with WS^2 form factors for the reaction ^{4}He+^{16}O at 54.1 MeV, Table 2.

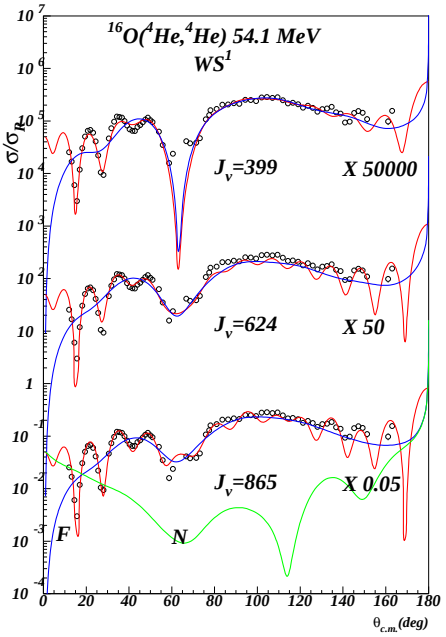

Figure 3: (Color online) F/N decomposition for the WS^1 potentials.

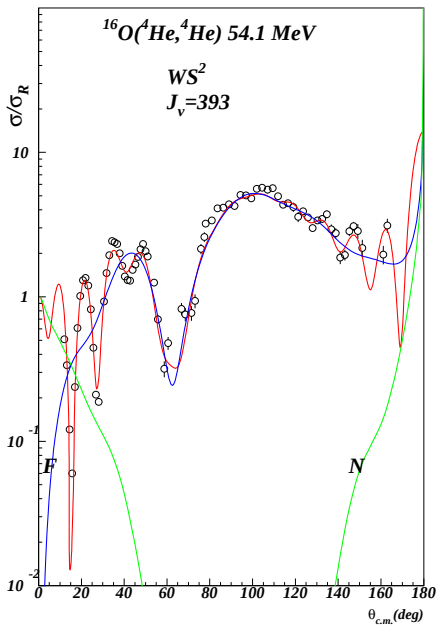

Figure 4: (Color online) F/N decomposition for the WS^2 potential.

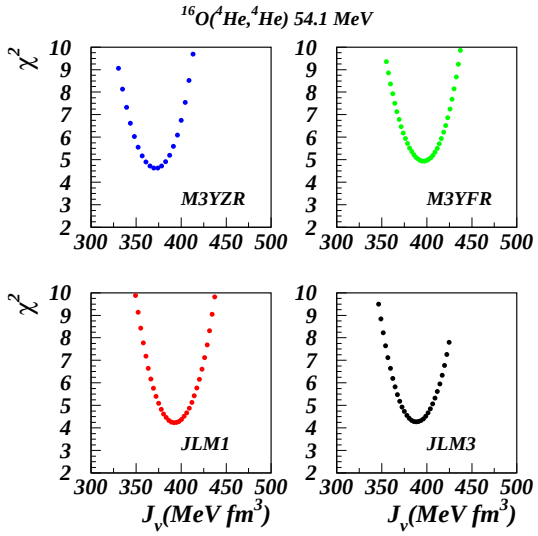

Figure 5: (Color online) Grid search with folding form factors. Unique solution, Table 3

pot	N_V	N_W	t_V	t_W	χ^2	σ_R	J_V	R_V	J_W	R_W
M3YZR	0.8400	0.1718	1.0178	0.8536	4.63	1083.	374.10	3.603	75.61	4.286
M3YFR	0.8250	0.1689	1.0020	0.8887	4.94	1069.	397.46	3.661	80.70	4.120
GOGNY1	0.6850	0.1420	1.0143	0.9147	5.81	1057.	401.73	3.657	82.67	4.049
GOGNY3	0.8800	0.1830	1.0278	0.9340	6.05	1058.	406.87	3.666	84.06	4.029
JLM1	0.6750	0.5947	0.9620	0.8801	4.23	1037.	391.99	3.626	77.48	4.076
JLM3	0.7250	0.6736	0.9577	0.8773	4.27	1042.	388.28	3.619	76.96	4.107

Table 3: Unique solutions obtained with folding form factors for the reaction ^{4}He+^{16}O at 54.1 MeV

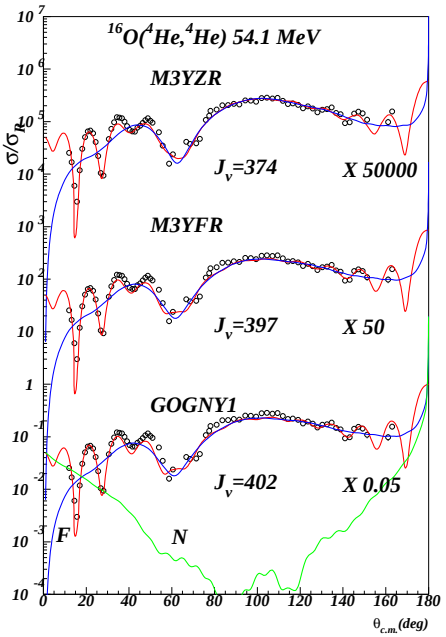

Figure 6: (Color online) F/N decomposition for the folding potentials from Table 3

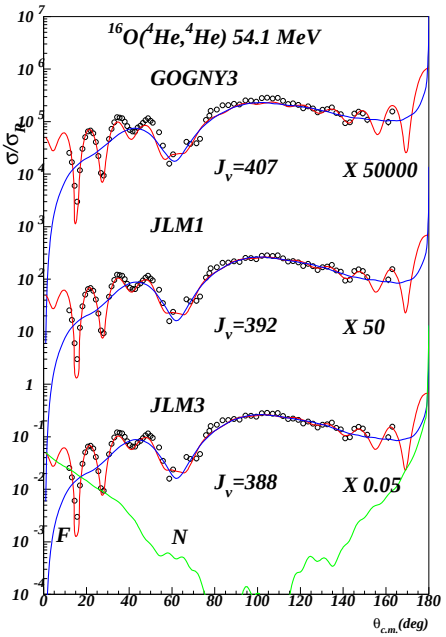

Figure 7: (Color online) F/N decomposition for the other folding potentials from Table 3

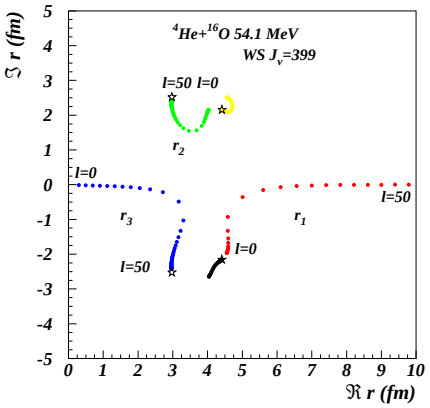

Figure 8: (Color online) Complex turning points for the WS potential with $J_V = 399$ MeV fm^3.

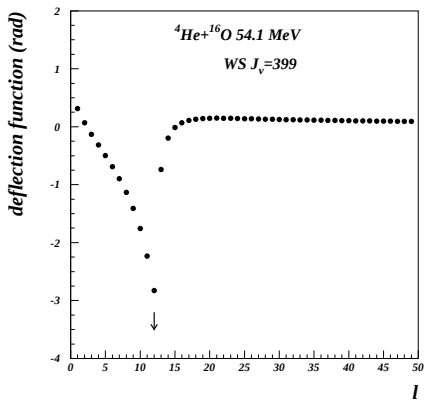

Figure 9: (Color online) Semiclassical deflection function for the WS potential with $J_V = 399$ MeV fm^3. The pattern is close to a near orbiting situation with the orbiting momentum $\ell \sim 12$.

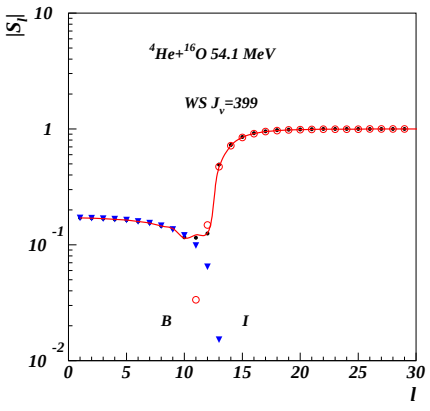

Figure 10: (Color online) Absorption profile for the WS potential with $J_V = 399$ MeV fm^3 (see text).

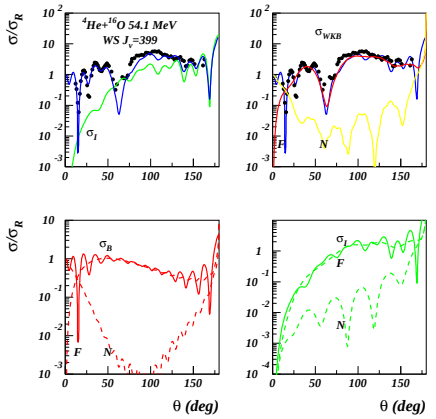

Figure 11: (Color online) Semiclassical (WKB) analysis of the reaction ^{4}He+^{16}O at 54.1 MeV based on the WS potential with $J_V = 399$ MeV fm^3 (see text).

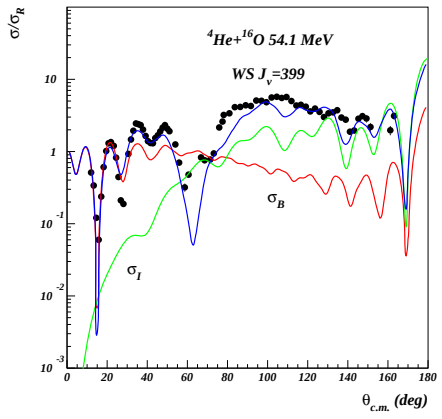

Figure 12: (Color online) The semiclassical (WKB) cross section is decomposed into barrier (B, red line) and internal barrier (I, green line). The deep Airy minimum appears as a strong interference of the B/I components. The internal barrier component dominates at large angles, reaching exceptionally large values ($\sigma_I/\sigma_R \sim 20$ at $\theta \sim 180°$)

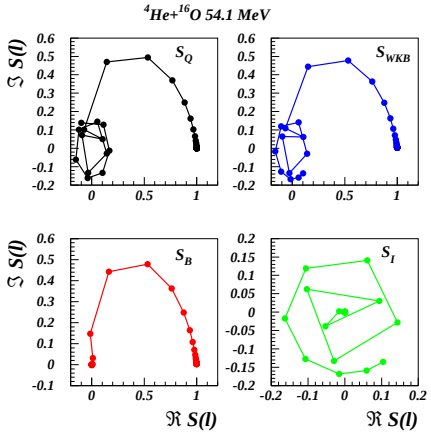

Figure 13: (Color online) Argand diagram for the semiclassical S-matrix based on the WS potential with $J_V = 399$ MeV fm^3. The trajectory for the S_{WKB} matches perfectly the exact quantum result S_Q. The internal barrier component, which reaches exceptionally large values, rotates several times around the origin suggesting the orbiting.

4 ^{4}He+^{28}Si at 18 MeV

We discuss here another reaction, ^{4}He+^{28}Si at $E_{lab} = 18$ MeV measured by Ahlfeld et al. [30]. The incident energy is quite low, just at the limit where the reaction mechanism starts to be dominated by direct interactions over compound elastic. The interest in this reaction resides in the fact that it displays a special kind of orbiting-butterfly scattering. The angular distribution is almost symmetric with respect to $\theta = 90^\circ$ and displays diffractive oscillations in the entire physical angular range. Our analysis go through the same steps as for the preceding reaction. Since the energy is quite low, we expect a significant number of discrete solutions with both WS and folding optical potentials see Tables 4 and 5. The χ^2 landscape is explored in Figures 14 and 22. Remarkably two solutions with $J_v \approx 200$ MeV fm^3 and $J_v \approx 300$ MeV fm^3 appear in all six model calculations. The far side/near side decomposition is shown in Figures 15-20 and 23. For all solutions there is a clear far side dominance and a particularly deeep Airy minimum near $\theta = 80^\circ$ for the solution with $J_v \approx 300$ MeV fm^3. This should in principle indicates a strongly refractive reaction mchanism . But we shall see that is not the case. The first hint is given by the large angle oscillations which can be fitted by a renormalized $P_8^2(\theta)$ amplitude which suggests the presence of a Regge pole near $\ell = 8$ For the moment we are interested if there are other traces of resonant scattering in our reaction. We show the Argand diagram for the folding S-matrix in Figure 16. The figure shows convingcingly that the corresponding folding potentials are phase equivalent since the S-matrix trajectories in angular momentum space are identical. Second, there is a cluster of points in the low angular momentum sector which in fact is a signature of the orbiting. The absorption profile for the same S-matix are shown in Figure 21. There is a significant odd-even staggering at low partial waves (multiple Regge poles).The arrow indicates the location of the main Regge pole near $\ell = 8$.

The trajectories of the complex turning points for the WS^1 potential with $J_v = 223$ MeV fm^3 are shown in Figure 26. The barrier turning point r_2 and the outer point r_1 have an unusual trajectory shape due to the fact that the imaginary component of the optical potential has complex poles located close to the real axis (right hand stars), see in Table 5 potentials with very small a_w. The calculation of the action integrals requires a careful numerical evaluation since the poles should be avoided. Figure 27 displays the semiclassical deflection function with a typical orbiting singularity near $\lambda = 9.5$. The semiclassical absorption profile, shown in Figure 28, indicate a quite strong internal barrier component. The semiclassical profile do not reproduce the exact Grühn-Wall spike (black dots) but still appears as a B/I interference near the orbiting momentum. The internal barrier component (I) is negligibly small beyond the orbiting momentum. The semiclassical cross section are cal-

culated and displayed in Figure 29 . The barrier component, typical for strong absorption, follows quite well the experimental cross section , though it is the internal barrier component which dominates the cross section at large angles. The Argand diagram shown in Figure 30. shows a strong orbiting effect in both semiclassical (WKB) and quantum (Q) S-matrix. The entire resonant effect is isolated into the internal barrier component (I). Finally we search the Regge poles directly from the data. We prceed as follows: we guess a reasonable background-two pole solution, as described in the preceding paper and then generate about 10^6 input solution by Monte Carlo for aur seraching code which minimises a standard χ^2 function. We are looking for solutions for which both the background and the pole component are unitary, since we want to isolate the pole contribution to the cross section. Two fully unitary solutions are given in Table 6 and confirms the preceding analysis with a main pole liocated near$\lambda = 8$

The cross sections obtained with this model are plotted in Fig.24. The butterfly effect is even more evident in this calculation The background component is important only at forward angles, while the pole component contributes significantly at all angles. The background absorption profile shown in Fig. 25 is typical for strong absorption regime while the Grühn-Wall spike of ecceptional amplitude appears here as carried out by the pole component alone.

5 Conclusion

We have analysed here two apparently obscure angular distribution for heavy ion scattering which proved to be extremely rich in information about the reaction mechanism. The first example α+^{16}O at 54.1 MeV show all characteristics of a strongly refractive reaction but proves to be in fact a typical example of heavy ion orbiting. A second examle, α+^{28}Si at 18.0 MeV taken at the limit where the direct interaction starts to dominate over the compound elastic, show a special case of heavy ion orbiting, butterfly scattering with diffractive oscillations in the entire physical angular range due to Regge pole dominance. In the light of our analysis it is evident that a lot of reactions dubbed improperly as ALAS (strong encrease of the cross section at large angles) should be reanalized since most if not all of them could be in fact cases of nuclear orbiting.

pot	N_V	N_W	t_V	t_W	χ^2	σ_R	J_V	R_V	J_W	R_W
M3YZR	0.4900	0.0673	0.8469	0.9997	4.47	1183.	220.80	4.649	30.63	3.946
	0.7450	0.0581	0.8675	1.2983	6.58	1287.	336.18	4.540	27.00	3.051
M3YFR	0.4300	0.0647	0.8750	1.1067	4.49	1141.	210.15	4.572	32.09	3.627
	0.6650	0.0539	0.8971	1.1402	6.13	1233.	325.48	4.461	26.78	3.522
GOGNY1	0.3600	0.0564	0.8900	1.1525	4.69	1138.	208.14	4.541	33.18	3.520
	0.5550	0.0432	0.9126	1.2495	5.64	1215.	321.34	4.430	25.58	3.251
JLM1	0.3550	0.2354	0.8367	1.1387	4.19	1143.	212.48	4.568	30.92	3.629
	0.5450	0.1889	0.8560	1.3226	5.92	1242.	326.64	4.466	25.09	3.133
JLM3	0.3900	0.3019	0.8321	1.1436	4.20	1138.	212.10	4.572	30.29	3.642
	0.6000	0.2502	0.8527	1.3011	6.10	1241.	326.77	4.463	25.35	3.209

Table 4: Discrete solutions with folding form factors for the reaction ^{4}He+^{28}Si at 18.0 MeV.

V	W	r_V	r_W	r_c	a_V	a_W	χ^2	σ_R	J_V	R_V	J_W	R_W
53.	3.44	0.9174	1.2304	1.0	0.9271	0.2423	4.43	1089.	223.	4.7611	24.	4.4982
88.	4.70	0.8756	1.2234	1.0	0.8542	0.2368	5.08	1140.	314.	4.4623	32.	4.4693
128.	5.70	0.8550	1.2244	1.0	0.7962	0.2270	5.45	1159.	414.	4.2585	39.	4.4659

Table 5: Discrete solutions with WS[1] form factors for the reaction ^{4}He+^{28}Si at 18.0 MeV.

Set	L	Δ	α	β	L_1	Δ_1	D_1	Γ_1	L_2	Δ_2	D_2	Γ_2	χ^2	σ_R
R1	8.14	4.00	-1.66	2.13	7.73	0.415	10.3	20.6	8.68	0.204	10.9	2.61	2.64	1680
R2	7.85	4.16	-1.67	2.37	7.98	0.421	13.6	27.4	8.06	0.413	11.3	1.38	2.69	1703

Table 6: Unitary solutions with Regge pole amplitudes for the reaction ^{4}He+^{28}Si at 18.0 MeV.

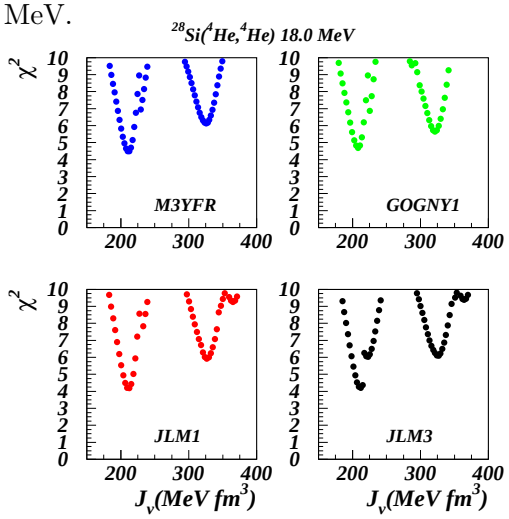

Figure 14: (Color online) Search for discrete solutions with folding form factors.

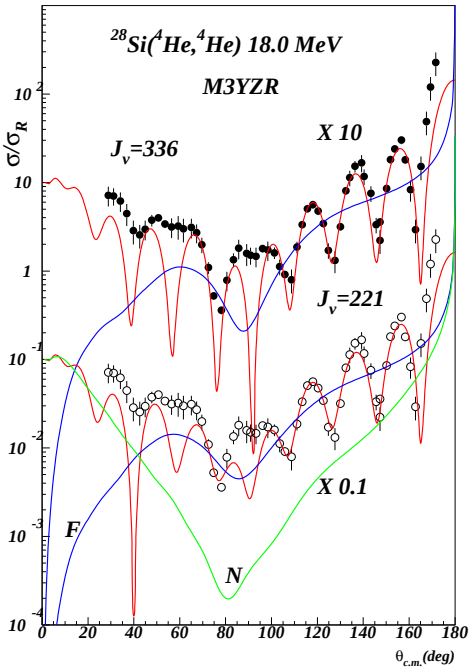

Figure 15: (Color online) F/N decomposition with M3YZR. There are normalization problems at forward angles.

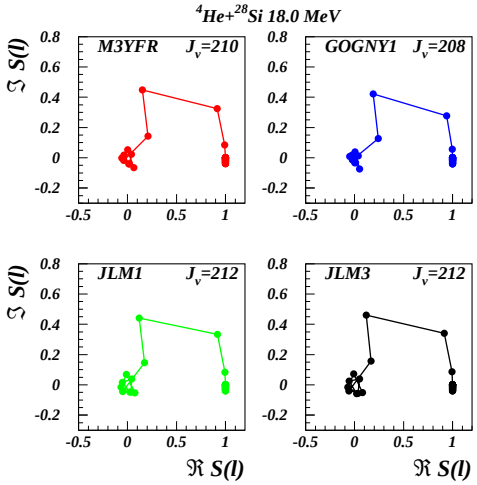

Figure 16: (Color online) Argand diagram for the S-matrix calculated with several folding solutions with real volume integral $J_V \sim 210$ MeV fm^3. The corresponding optical potentials are fully phase equivalent.

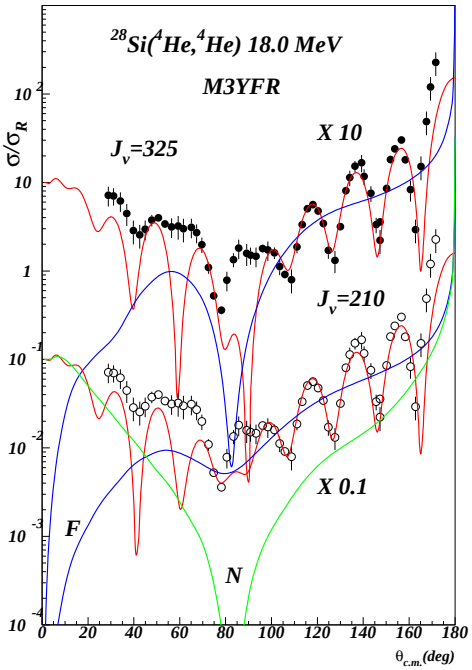

Figure 17: (Color online) F/N decomposition with M3YFR.

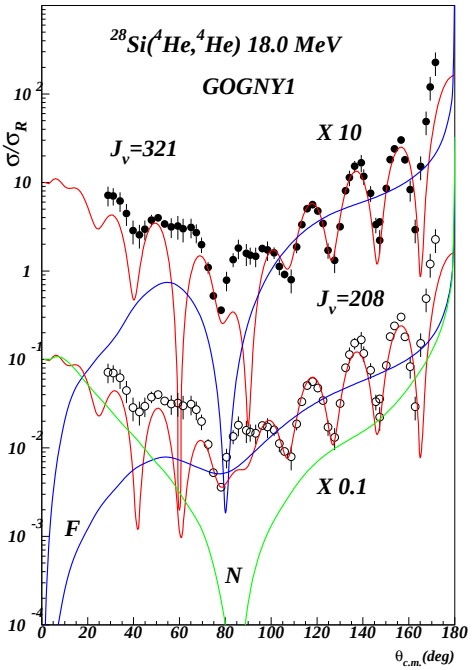

Figure 18: (Color online) F/N decomposition with GOGNY1.

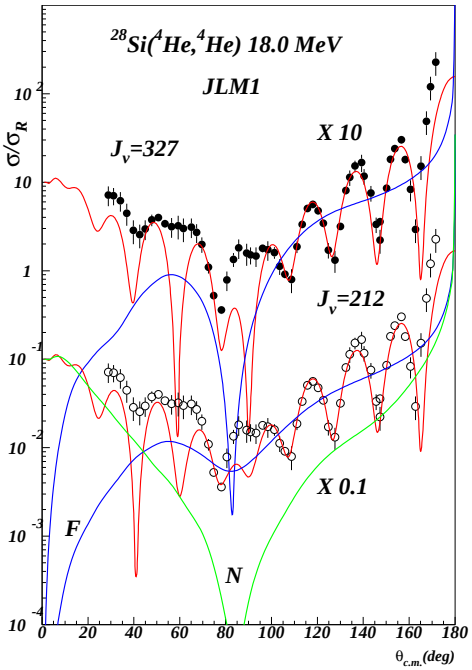

Figure 19: (Color online) F/N decomposition with JLM1.

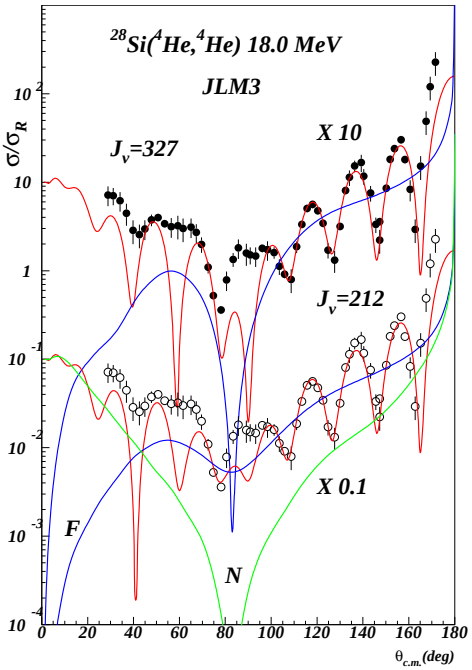

Figure 20: (Color online) F/N decomposition with JLM3.

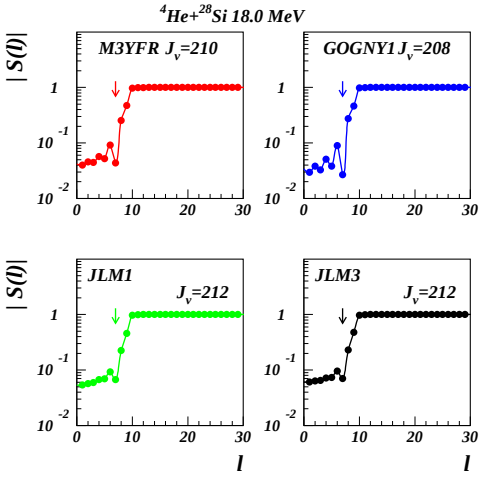

Figure 21: (Color online) Absorption profile calculated with several folding solutions. The arrows indicate the position of the Regge pole.

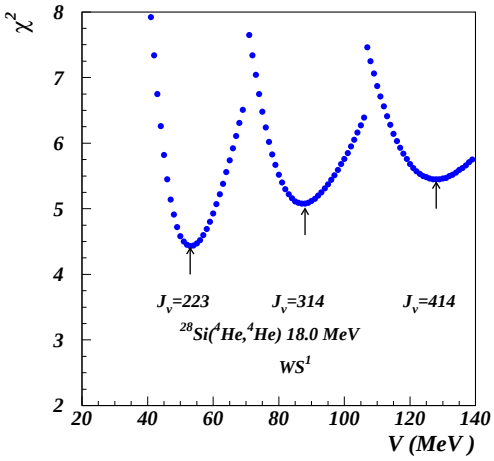

Figure 22: (Color online) Search for discrete solutions with WS^1 form factors.

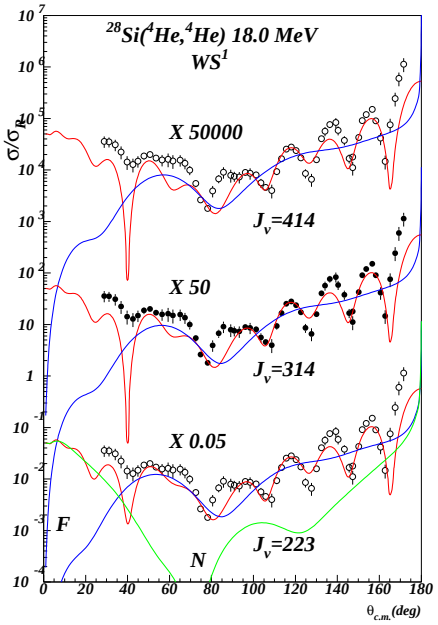

Figure 23: (Color online) F/N decomposition with WS^1. This calculation did not solved the normalization problem at forward angles.

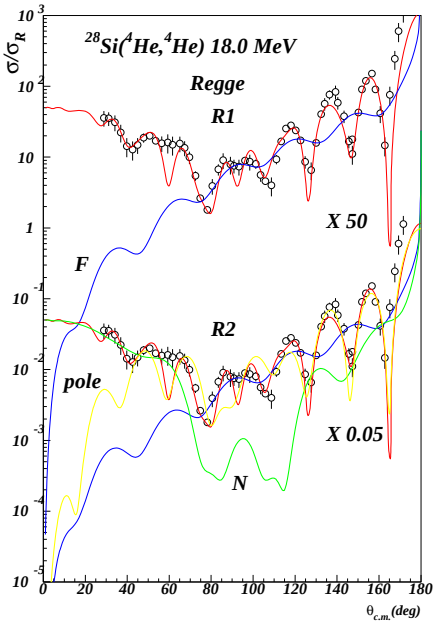

Figure 24: (Color online) F/N decomposition using Regge pole amplitudes. The pole components dominate the cross section in the entire angular range. This calculation solved the normalization problem at forward angles.

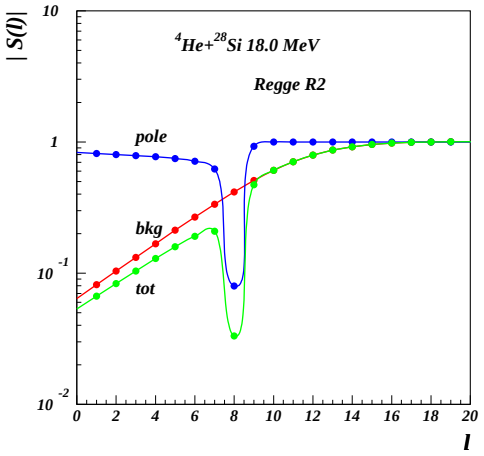

Figure 25: (Color online) Absorption profile using Regge pole amplitude R2. The main pole located near $\ell = 8$ produced a deep Grühn-Wall spike in the total S-matrix.

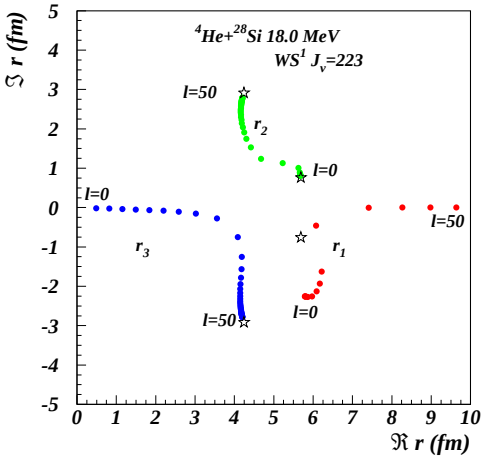

Figure 26: (Color online) Complex turning point trajectory for the WS^1 potential with real volume integral $J_V = 223$ MeV fm^3. Unusual shape of the barrier turning point trajectory (r_2 green). This starts near the pole of the imaginary potential and ends near the pole of the real potential (stars).

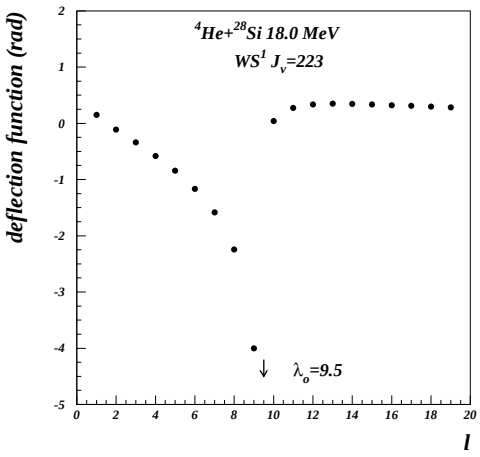

Figure 27: (Color online) Deflection function. The orbiting angular momentum is $\lambda_0 = 9.5$.

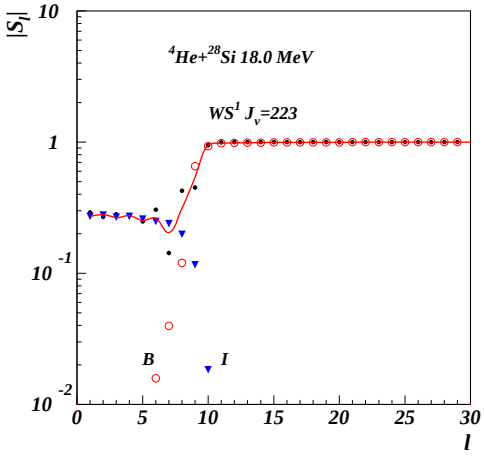

Figure 28: (Color online) Semiclassical (WKB) absorption profile red curve. The quantum mechanical solution (black dots) is shown for comparison. The WKB solution is decomposed into barrier (B) and internal barrier (I) components. The internal barrier component is negligibly small beyond the orbiting angular momentum.

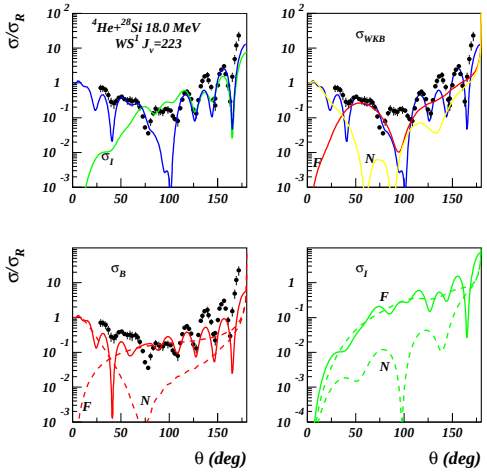

Figure 29: (Color online) Semiclassical (WKB) cross section compared with the data. The regular oscillations at large angles are triggered by the barrier component. But their amplitude is determined by the internal barrier component (green curve). The B/I components are further decomposed into F/N subcomponents.

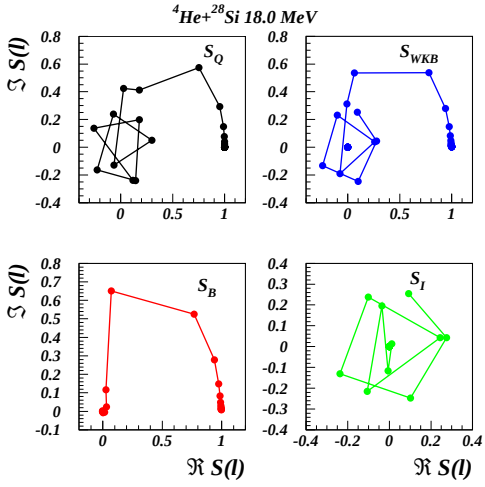

Figure 30: (Color online) Argand diagram for the semiclassical (WKB) S-matrix is compared with the exact quantum mechanical result (Q). The orbiting effect is isolated into the internal barrier component (I).

Acknowledgements

This work was partly supported by CNCSIS Romania, under program PN-II-PCE-55/2011 and PN-II-ID-PCE-0299/2012, and partly by IN2P3, France.

References

[1] K. W. McVoy, Phys. Rev. C **3**, 1104 (1971).

[2] T. E. O. Ericson, Preludes in Theoretical Physics, eds, A. de-Shalit, L. Van Hove and H. Feshbach, North Holland, 1965.

[3] R. Anni, Phys. Rev. C **63**, 031601R (2001).

[4] C. R. Grühn and N. S. Wall, Nucl. Phys. **81**, 161 (1966).

[5] F. Michel, G. Reidemeister and S. Ohkubo, Phys. Rev. Lett. **89**, 152701 (2002);ibidem, Phys. Rev. C **63**, 034620 (2001).

[6] P. Fröbrich and R. Lipperheide, *Theory of Nuclear Reactions*, Clarendon Press, Oxford, 1996.

[7] K. W. Ford and J. A. Wheeler, Ann. Phys. (N. Y.) **7**, 259 (1959).

[8] D. M. Brink and N. Takigawa, Nucl. Phys. **A279**, 159 (1977).

[9] A. A. Ogloblin *et al.*, Phys. Rev. C **62**, 044601 (2000).

[10] N. Anantaraman, H. Toki and G. F. Bertsch, Nucl. Phys. **A398**, 269 (1983).

[11] J. P. Jeukenne, A. Lejeune and C. Mahaux, Phys. Rev. **C16**, 80 (1977).

[12] M. Beiner and R. J. Lombard, Ann. Phys. (N.Y.) **86**, 262 (1974).

[13] I. Angeli, Heavy Ion Physics, **8**, 23 (1998).

[14] Dao T. Khoa, Hoang Sy Than, Tran Hoai Nam, Marcella Grasso, and Nguyen Van Giai Phys. Rev. **C 69**, 044605 (2004).

[15] F. Carstoiu and M. Lassaut, Nucl. Phys. **597**, 269 (1996).

[16] Dao T. Khoa, Phys. Rev. **C63**, 034007 (2001).

[17] X. Campi and A. Bouyssy, Phys. Lett. **73B**, 263 (1978).

[18] J. W. Negele and K. Yazaki, Phys. Rev. Lett. **47**, 71 (1981).

[19] D. Gogny, *Proc. Int. Conf. on Nucl. Physics, Munich 1973, eds J. de Boer and H. J. Mang, Vol. 1, p. 48.*

[20] D. H. Youngblood, H. L. Clark and Y.-W. Lui, Phys. Rev. Lett. **82**, 691 (1999).

[21] G. Colo, N. Van Giai, P. F. Bortignon and M. R. Quaglia, Phys. Lett. **B485**, 362 (2000).

[22] J. P. Auger and R. J. Lombard, Phys. Lett. **90B**, 200 (1980).

[23] L. Trache, A. Azhari, H. L. Clark, C. A. Gagliardi, Y.-W. Lui, A. M. Mukhamedzhanov, X. Tang, N. Timofeyuk, R. E. Tribble and F. Carstoiu, Phys. Rev. **C61**, 024612 (2000).

[24] H.Abele,H.J.Hauser,A.Korber,W.Leitner,R.Neu, H.Plappert,T.Rohwer,G.Staudt,M.Strasser,S.Welte, M.Walz,P.D.Eversheim,F.Hinterberger, Z.Physik **A326** 373,1987.

[25] H. Abele and G. Staudt, Phys. Rev. **C47**, 742 (1993).

[26] D. A. Goldberg, S. M. Smith and G. F. Burdzik, Phys. Rev. **C10**, 1362 (1974).

[27] Dao T Khoa, W von Oertzen, H G Bohlen and S Ohkubo, ArXiv:nucl-th/0612100v1 (2006).

[28] F. Michel, J. Albinski, P. Belery, Th. Delbar, Gh. Gregoire, B.Tasiaux and G. Reidemeister Phys. Rev. **C28**, 1904 (1983).

[29] Florin Carstoiu, Livius Trache, Robert E.Tribble, Carl A. Gagliardi Phys. Rev. **C70** 054610, (2004)

[30] C. E. Ahlfeld, G. E. Assousa, R. A. Lasalle, W. J .Thompson, H. A. Van Rinsvelt, N. P. Heydenburg, Nucl. Phys **A191** 137(1972).

[31] T. Al-Abdullah, F. Carstoiu, X. Chen, H. L. Clarke, C. A. Gagliardi, Y.-W. Lui, A. Mukhamedzhanov, G. Tabacaru, Y. Takimoto, L. Trache, R.E.Tribble, Y. Zhai Phys. Rev. C **89**, 025809 (2014).

[32] T. Al-Abdullah, F. Carstoiu, C. A. Gagliardi, G. Tabacaru, L. Trache and R. E. Tribble. Phys. Rev. C **89**, 064602 (2014).